Turkish Journal of Chemistry

Volume 42 | Number 1 Article 15

1-1-2018

Cu(II) immobilized on Fe$_{3}$O$_{4}$ @Agarose nanomagnetic catalyst functionalizedwith ethanolamine phosphate-salicylaldehyde Schiff base: a magnetically reusablenanocatalyst for preparation of 2-substituted imidazolines, oxazolines, andthiazolines

ZEINAB ZAREI

BATOOL AKHLAGHINIA

TÜBİTAK

Turkish Journal of Chemistry

http://journals.tubitak.gov.tr/chem/

Research Article

Turk J Chem
(2018) 42: 170 – 191

doi:10.3906/kim-1704-53

Cu(II) immobilized on Fe_3O_4@Agarose nanomagnetic catalyst functionalized with ethanolamine phosphate–salicylaldehyde Schiff base: a magnetically reusable nanocatalyst for preparation of 2-substituted imidazolines, oxazolines, and thiazolines

Zeinab ZAREI, Batool AKHLAGHINIA*
Department of Chemistry, Faculty of Sciences, Ferdowsi University of Mashhad, Mashhad, Iran

Received: 24.04.2017 • **Accepted/Published Online:** 03.11.2017 • **Final Version:** 08.02.2018

Abstract: Herein we synthesized Cu(II) immobilized on Fe_3O_4@Agarose functionalized with ethanolamine phosphate–salicylaldehyde Schiff base (Fe_3O_4@Agarose/SAEPH$_2$/Cu(II)) as a new and cost-effective nanomagnetic catalyst. The nanomagnetic catalyst was characterized by FT-IR, XRD, VSM, SEM-EDX, TEM, TGA, and ICP techniques and it was found that the particles were about 9–25 nm in size and spherical with entrapment of the Fe_3O_4 particles in the hollow pore structure of the agarose. The prepared nanomagnetic catalyst showed excellent activity for preparation of 2-substituted imidazolines, oxazolines, and thiazolines. The catalyst is easy to prepare and exhibits higher catalytic activity than some commercially available copper sources. More importantly, this nanomagnetic catalyst can be easily recovered by using a permanent magnet and reused for at least seven cycles without significant deactivation.

Key words: Agarose, Schiff base complex, nanomagnetic catalyst, 2-substituted imidazolines, 2-substituted oxazolines and 2-substituted thiazolines

1. Introduction

Heterocyclic compounds are essential to life and found in the structures of many biologically active natural products.[1] The largest portion of chemical entities as a part of many natural products, fine chemicals and biologically active pharmaceuticals are made up of nitrogen containing heterocyclic molecules which are vital for enhancing the quality of life.[1] Among a large variety of nitrogen-containing heterocyclic compounds imidazolines, oxazolines, and thiazolines, as an important class of natural and synthetic products, are of interest because many of them exhibit useful biological activities and clinical applications.[2] Moreover, they are known as important intermediates in organic transformations.[3–5] There are numerous methods for the synthesis of 2-imidazolines, 2-oxazolines, and 2-thiazolines from different precursors such as carboxylic acids,[6,7] aldehydes,[8–11] amides,[12] thioamides,[13] esters,[14,15] aziridines,[16–19] anthraquinone,[20] carbene complex,[21] and nitriles[22–24] under various reaction conditions and a variety of homogeneous and heterogeneous catalysts. In spite of the potential utility of the above-mentioned procedures for the synthesis of these nitrogen-containing heterocycles, some of these methods suffer from one or more disadvantages, such as harsh reaction conditions (strong acidic conditions), use of stoichiometric amounts of catalysts, use of complex and expensive reagents and toxic solvents, long reaction times, and low yields of products. Therefore, in order to remove these limi-

*Correspondence: akhlaghinia@um.ac.ir

tations, the introduction of a new and environmentally benign catalytic procedure with high catalytic activity, recyclability, and simple workup for the preparation of these compounds under neutral, mild, and practical conditions is of prime interest.

Nanomagnetic catalysts have received much attention in organic chemistry due to their easy separation from the reaction mixture, clean forward reaction, and remarkable physical and chemical properties through controlling the particle size and high surface area.[25] Nowadays, agarose (linear polysaccharide) is well known as an excellent coating for Fe_3O_4 NPs due to high surface area and its good dispersion,[26,27] which prevent the aggregation of magnetic nanoparticles.

In recent years, Schiff bases have been found as efficient ligands for stable complexation with different metals, because of their vital roles in medicine and complexation chemistry.[28] Among them, copper–Schiff base complexes have received more attention due to their low cost, nontoxicity, high electrical conductivity, high corrosion resistance, and Lewis acid activity.[29] With respect to these advantages, in the present study, preparation of Fe_3O_4 NPs with an outer shell of agarose functionalized by the Schiff base (via the condensation reaction of ethanolamine phosphate with salicylaldehyde) and immobilization of Cu(II) ions on its surface has been implemented and reported for the first time, as a novel and efficient nanomagnetic catalyst for successful synthesis of 2-imidazolines, 2-oxazolines, and 2-thiazolines (Scheme 1).

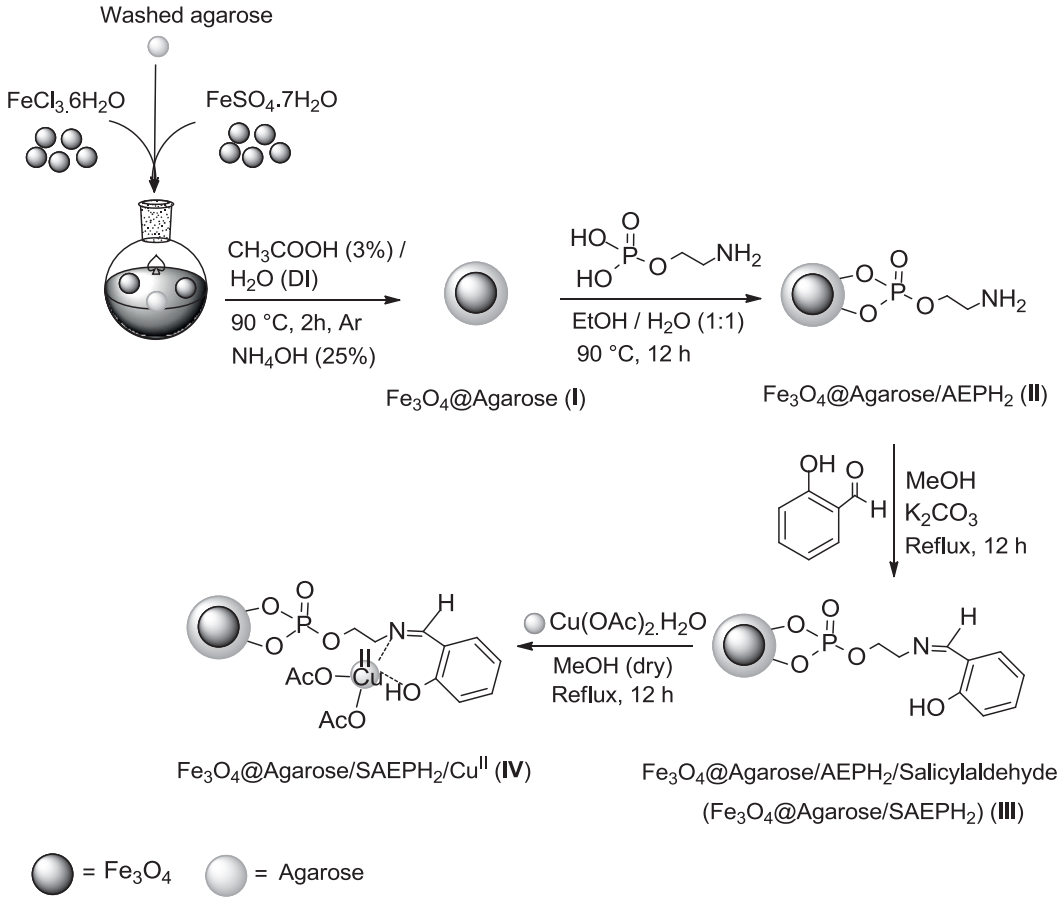

Scheme 1. Preparation of Cu(II) immobilized on Fe_3O_4@Agarose nanomagnetic catalyst functionalized with ethanolamine phosphate–salicylaldehyde Schiff base (Fe_3O_4@Agarose/$SAEPH_2$/Cu(II)).

2. Results and discussion

2.1. Characterization of catalyst

The chemical structure and detailed morphology of the prepared catalyst were characterized by techniques including Fourier transform infrared spectroscopy (FT-IR), thermogravimetric analysis (TGA), transmission electron microscopy (TEM), scanning electron microscopy (SEM), energy-dispersive X-ray analysis (EDS), vibrating sample magnetometer (VSM), X-ray powder diffraction (XRD), and inductively coupled plasma (ICP), which confirmed the functionalization of Fe_3O_4@Agarose nanomagnetic catalyst according to the pathway shown in Scheme 1.

The FT-IR spectrum of Fe_3O_4@Agarose nanomagnetic catalyst (**I**) (Figure 1a) showed a broad band at 3552–3019 cm^{-1} due to O–H stretching vibration modes of both iron oxide and agarose.[30] Moreover, several bands at 2929, 1073, and 929 cm^{-1} were assigned to the asymmetric stretching vibrations of CH_2 groups, the C–O–C bridge, and 3,6-anhydrogalactose units, respectively. Furthermore, the medium band at 588 cm^{-1} was related to the stretching vibration of the Fe–O bond, which was identified as an octahedral site from the Fe_3O_4 core.

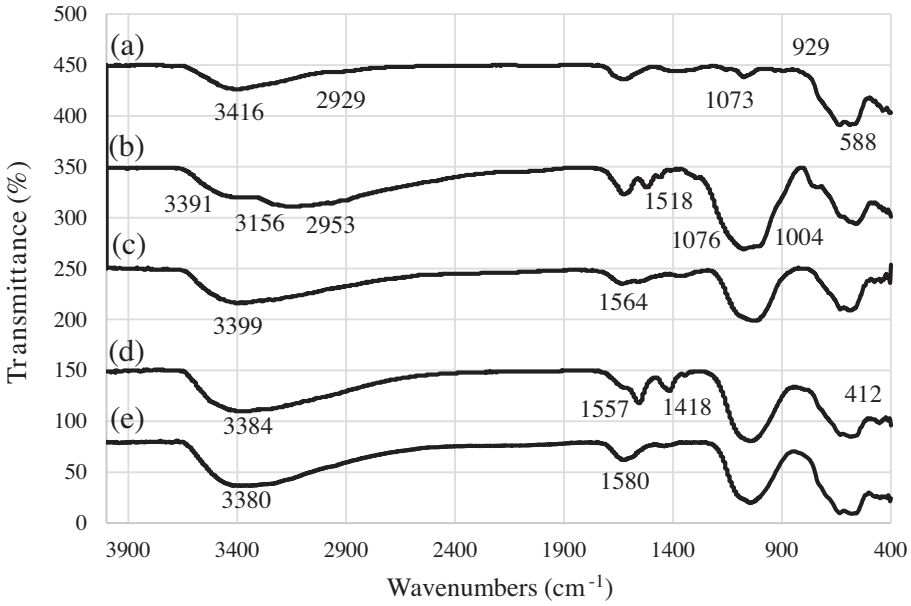

Figure 1. FT-IR spectra of (a) Fe_3O_4@Agarose (**I**), (b) Fe_3O_4@Agarose/$AEPH_2$ (**II**), (c)Fe_3O_4@Agarose/$SAEPH_2$ (**III**),(d)Fe_3O_4@Agarose/$SAEPH_2$/Cu(II)(**IV**), and (e) 7th reused Fe_3O_4@Agarose/$SAEPH_2$/Cu(II).

In the FT-IR spectrum of Fe_3O_4@Agarose/$AEPH_2$ (**II**) (Figure 1b), two absorption bands appearing at 3391 and 3156 cm^{-1} were attributed to the stretching vibration modes of NH_2 groups. Meanwhile, the existence of CH_2 groups has been proved by the appearance of the broader band around 2953–2800 cm^{-1}, which was covered by stretching vibrations of the C–H bonds of agarose. Furthermore, another band at 1518 cm^{-1} could be ascribed to the bending vibration of the N–H bond.[31] It is worth noting that the stretching vibration bands of P=O and O–P–O bonds were covered by the asymmetric stretching vibration bands of the C–O–C, bridge which caused a broad absorption band at 1153–1004 cm^{-1}.[32]

The FT-IR spectrum of Fe_3O_4@Agarose/$SAEPH_2$ (**III**) (Figure 1c) showed an absorption band at 1564 cm^{-1} due to the C=N stretching vibration[33] and the relatively broad band corresponding to O–H

stretching vibration mode at around 3596–3064 cm^{-1}, which confirmed the successful formation of Schiff base on the surface of functionalized Fe_3O_4@Agarose. In addition, coordination of Fe_3O_4@Agarose/$SAEPH_2$ to $Cu(OAc)_2.H_2O$ (Figure 1d) was corroborated by the decrease in the intensities and frequencies of absorption bands of O–H and C=N bonds (3384, 1557 cm^{-1} due to stretching vibrations modes of O–H and C=N, respectively). Furthermore, the appearance of a broad absorption band with low intensity at around 1479–1401 cm^{-1} was attributed to the asymmetric and symmetric stretching vibrations of acetate ions (OAc), which revealed that the acetate ions were still connected to Cu(II).[32] Additionally, the absorption band at 412 cm^{-1} can be attributed to the Cu–N stretching vibration.[34,35]

The crystal structure of Fe_3O_4@Agarose/$SAEPH_2$/Cu(II) was characterized by X-ray powder diffraction (XRD) analysis. As seen in Figure 2, the XRD pattern showed ten diffraction peaks. The peaks that appeared at $2\Theta = 19.0°$, $30.28°$, $35.67°$, $43.36°$, $53.8°$, $57.36°$, $62.99°$, $71.48°$, $74.55°$, and $75.56°$ could be indexed to the (111) (220), (311), (400), (422), (511), (440), (620), (533), and (622) planes of Fe_3O_4 NPs in the cubic phase. This result agrees with the standard data published for the cubic structure of Fe_3O_4 (JCPDS: 19-0629).[36–38] In addition, the broad peak positioned at $2\Theta = 20°$–$25°$ confirmed the presence of amorphous agarose coated on the Fe_3O_4NPs.[39] It is noteworthy that no peak corresponding to impurity was detected, which indicated high purity of the prepared nanocatalyst. Furthermore, the crystalline size of the synthesized catalyst was about 9 nm according to the Debye–Scherrer equation $d = K\lambda/(\beta\cos\theta)$.

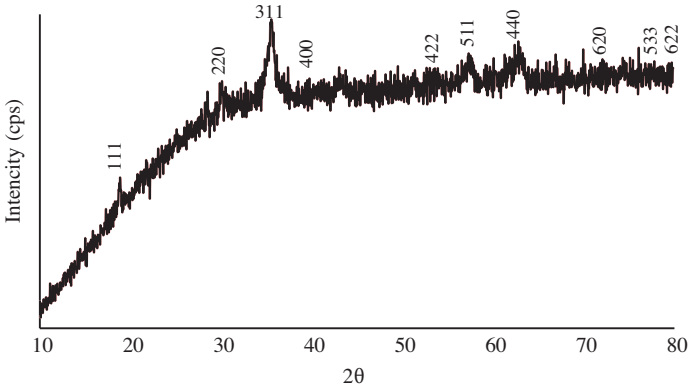

Figure 2. The XRD pattern of Fe_3O_4@Agarose/$SAEPH_2$/Cu(II).

To elucidate the morphology and size of the synthesized nanomagnetic catalyst, Fe_3O_4@Agarose/$SAEPH_2$/Cu(II) was analyzed by SEM and TEM (Figures 3a–3d). It is evident from SEM images (Figures 3c and 3d) that agarose coated the Fe_3O_4 NPs and formed polymer shells with a nearly spherical morphology. TEM micrographs and size distributions (9–25 nm) of catalyst, which are shown in Figures 3a and 3b, indicate that Fe_3O_4@Agarose/$SAEPH_2$/Cu(II) are spherical and 9–25 nm in size. The TEM results reveal the entrapment of the Fe_3O_4 particles in the hollow pore structure of agarose, which prevented the agglomeration of small particles and resulted in good dispersity of Fe_3O_4 NPs in the agarose matrix.[30,38]

Furthermore, an energy dispersive spectrometer (EDS) confirmed the existence of C, O, P, Fe, and Cu elements in the nanocatalyst as shown in Figure 3e. It is clear that copper was successfully immobilized on the surface of the Fe_3O_4@Agarose/$SAEPH_2$ due to the high intensity of Cu(II). In addition, there are no impurity elements in the catalyst structure.

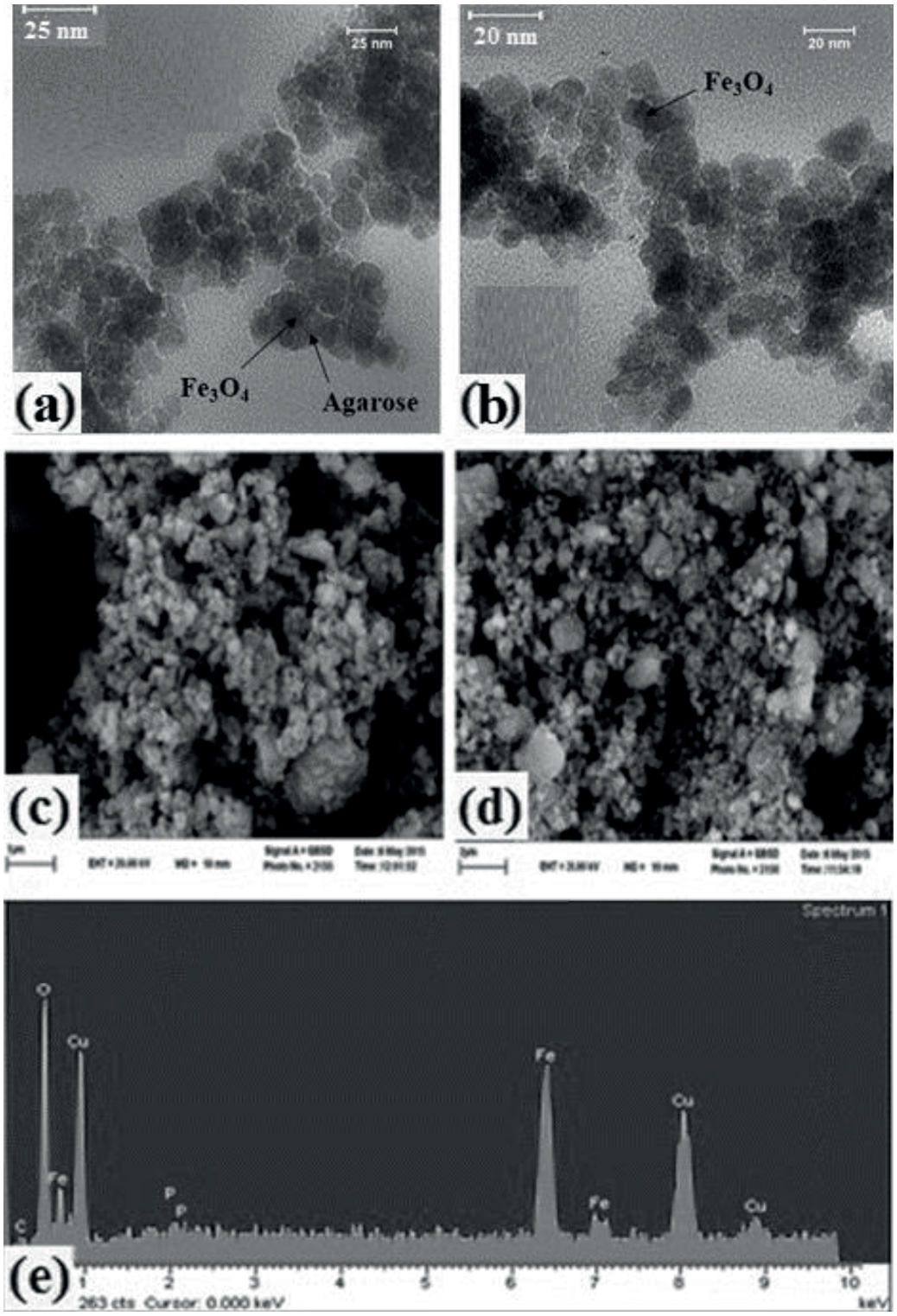

Figure 3. (a, b) TEM images of Fe_3O_4@Agarose/SAEPH$_2$/Cu(II), (c, d) SEM images of Fe_3O_4@Agarose/SAEPH$_2$/Cu(II) with 20,000× and 40,000× magnification, and (e) The EDS analysis of Fe_3O_4@Agarose/SAEPH$_2$/Cu(II).

The magnetic behavior of the catalyst was investigated using a vibrational sampling magnetometer (VSM) at room temperature. As can be seen in Figures 4a and 4b, the hysteresis loops of Fe_3O_4@Agarose nanomagnetic catalyst (Figure 4a) and Fe_3O_4@Agarose/$SAEPH_2$/Cu(II) (Figure 4b) were completely reversible, which indicated superparamagnetic behaviour,[40] due to the small size of the magnetic NPs in the core. Moreover, the curve indicated that the saturated magnetization values of Fe_3O_4@Agarose nanomagnetic catalyst and Fe_3O_4@Agarose/$SAEPH_2$/Cu(II) were about 59.64 emu/g and 32.47 emu/g, respectively, and it was lower than that of uncoated Fe_3O_4 NPs.[41] Likewise, a significant decrease in the saturation magnetization value of Fe_3O_4@Agarose/$SAEPH_2$/Cu(II), compared to the value of Fe_3O_4@Agarose, confirmed the successful functionalization of the Fe_3O_4@Agarose surface.

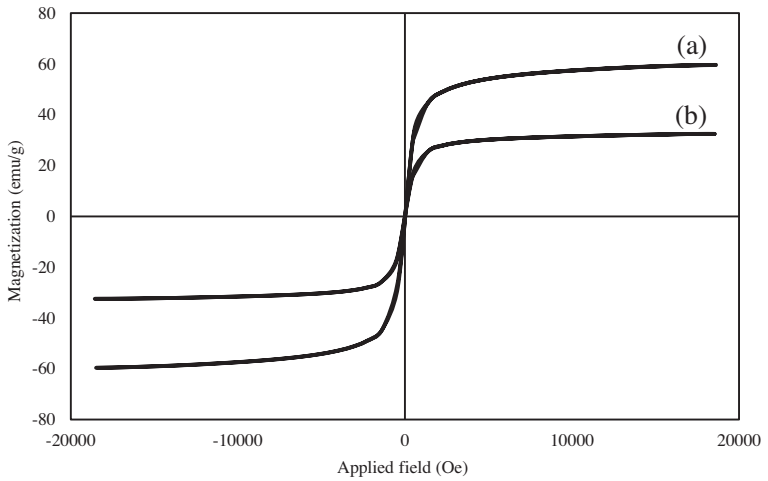

Figure 4. Magnetization curves of (a) Fe_3O_4@Agarose and (b) Fe_3O_4@Agarose/$SAEPH_2$/Cu(II).

To verify the thermal stability of the catalyst, thermogravimetric analysis of Fe_3O_4@Agarose, Fe_3O_4@Agarose/$AEPH_2$, and Fe_3O_4@Agarose/$SAEPH_2$/Cu(II) were studied under air atmosphere at the heating rate of 10 °C/min from room temperature to 950 °C (Figures 5a–5c). The TGA thermogram of Fe_3O_4@Agarose nanomagnetic catalyst (Figure 5a) showed two regions of weight losses. The first stage can be ascribed to the loss of physically adsorbed water (weight loss 2%, 23–180 °C). The second stage showed a weight loss owing to decomposition of agarose (weight loss 2.76 %, 180–400 °C).[39] As previously reported in the literature, at the second stage crystal phase transformation from Fe_3O_4 to γ-Fe_2O_3 occurred.[25]

Similarly, thermal decomposition of Fe_3O_4@Agarose/$AEPH_2$ (Figure 5b) happened in two stages of weight losses. It is clear that the first decomposition stage corresponded to the loss of moisture and physically adsorbed water on the surface of catalyst (weight loss 2.10%, 23–150 °C). In comparison, a greater weight loss in the second step that occurred at lower temperature can be attributed to the presence of organic segment on the surface of Fe_3O_4@Agarose nanomagnetic catalyst (weight loss 5.41%, 150–550 °C). In addition, the TGA thermogram of Fe_3O_4@Agarose/$SAEPH_2$/Cu(II) (Figure 5c) showed two major weight loss stages. The first stage was mainly related to the evaporation of moisture and physically absorbed water on the catalyst surface (weight loss 2.73%, 23–120 °C). The second one, which occurred at 120–645 °C (weight loss 11.01%), corresponded to the complete decomposition of Schiff base ligand and agarose in the structure of catalyst. According the results obtained from the TGA thermogram, the amount of Schiff base ligand supported on Fe_3O_4@Agarose nanocatalyst was estimated to be 2.5 mmol/g.

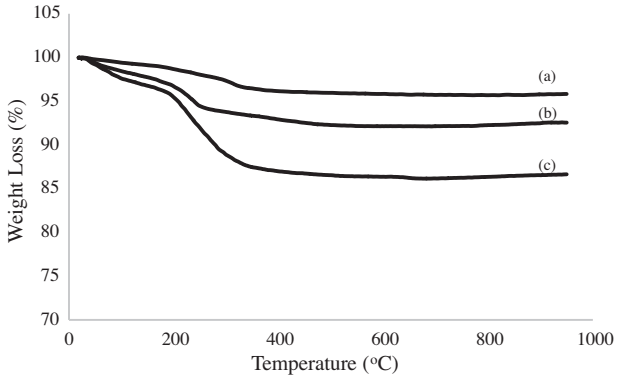

Figure 5. TGA thermogram of (a) Fe_3O_4@Agarose, (b) Fe_3O_4@Agarose/$AEPH_2$, and (c) Fe_3O_4@Agarose/$SAEPH_2$/Cu(II).

The total copper content in freshly prepared catalyst was determined by ICP analysis to be 179,560 ppm, 0.17 g, or 2.82 mmol of Cu per 1 g of catalyst.

2.2. Catalytic synthesis of 2-imidazolines, 2-oxazolines, and 2-thiazolines derivatives in the presence of Fe_3O_4@Agarose/$SAEPH_2$/Cu(II)

In continuation of our interest in the preparation of heterocyclic compounds and also application of heterogeneous catalysts for development of useful synthetic methodologies,[32,39,42–65] herein a simple, efficient, and high-yielding synthetic method for 2-imidazolines, 2-oxazolines, and 2-thiazolines derivatives from the reaction of nitrile compounds with ethanediamine, 2-aminoethanol, and 2-aminoethanthiolhydrochloride in the presence of Fe_3O_4@Agarose/$SAEPH_2$/Cu(II) is described (Scheme 2).

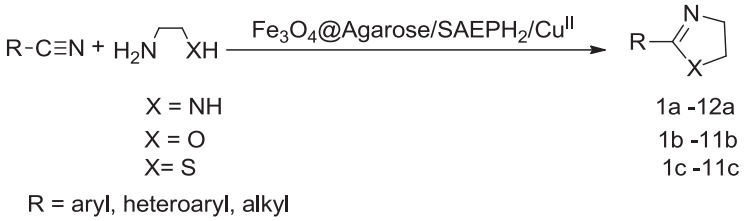

Scheme 2. Preparation of 2-imidazolines, 2-oxazolines, and 2-thiazolines derivatives in the presence of Fe_3O_4@Agarose/$SAEPH_2$/Cu(II).

We started to study the preparation of 2-imidazolines by examining the reaction of benzonitrile with ethanediamine as a model reaction (Table 1). The model reaction was performed using different molar ratios of substrates and catalyst, at various temperatures, and in different polar and nonpolar solvents. With the goal of performing the synthesis in the absence of solvent as a special advantage of the method, the model reaction was carried out under solvent-free conditions. As observed, the best result was obtained in the reaction of benzonitrile (1 mmol), ethanediamine (1.5 mmol), and Fe_3O_4@Agarose/$SAEPH_2$/Cu(II) (14 mol% contains 0.14 mmol, 0.008 g, and 128,257 ppm, of Cu) at 100 °C under solvent-free conditions (Table 1, entry 7). To prove the reaction was indeed involving Fe_3O_4@Agarose/$SAEPH_2$/Cu(II) as an effective catalyst, we carried out several control experiments. In the absence of any catalyst, no desired product was formed even after a long period of time (Table 1, entry 1). We observed that very low yield of the desired product was obtained when

the reaction was carried out in the presence of Fe_3O_4 NPs, Fe_3O_4@Agarose (**I**), Fe_3O_4@Agarose/$AEPH_2$ (**II**), Fe_3O_4@Agarose/$SAEPH_2$ (**III**), and $Cu(OAc)_2.H_2O$, consecutively (Table 1, entries 2–6). At the same reaction conditions and by applying 14 mol% of Fe_3O_4@Agarose/$SAEPH_2$/Cu(II), 2-phenyl-4,5-dihydro-1*H*-imidazole was obtained in high yield (Table 1, entry 7). The effect of reaction temperature on the yield of reaction is another important factor that was studied. The reaction rate decreased when the reaction was performed at 90 °C and 80 °C (Table 1, entries 8 and 9). As shown in Table 1, applying 13 mol% (contains 0.13 mmol, 0.008 g, and 102,605 ppm of Cu) of catalyst led to formation of 2-phenyl-4,5-dihydro-1*H*-imidazole in low yield and in a longer reaction time, while using additional amounts of catalyst gave the same result as entry 7 (entries 10 and 11). At the same reaction conditions, performing the reaction in solvents such as DMSO, DMF, CH_3CN, THF, 1,4-dioxane, and toluene produced the desired product with lower yield and in longer reaction time (Table 1, entries 12–17) and no product was obtained in H_2O (Table 1, entry 18). To study the effect of various molar ratios of reactants, lower yield of product was obtained by using 1/1.2 molar ratio of benzonitrile/ethanediamine (Table 1, entry 19) and, interestingly, increasing the molar ratio of benzonitrile/ethanediamine had no significant effect on the reaction progress (Table 1, entry 20).

Building on this we wished to expand the reaction to the synthesis of 2-oxazolines as other important *N*-heterocyclic compounds that are found in a wide variety of biologically active natural products and enzyme inhibitors. Changing the nucleophile from ethanediamine to 2-aminoethanol would afford a range of substituted benzoxazoles (Table 2). Based on the proposed mechanism in Scheme 3, the results obtained from our recent study,[42] and Table 2, formation of **IV** by intramolecular cyclization of **II** and subsequent ammonia elimination from **III** was considered a difficult step towards the construction of *N*-heterocyclic compounds. Under the optimized reaction conditions established for preparation of 2-imidazolines, 2-phenyl-4,5-dihydro-1,3-oxazole was not synthesized even after 12 h (Table 2, entry 1). Increasing the reaction temperature improved the yield of the desired product but by leaving a considerable amount of **II** (Table 2, entry 2). Furthermore, an additional amount of catalyst does not enhance the yield of the desired product (Table 2, entry 3). The effect of different solvents was also studied on the model reaction. According to the above results (obtained from Table 2), it was found that DMF was the best choice in terms of obtaining the desired *N*-heterocyclic compound (Table 2, entries 4–11). To achieve good yield of the desired product, the effect of temperature was evaluated in DMF and it was found that the reaction proceeded more efficiency by reducing temperature to 110 °C, and at 100 °C intramolecular cyclization was slowed down (Table 2, entries 12–14). The results obtained from Table 2 led us to conclude that intramolecular cyclization and ammonia elimination steps are strongly dependent on solvent polarity. To provide more polar media, the model reaction was carried out in DMSO. As seen, the product was gained with excellent yield under the same reaction conditions at 110 °C (Table 2, entry 15). The effect of different parameters such as temperature, molar ratios of reactants, and catalyst loading on the model reaction was also examined in DMSO. At lower reaction temperature (100 °C) the reaction proceeded the same as at 110 °C (Table 2, entry 16), while further decreasing temperature led to lower yield of product (Table 2, entry 17). According to this study, increasing the molar ratio of reactants did not improve the reaction rate (Table 2, entry 18), while lower amounts of reactants decreased the reaction rate considerably (Table 2, entry 19). In addition, lower catalyst loading caused lower conversion, whereas additional amounts of catalyst had no considerable effect on the reaction yield and reaction rate (Table 2, entries 20 and 21). Thus, the data in Table 2 revealed that the best result was obtained by using 1/1.5 molar ratio of benzonitrile/ 2-aminoethanol in the presence of 14 mol% of Fe_3O_4@Agarose/$SAEPH_2$/Cu(II) in DMSO at 100 °C (Table 2, entry 16).

Table 1. Preparation of 2-phenyl-4,5-dihydro-1*H*-imidazole catalyzed by Fe_3O_4@Agarose/SAEPH$_2$/Cu(II) under different reaction conditions.

Entry	Molar ratio of (benzonitrile/ ethanediamine)	Catalyst (mol %)	Solvent	Temp (°C)	Time (h)	Isolated yield (%)
1	1/1.5	0	-	100	24	0
2[a]	1/1.5	0.05 (g)	-	100	24	20
3[b]	1/1.5	0.05 (g)	-	100	24	20
4[c]	1/1.5	0.05 (g)	-	100	24	20
5[d]	1/1.5	0.05 (g)	-	100	24	20
6[e]	1/1.5	2.6	-	100	24	65
7	1/1.5	14	-	100	3	95
8	1/1.5	14	-	90	12	80
9	1/1.5	14	-	80	12	60
10	1/1.5	13	-	100	12	70
11	1/1.5	15	-	100	3	95
12	1/1.5	14	DMSO	100	12	15
13	1/1.5	14	DMF	100	12	45
14	1/1.5	14	CH_3CN	100	12	30
15	1/1.5	14	THF	100	12	80
16	1/1.5	14	1,4-dioxane	100	12	70
17	1/1.5	14	toluene	100	12	80
18	1/1.5	14	H_2O	100	24	0
19	1/1.2	14	-	100	12	70
20	1/2	14	-	100	3	95

[a]The reaction was performed in the presence of Fe_3O_4 NP. [b]The reaction was performed in the presence of Fe_3O_4@Agarose (**I**). [c]The reaction was performed in the presence of Fe_3O_4@Agarose/AEPH$_2$ (**II**). [d]The reaction was performed in the presence of Fe_3O_4@Agarose/SAEPH$_2$(**III**).[e]The reaction was performed in the presence of $Cu(OAc)_2.H_2O$.

The efficiency of Fe_3O_4@Agarose/SAEPH$_2$/Cu(II) was also examined in the reaction of benzonitrile with 2-aminoethanthiolhydrochloride to produce 2-phenyl-4,5-dihydro-1,3-thiazole under different reaction conditions (Table 3). To study the role of Fe_3O_4@Agarose/SAEPH$_2$/Cu(II) in the preparation of 2-phenyl-4,5-dihydro-1,3-thiazole, the reaction was conducted in the absence of any catalyst (Table 3, entry 1). As observed, in the absence of any catalyst and base in solvent-free conditions at 90 °C, very low yield of the desired product was obtained. In the same reaction conditions and in the presence of 13 mol% of catalyst, the yield of this condensation reaction was increased to 50% (Table 3, entry 2). Interestingly, using NaOH as base in the reaction mixture improved the reaction rate considerably (Table 3, entries 3–6). We assumed that addition of a small amount of base (NaOH) will make a fraction of amine available for the reaction, which upon condensation will release an equivalent amount of ammonia. Ammonia as a proton scavenger may assist the reaction further. Hence, 2.5 mol% of sodium hydroxide was added as promoter to initiate the reaction. Indeed, by employing

Table 2. Preparation of 2-phenyl-4,5-dihydro-1,3-oxazole catalyzed by Fe_3O_4@Agarose/SAEPH$_2$/Cu(II) under different reaction conditions.

Entry	Molar ratio of (benzonitrile/ 2-aminoethanol)	Catalyst (mol%)	Solvent	Temp (°C)	Time (h)	Isolated yield of II/V (%)[a]
1	1/1.5	14	-	100	12	95/0
2	1/1.5	14	-	170	12	20/80
3	1/1.5	15	-	170	12	20/80
4	1/1.5	14	DCM	reflux	24	0/0
5	1/1.5	14	1,4-dioxane	reflux	24	0/0
6	1/1.5	14	H_2O	reflux	12	60/40
7	1/1.5	14	toluene	reflux	12	0/0
8	1/1.5	14	THF	reflux	12	0/0
9	1/1.5	14	CH_3CN	reflux	12	30/40
10	1/1.5	14	CH_3NO_2	reflux	12	20/60
11	1/1.5	14	DMF	130	4	0/95
12	1/1.5	14	DMF	120	4	0/95
13	1/1.5	14	DMF	110	4	0/95
14	1/1.5	14	DMF	100	12	10/90
15	1/1.5	14	DMSO	110	4	0/95
16	1/1.5	14	DMSO	100	4	0/95
17	1/1.5	14	DMSO	90	4	10/90
18	1/2	14	DMSO	100	4	0/95
19	1/1.2	14	DMSO	100	4	0/90
20	1/1.5	13	DMSO	100	4	0/90
21	1/1.5	15	DMSO	100	4	0/95

[a] **II** and **V** correspond to intermediate **II** and final product **V** in Scheme 3.

this strategy, the reaction occurred satisfactorily in the desired direction. Then a variety of solvents were screened, and it was clearly demonstrated that no appreciable reaction occurred between benzonitrile and 2-aminoethanthiolhydrochloride (in the presence of base) in H_2O, DMSO, CH_2Cl_2, 1,4-dioxane, and toluene (Table 3, entries 7–11). To achieve good yield of the desired product, the reaction was performed using different amounts of catalyst and different molar ratios of benzonitrile/2-aminoethanthiolhydrochloride separately (Table 3, entries 12–15). According to the results obtained from Table 3, it seems that 13 mol% of catalyst and 1/1.2 molar ratio of benzonitrile/2-aminoethanthiolhydrochloride gave the best yield of 2-phenyl-4,5-dihydro-1,3-thiazole. Decreasing the reaction temperature was not helpful, as it only decreased the rate of the reaction without altering the outcome of the reaction (Table 3, entries 16 and 17).

With these optimal reaction conditions in hand (Table 1, entry 7; Table 2, entry 16; Table 3, entry 5), the scope of the reaction was investigated by employing a variety of aromatic, heteroaromatic, and aliphatic nitriles with ethanediamine/ or 2-aminoethanol/ or 2-aminoethanthiolhydrochloride. The results are summarized in Table 4. Gratifyingly, our initial attempt at this transformation worked well, 2-imidazolines being

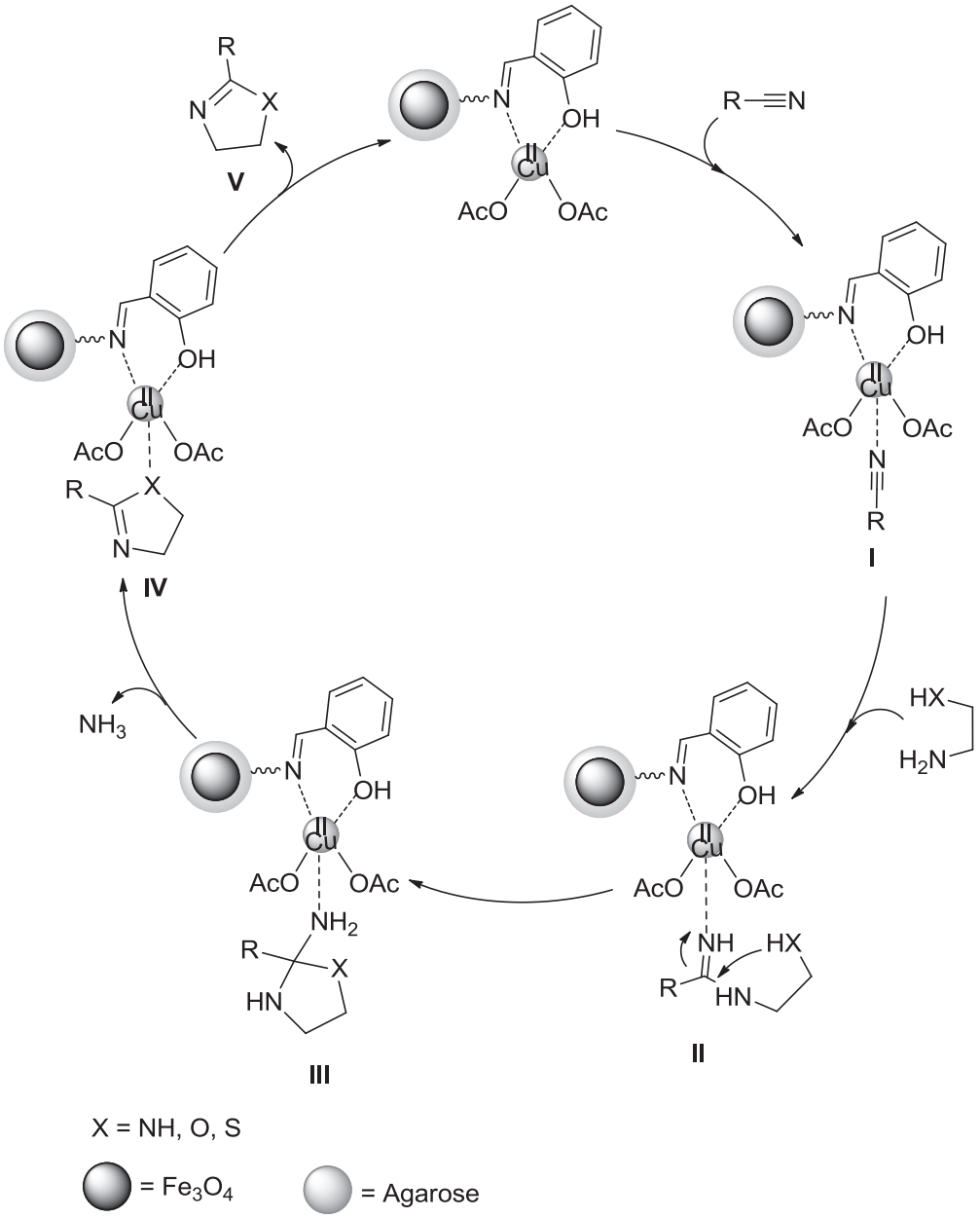

Scheme 3. Proposed mechanism for the synthesis of 2-substituted imidazolines, oxazolines, and thiazolines catalyzed in the presence of Fe_3O_4@Agarose/SAEPH$_2$/Cu(II).

formed cleanly in 1.5–10 h. The reaction is also tolerant of more substituted aromatic and heteroaromatic nitriles as well as aliphatic nitriles with ethanediamine giving the desired products 1a–12a in 75%–95% isolated yields. Electron-withdrawing and electron-donating groups attached to the phenyl ring influenced the reaction rate considerably. High yields of 2-imidazolines were obtained in short reaction time with aromatic nitriles bearing electron-withdrawing substituents, whereas aromatic nitriles substituted with electron-releasing groups gave only moderate yields in longer reaction times (e.g., compare entries 2 and 3 with 6–8). Bis-imidazoline can also be prepared under the same reaction conditions by applying 1/3 molar ratio of tereph-

Table 3. Preparation of 2-phenyl-4,5-dihydro-1,3-thiazole catalyzed by Fe_3O_4@Agarose/SAEPH$_2$/Cu(II) under different reaction conditions.

Entry	Molar ratio of benzonitrile /2-aminoethanthiolhydrochloride	Catalyst (mol %)	Base (mol%)	Solvent	) Temp (°C)	Time (min)	Isolated yield (%)
1	1/1.2	-	-	-	90	20	10
2	1/1.2	13	-	-	90	20	50
3	1/1.2	13	1	-	90	20	80
4	1/1.2	13	2	-	90	20	87
5	1/1.2	13	2.5	-	90	20	95
6*	1/1.2	13	2.5	-	90	20	60
7	1/1.2	13	2.5	H_2O	90	20	5
8	1/1.2	13	2.5	DMSO	90	20	10
9	1/1.2	13	2.5	CH_2Cl_2	reflux	20	0
10	1/1.2	13	2.5	1,4-dioxane	90	20	0
11	1/1.2	13	2.5	toluene	90	20	0
12	1/1.2	14	2.5	-	90	20	95
13	1/1.2	12	2.5	-	90	20	87
14	1/1.5	13	2.5	-	90	20	95
15	1/1	13	2.5	-	90	20	90
16	1/1.2	13	2.5	-	85	20	85
17	1/1.2	13	2.5	-	80	20	78

* The reaction was performed in the presence of NaOAc.

thalonitrile/ethanediamine. Thus, the reaction of 1,4-dicyanobenzene (terephthalonitrile) with ethanediamine in the presence of Fe_3O_4@Agarose/SAEPH$_2$/Cu(II) afforded 1,4-phenylenebis-imidazolines in 90% isolated yield (Table 4, entry 5). Reactive nitriles such as nicotinonitrile, isonicotinonitrile, and thiophene-2-carbonitrile gave the desired products quickly in good isolated yields (Table 4, entries 9–11), while aliphatic nitriles produced the corresponding 2-imidazolines in moderate rates (Table 4, entry 12). The versatility of the present method was extended to preparation of 2-oxazolines. 2-Aminoethanol reacted more slowly than ethanediamine. In all cases, a high yield of 2-oxazolines (1b–11b) was obtained but in a longer reaction time. It is also interesting to note that alkylnitriles did not afford the corresponding 2-oxazolines under the same reaction conditions. These results indicate that the method is selective for the reaction of aromatic and heteroaromatic nitriles as aliphatic nitriles are unreactive under these conditions. The reaction of various aromatic, heteroaromatic, and aliphatic nitriles under the optimized reaction conditions (Table 3, entry 5) was carried out to elucidate the limitations and chemoselectivity of 2-thiazolines formation in the presence of Fe_3O_4@Agarose/SAEPH$_2$/Cu(II). The reactions of 2-aminoethanthiolhydrochloride took place more quickly and the desired 2-thiazolines (1c–11c) were obtained in 80%–95% isolated yields due to higher nucleophilicity of SH than OH and NH_2 groups. As was the case for 2-aminoethanol, valeronitrile was not converted to the corresponding 2-thiazoline under the same reaction conditions.

In our study, the progress of the reaction was monitored by disappearance of starting materials and formation of intermediate **II** (Scheme 3) on TLC. Disappearance of intermediate **II** and further formation of

Table 4. Preparation of 2-phenyl-4,5-dihydro-1,3-thiazole catalyzed by Fe_3O_4@Agarose/SAEPH$_2$/Cu(II) under different reaction conditions.

Entry	R	Product	Time (h) / Isolated Yield (%)
1	C_6H_5	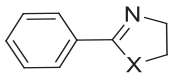	3 / 95 X= NH (**1 a**) 4 / 95 X= O (**1 b**) 0.5 / 95 X= S (**1 c**)
2	4-ClC_6H_4	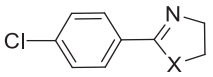	1.5 / 90 X= NH (**2 a**) 3 / 90 X= O (**2 b**) 0.25 / 93 X= S (**2 c**)
3	4-BrC_6H_4	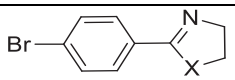	1.5 / 85 X= NH (**3 a**)
4	4-$NO_2C_6H_4$	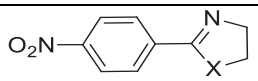	10*/ 85 X= S (**4 c**)
5**	4-CNC_6H_4	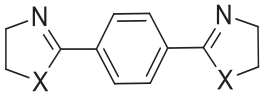	2/ 90 X= NH (**5 a**)
6	3-MeC_6H_4	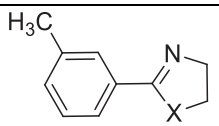	4 / 90 X= NH (**6 a**) 6 / 85 X= O (**6 b**) 2 / 80 X= S (**6 c**)
7	4-EtOC_6H_4	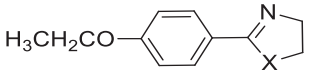	5 / 85 X= NH (**7 a**) 8 / 70 X= O (**7 b**)
8	3,4,5-TriMeC_6H_2	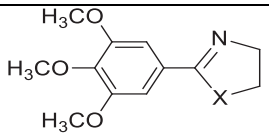	10 / 75 X= NH (**8 a**)
9	3-Pyridyl	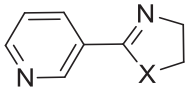	2 / 85 X= NH (**9 a**) 3/ 85 X= O (**9 b**) 1/ 90 X = S(**9 c**)
10	4-Pyridyl	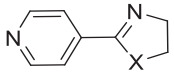	2 / 90 X= NH (**10 a**) 3 / 75 X = O (**10 b**) 1 / 95 X = S (**10 c**)
11	2-Thienyl	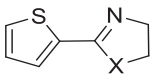	1.5 / 85 X= NH (**11 a**) 2/ 80 X= O (**11 b**) 1/ 90 X= S (**11 c**)
12	CH_3-$(CH_2)_3$	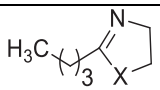	10 / 85 X= NH (**12 a**)

* The reaction was performed in the presence of NaOAc.

2-substituted imidazolines, oxazolines, and thiazolines confirmed the completion of the reaction. In addition, in the FT-IR spectrum, the CN stretching frequency at 2260–2210 cm^{-1} was removed and three absorption bands appeared at 3297–3118 cm^{-1}, 1661–1594 cm^{-1}, and 1544–1506 cm^{-1} due to NH stretching, C=N stretching

and NH bending vibrations, respectively, which confirmed the formation of 2-imidazolines. Formation of 2-oxazolines was established by the presence of two absorption bands at 1650–1649 cm^{-1} and 1078–1075 cm^{-1} attributed to C=N and C–O groups of 2-oxazolines, respectively. FT-IR spectra of 2-thiazolines show absorption bands around 1591 cm^{-1} and 928 cm^{-1} corresponding to C=N and C–S bonds.

In the ^{1}H NMR spectra, the appearance of a resonating signal at 4.83–4.54 ppm was attributed to the NH of 2-imidazolines. Furthermore, in the ^{13}C NMR spectra, the signals at 168.8–164.7 ppm, 163.7 ppm, and 168.7–161.6 ppm were attributed to the quaternary carbon atoms, which revealed the formation of 2-imidazolines, 2-oxazolines, and 2-thiazolines, respectively.

Most of the products were known and characterized by mass spectrometry and comparison of their melting points with known compounds. The structure of some selected products was further confirmed by the FT-IR, ^{1}H NMR, and ^{13}C NMR spectroscopy.

Based on the results reported previously, a plausible mechanism was suggested for the formation of 2-substituted imidazolines, oxazolines, and thiazolines (Scheme 3).[66,67] First the nitrile compound is activated via coordination to Cu(II), which generates structure **I**. Then the fast nucleophilic attack of the NH_2 group of ethanediamine/ or 2-aminoethanol/ or 2-aminoethanthiolhydrochloride to activated nitrile compound produces the intermediate **II**. The structure of intermediate **II** was studied by FT-IR spectroscopy and mass spectrometry. When X=NH or O or S was present a broad absorption band at 3370 or 3481 or 2263 cm^{-1} showed the stretching vibrations of NH_2 or OH or SH groups of intermediate **II**. The presence of HN–C=NH linkage of the corresponding intermediate **II** of 2-imidazoline or 2-oxazoline or 2-thiazoline was also confirmed by the appearance of another strong absorption band at 3172 or 3415 or 3424 cm^{-1} and a medium intensity band at 1658 or 1642 or 1675 cm^{-1}, which are assigned to corresponding NH and C=NH bonds, respectively. Asymmetric and symmetric vibration modes of methylene groups ($-CH_2$) appeared at 2917 and 2770 cm^{-1} (X=NH), 2953 and 2924 cm^{-1} (X=O), and 2914 and 2814 cm^{-1} (X=S). Existence of a molecular ion peak at m/z 163 or 164 or 180 in the mass spectra confirmed the formation of intermediate **II** (X=NH or O or S) (see Supporting Information, Figures 81–86).

An intramolecular cyclization in intermediate **II** produced **III** via nucleophilic attack of NH_2 or OH or SH to C=NH. Faster formation of 2-thiazolines than 2-imidazolines and 2-oxazolines (based on the results obtained from Table 4) led us to conclude that intramolecular cyclization of intermediate **II** should be the rate determining step of the reaction. The higher nucleophilicity leads to faster intramolecular cyclization.

Finally, upon the rapid extrusion of ammonia from **III**, corresponding 2-substituted imidazoline, oxazoline, and thiazoline were obtained and Fe_3O_4@Agarose/SAEPH_2/Cu(II) released from the product for the next catalytic cycle. It is clear that the reaction mechanism is still disputable and it needs further study.

To ascertain the five-membered ring formation the HMBC spectrum of 2-(3-methylphenyl) imidazoline (6a) was recorded (Figure 6). As can be seen, methyl protons (δ_H 2.38) showed correlations with C-6, C-7, C-8, and C-9. In the aromatic ring, H-9 and H-10 have correlations with C-8 and C-11, respectively. Moreover, cross-peaks were observed between H-11 (δ_H 7.55) and C-9 and between H-7 (δ_H 7.66) and C-2, C-9, C-10, and C-11. Furthermore, the HMBC spectrum showed strong 3-bond correlation between H-4 and H-5 and C-2, which established the five-membered ring formation. This suggested the presence of a quaternary carbon, which was followed by extrusion of NH_3.

To investigate the heterogeneous nature of Fe_3O_4@Agarose/SAEPH_2/Cu(II), the hot filtration test was carried out on the model reaction under the optimized reaction conditions. In this test, a mixture of

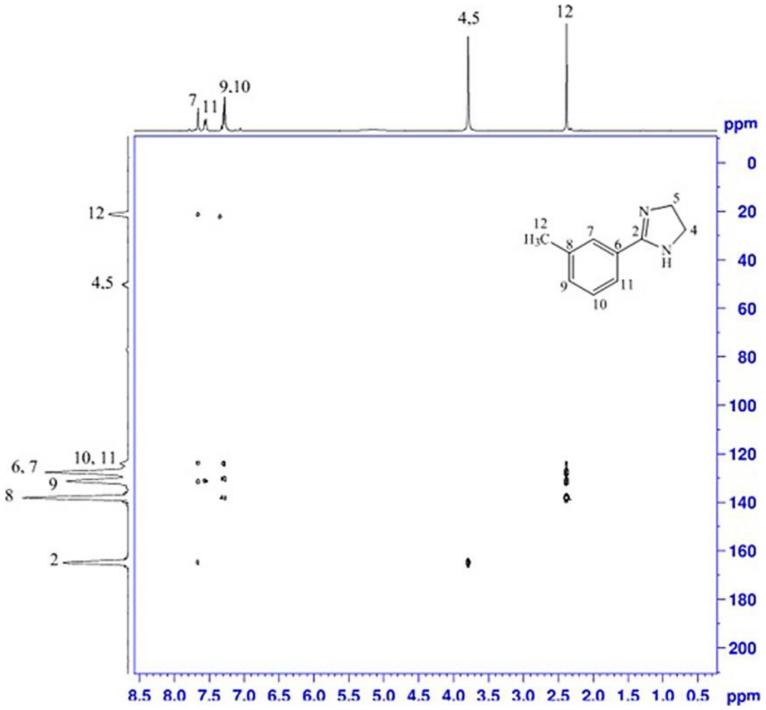

Figure 6. HMBC spectrum of 2-(3-methylphenyl) imidazoline (**6a**).

Fe_3O_4@Agarose/SAEPH$_2$/Cu(II) (0.05 g, 14 mol%), benzonitrile (0.1 g, 1 mmol), and ethanediamine (0.09 g, 1.5 mmol) was heated at 100 °C under solvent-free conditions for 1.5 h. After 70% conversion, the catalyst was magnetically separated from the reaction mixture and then the reaction was continued for an additional time (1.5 h). No further product formation was observed, which was monitored by TLC. This result clearly demonstrates that no leaching of Cu(II) took place during the reaction, and Fe_3O_4@Agarose/SAEPH$_2$/Cu(II) is truly heterogeneous in nature.

The reusability of the catalyst is one of the main benefits and it makes it useful and economic for commercial applications. Thus, reusability of catalyst was studied in preparation of 2-phenyl-4,5-dihydro-1*H*-imidazole under optimized reaction conditions. After completion of the reaction, ethyl acetate (10 mL) was added to the reaction mixture and the catalyst was magnetically separated and washed with boiled ethyl acetate several times to remove all organic compounds (Figures 7a and 7b). Then the catalyst was dried at 70 °C for 5 h and used in the next run of the model reaction. The catalytic activity of the catalyst remained without significant loss of activity for seven successive runs as can be seen in Figure 8. These results confirmed the excellent stability of the prepared catalyst during the recovery process. Moreover, as can be seen in Figure 1e, the presence of an absorption band at 419 cm^{-1} due to Cu–N stretching vibration was evidence of the stability of the catalyst after seven cycles. ICP analysis showed that freshly prepared catalyst contains 179,560 ppm, 0.17 g, or 2.82 mmol of Cu per 1 g of catalyst, while the 7th reused catalyst contains 171,160 ppm, 0.17 g, or 2.69 mmol of Cu per 1 g of catalyst. This indicates that 96% of Cu(II) could be found in the structure of the catalyst after seven runs.

To show the efficiency of the catalyst, we compared various reported methods of 2-phenyl-4,5-dihydro-1*H*-imidazole and 2-phenyl-4,5-dihydro-1,3-oxazole preparations with Fe_3O_4@Agarose/SAEPH$_2$/Cu(II) (Table 5). The remarkable feature of Fe_3O_4@Agarose/SAEPH$_2$/Cu(II) is that it can be simply separated from the reaction

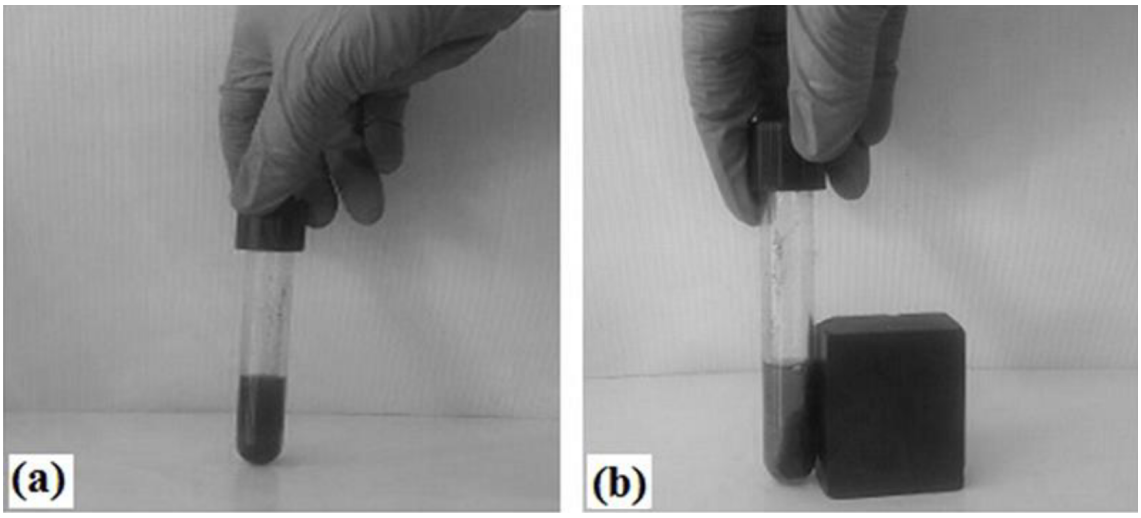

Figure 7. Photograph of the (a) catalyst dispersed in the reaction mixture and (b) magnetic separation of the catalyst from the reaction medium.

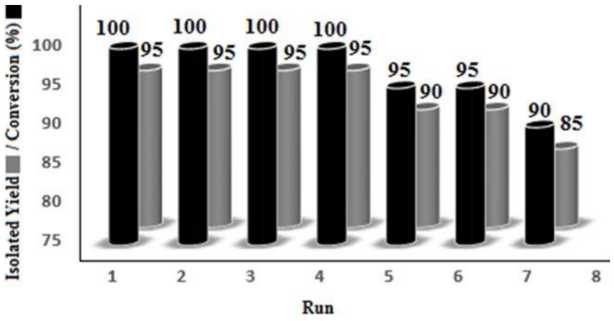

Figure 8. Synthesis of 2-phenyl-4,5-dihydro-1*H*-imidazole in the presence of reused Fe_3O_4@Agarose/SAEPH$_2$/Cu(II) nanocatalyst.

mixture by applying an external magnetic field, in comparison with the previously reported methods. Moreover, in the presence of Fe_3O_4@Agarose/SAEPH$_2$/Cu(II), 2-phenyl-4,5-dihydro-1*H*-imidazole and 2-phenyl-4,5-dihydro-1,3-oxazole were produced at lower temperature and with higher yields than the methods reported in entries 7, 8, and 15 (Table 5). Comparatively, the current study affords the desired products by using nontoxic, more abundant, and low cost metallic complex (e.g., compared with entries 9 and 10).

3. Experimental

3.1. General

All chemical reagents and solvents were purchased from Merck and Sigma-Aldrich and were used as received without further purification.

The melting points of products were determined with an Electrothermal Type 9100 melting point apparatus. The FT-IR spectra were provided on pressed KBr pellets using an AVATAR 370 FT-IR spectrometer (Therma Nicolet spectrometer, USA) at room temperature in the range between 4000 and 400 cm^{-1}. The NMR spectra were obtained in Bruker Avance 300 MHz instruments (Germany) in $CDCl_3$. Elemental analysis was performed using a Thermo Finnigan Flash EA 1112 Series instrument. Mass spectra were recorded with a

Table 5. Comparison efficiency of various catalysts in the synthesis of 2-phenyl-4,5-dihydro-1*H*-imidazole and 2-phenyl-4,5-dihydro-1,3-oxazole.

Entry*	Catalyst	Conditions	Temp (°C)	Time (min)	Yield (%)	Ref.
1	$H_4SiW_{12}O_{40}$-SiO_2	solvent-free	116	45	90	68
2	Cu(II)-(IAA**)$_2$	solvent-free	116	240	87	69
3	P_2S_5	solvent-free	116	5	93	70
4	CS_2	solvent-free	116	35	75	71
5	Sodium Hydrosulfide	solvent-free	116	120	89	67
6	*p*-Toluenesulfonic acid	solvent-free	116	35	92	72
7	$ZrOCl_2.8H_2O$	solvent-free	116	160	70	73
8	Sulfur	ultrasonic irradiation	116	5	90	74
9	Cu(II)/NaOAc/I_2	toluene	110	240	90	66
10	[Ru (CO)(L***)(PPh_3)$_2$]	solvent-free	80	180	83	75
11	Highly sulfonated carbon	solvent-free	116	210	92	24
12	$H_3PW_{12}O_{40}$	solvent-free	100	210/ 270	85/82	76
13	Dowex-50 W	solvent-free	80	180 /210	85/74	77
14	Trichloroisocyanuric acid	solvent-free	110	60/240	95/90	78
15	Silica sulfuric acid	solvent-free	116	210/ 390	92/65	79
16	Fe_3O_4@Agarose/SAEPH_2/Cu(II)	solvent-free /DMSO	100	180/ 240	95/95	Present study

*Entries 1–10 correspond to the time and yield of 2-phenyl-4,5-dihydro-1*H* imidazole and entry 11 corresponds to the time and yield of 2-phenyl-4,5-dihydro-1,3-oxazole. In entries 12–15, the left number corresponds to the time and yield of 2-phenyl-4,5-dihydro-1*H* imidazole and the right number corresponds to the time and yield of 2-phenyl-4,5-dihydro-1,3-oxazole respectively. **Indole-3-acetic acid (IAA). ***Pyridoxal N(4)-substituted thiosemicarbazone hydrochloride (L).

CH7A Varianmat Bremem instrument (Germany) at 70 eV electron impact ionization, in m/z (rel%). TGA analysis was carried out on a Shimadzu Thermogravimetric Analyzer (TG-50, Switzerland) in the temperature range of 25–950 °C at a heating rate of 10 °C min^{-1} under air atmosphere. Transmission electron microscopy (TEM) was performed with a Leo 912 AB microscope (Zeiss, Germany) with an accelerating voltage of 120 kV. SEM images were also recorded using a Leo 1450 VP scanning electron microscope operating at an acceleration voltage of 20 kV. Elemental compositions were determined with a Leo 1450 VP scanning electron microscope equipped with an SC7620 energy dispersive spectrometer (SEM-EDS) presenting a 133 eV resolution at 20 kV. The crystal structure of catalyst was analyzed by XRD using a D8 ADVANCE-Bruker diffractometer operated at 40 kV and 30 mA utilizing CuKα radiation (λ= 0.154 Å). The magnetic property of catalyst was measured using a vibrating sample magnetometer (VSM, 7400 Lake Shore). Inductively coupled plasma (ICP) was carried out on an Arcos spectrometer, 76004555 model, Germany. All of the products were known compounds and characterized by mass spectrometry and comparison of their melting points with known compounds. The structure of selected products was further confirmed by the FT-IR, ^{1}H NMR, and ^{13}C NMR spectroscopy. All yields refer to isolated products after purification by recrystallization or thin layer chromatography.

3.2. Preparation of Fe_3O_4@Agarose nanomagnetic catalyst (I)

First 2.00 g of washed agarose [80] was dissolved in 80 mL of acetic acid (3%) at 90 °C, in a 500-mL three-necked flask equipped with an argon gas inlet tube and dropping funnel. Then $FeCl_3.6H_2O$ (2.1 g, 8 mmol) and

$FeSO_4.7H_2O$ (1.08 g, 4 mmol) were added sequentially to the resulting solution. The mixture was magnetically stirred for 1 h at 90 °C, and then aqueous ammonia (25%, 25 mL) was added dropwise into the homogeneous dispersed system until the pH increased to 12. After 1 h, a brown/black precipitate was collected by an external magnetic field and washed subsequently with deionized water until the pH reached 7. The product from this system was magnetized for 20 min by an external magnet. The powder of Fe_3O_4@Agarose nanomagnetic catalyst (**I**) was obtained (4 g) by drying at 50 °C in an oven for 12 h. The catalyst was then cooled to room temperature and stored in a closed vial at room temperature.

3.3. Preparation of Fe_3O_4@Agarose/$AEPH_2$ (II)

Fe_3O_4@Agarose nanomagnetic catalyst (**I**) (2 g) was dispersed in 30 mL of deionized water/ethanol (1/1, v/v), and then ethanolamine phosphate (2 g, 14 mmol) was added under vigorous stirring (1500 rpm). Then the reaction mixture was stirred at 90 °C for 12 h. Afterward, the Fe_3O_4@Agarose/$AEPH_2$ (**II**) as a dark brown magnetic precipitate was collected by an external magnetic field and washed repeatedly with hot water (2 × 100 mL) and dried at 50 °C for 12 h. Then the obtained catalyst (3.80 g) was cooled to room temperature and stored in a closed vial at room temperature.

3.4. Preparation of Fe_3O_4@Agarose/$SAEPH_2$ (III)

Fe_3O_4@Agarose/$AEPH_2$ (**II**) (2 g) was added to the mixture of salicylaldehyde (2 g, 16 mmol) and K_2CO_3 (2.20 g, 16 mmol) in methanol (30 mL) and refluxed for 12 h. After that, the resulting suspension was magnetically separated by an external field, washed several times with methanol (2 × 50 mL), and dried at 50 °C for 12 h. Then the obtained catalyst (3.50 g) was cooled to room temperature and stored in a closed vial at room temperature.

3.5. Preparation of Fe_3O_4@Agarose/$SAEPH_2$/Cu(II) (IV)

$Cu(OAc)_2.H_2O$ (2 g, 10 mmol) was added to a suspension of Fe_3O_4@Agarose/$SAEPH_2$ (**III**) (2 g) in dry methanol (30 mL). The resulting mixture was stirred under reflux conditions for 12 h. Subsequently, the light brown precipitate was collected by an external magnetic field, washed repeatedly with water (2 × 100 mL), and dried at 70 °C for 5 h. The obtained catalyst (3.90) was then cooled to room temperature and stored in a closed vial at room temperature.

3.6. Typical procedure for preparation of 2-phenyl-4,5-dihydro-1*H*-imidazole catalyzed in the presence of Fe_3O_4@Agarose/$SAEPH_2$/Cu(II)

A mixture of benzonitrile (0.1 g, 1 mmol), ethanediamine (0.09 g, 1.5 mmol), and Fe_3O_4@Agarose/$SAEPH_2$/Cu(II) nanomagnetic catalyst (0.05 g, 14 mol%) was stirred at 100 °C. The progress of the reaction was monitored by TLC. After completion of the reaction, the nanomagnetic catalyst was separated with an external magnetic field and the crude product was recrystallized from *n*-hexane to afford the pure 2-phenyl-4, 5-dihydro-1*H*-imidazole (0.13 g, 95%). The nanomagnetic catalyst was washed with hot ethyl acetate several times to remove unreacted starting materials and then was dried at 70 °C for 5 h and used in the next run.

3.7. Typical procedure for preparation of 2-phenyl-4,5-dihydro-1,3-oxazole catalyzed in the presence of Fe_3O_4@Agarose/SAEPH$_2$/Cu(II)

Benzonitrile (0.1 g, 1 mmol), 2-aminoethanol (0.09 g, 1.5 mmol), and Fe_3O_4@Agarose/SAEPH$_2$/Cu(II) nanomagnetic catalyst (0.05 g, 14 mol%) were added to DMSO (2 mL) at 100 °C. The resultant mixture was stirred and controlled by TLC. After completion of the reaction, the reaction mixture was cooled and the nanomagnetic catalyst was separated by an external magnetic field. Then water (2 × 10 mL) was added to the reaction mixture and the mixture was extracted with ethyl acetate (2 × 10 mL). The organic layer was evaporated and the residue was purified by thin layer chromatography using ethyl acetate/*n*-hexane (1/1) as eluent. The pure 2-phenyl-4,5-dihydro-1,3-oxazole was obtained with a 95% yield (0.13 g).

3.8. Typical procedure for preparation of 2-phenyl-4,5-dihydro-1,3-thiazole catalyzed in the presence of Fe_3O_4@Agarose/SAEPH$_2$/Cu(II)

Fe_3O_4@Agarose/SAEPH$_2$/Cu(II) (0.04 g, 13 mol%) was added to a mixture of benzonitrile (0.1 g, 1 mmol), 2-aminoethanthiolhydrochloride (0.13 g, 1.2 mmol), and NaOH (0.0009 g, 0.02 mmol). Then the mixture was stirred at 90 °C. After completion of the reaction (monitored by TLC), the resultant mixture was dissolved in ethyl acetate and the catalyst was collected by magnetic field. The corresponding product was purified by thin layer chromatography using *n*-hexane/EtOAc (2:1) as eluent to give pure 2-phenyl-4,5-dihydro-1,3-thiazole as yellow oil in a high yield (95%, 0.14 g).

4. Conclusions

We successfully synthesized Fe_3O_4@Agarose/SAEPH$_2$/Cu(II) as a new, inexpensive, nontoxic, and magnetically reusable nanomagnetic catalyst and characterized it using FT-IR, XRD, VSM, SEM-EDX, TEM, TGA, and ICP techniques. It was found that the particles were about 9–25 nm in size and spherical with entrapment of the Fe_3O_4 particles in the hollow pore structure of the agarose. The new heterogeneous and magnetically reusable nanomagnetic catalyst was used as an efficient catalyst for the preparation of 2-imidazolines, 2-oxazolines, and 2-thiazolines by the reaction of nitrile compounds with ethanediamine or 2-aminoethanol or 2-aminoethanthiol hydrochloride. The reaction mechanism is proposed to go through the rapid formation of intermediate **II**, which was then converted to the desired product by intramolecular cyclization and subsequent evolution of ammonia. Moreover, the nanomagnetic catalyst could be magnetically separated from the reaction mixture, which offers simple work-up and high yields. The catalytic activity of the nanomagnetic catalyst was not decreased drastically even after seven consecutive cycles. Simple separation, easy handling, and recycling of the catalyst make this method attractive for organic chemists.

Acknowledgment

The authors gratefully acknowledge the partial support of this study by Ferdowsi University of Mashhad Research Council (Grant no. p/3/29781).

References

1. Shatarian, H. R.; Khorami, F.; Amirzadeh, A.; Doostmohammadi, R.; Ghashang, M. *J. Iran. Chem. Res.* **2009**, *2*, 57-62.
2. Gant, T. G.; Meyers, A. I. *Tetrahedron* **1994**, *50*, 2297-2360.

3. Puntener, K.; Hellman, M. D.; Kuester, E.; Hegedus, L. S. *J. Org. Chem.* **2000**, *65*, 8301-8306.
4. Atzrodt, J.; Derdau, V.; Kerr, W. J.; Reid, M.; Rojahn, P.; Weck, R. *Tetrahedron* **2015**. DOI: 10.1016/j.tet.2015.02.029.
5. Enright, R. N.; Grinde, J. L.; Wurtz, L. I.; Paeth, M. S.; Wittman, T. R.; Cliff, E. R.; Sankari, Y. T.; Henningsen, L. T.; Tan, C.; Scanlon, J. D.; et al. *Tetrahedron* **2016**, *72*, 6397-6408.
6. Cwik, A.; Hell, Z.; Hegedus, A.; Finta, Z.; Horvath, Z. *Tetrahedron Lett.* **2002**, *43*, 3985-3987.
7. Seijia, J. A.; Vázquez-Tato, M. P. V.; Crecente-Campo, J. *Tetrahedron* **2008**, *64*, 9280-9285.
8. Fujioka, H.; Murai, K.; Kubo, O.; Ohba, Y.; Kita, Y. *Tetrahedron* **2007**, *63*, 638-643.
9. Karade, N. K.; Tiwari, G. B.; Gamparvar, S. V. *Synlett* **2007**, *12*, 1921-1924.
10. Ishihara, M.; Togo, H. *Tetrahedron* **2007**, *63*, 1474-1480.
11. Cocconcelli, G.; Diodato, E.; Caricasole, A.; Gaviraghi, G.; Genesio, E.; Ghiron, C.; Magnoni, L.; Pecchioli, E.; Plazzi, P. V.; Terstappen, G. C. *Bioorgan. Med. Chem.* **2008**, *16*, 2043-2052.
12. Brain, C. T.; Hallett, A.; Ko, S. Y. *Tetrahedron Lett.* **1998**, *39*, 127-130.
13. Pathak, U.; Bhattacharyya, S.; Mathur, S. *RSC Adv.* **2015**, *5*, 4484-4488.
14. Zhou, P.; Blubaum, J. E.; Burns, C. T.; Natale, N. R. *Tetrahedron Lett.* **1997**, *38*, 7019-7020.
15. Ikgul, B.; Gunes, D.; Sirkecioglu, O.; Bicak, N. *Tetrahedron Lett.* **2010**, *51*, 5313-5315.
16. Ghorai, M. K.; Ghosh, K.; Das, K. *Tetrahedron Lett.* **2006**, *47*, 5399-5403.
17. Gandhi, S.; Bisai, A.; Prasad, B. A.B.; Singh, V. K. *J. Org. Chem.* **2007**, *72*, 2133-2142.
18. Kuszpit, M. R.; Wulf, W. D.; Tepe, J. J. *J. Org. Chem.* **2011**, *76*, 2913-2919.
19. Li, R.; Jiang, H.; Liu, W. Y.; Gu, P. M.; Li, X. Q. *Chinese. Chem. Lett.* **2014**, *25*, 583-585.
20. Vasilevsky, S. F.; Davydova, M. P.; Mamatyuk, V. I.; Tsvetkov, N.; Hughes, A.; Baranov, D. S.; Alabugin, L. V. *Aust. J. Chem.* **2017**. DOI: 10.1071/CH17026.
21. Raubenheimer, H. G.; Cronje, S. *J. Organomet. Chem.* **2001**, *617-618*, 170-181.
22. Mohammadpoor-Baltork, I.; Khosropour, A. R.; Hojati, S. F. *Synlett* **2005**, 2747-2750.
23. Mirkhani, V.; Mohammadpoor-Baltork, I.; Moghadam, M.; Tangestaninejad, S.; Abdoullahi-Alibeik, M.; Kargar, H. *Appl. Catal. A: Chem.* **2007**, *325*, 99-104.
24. Mirkhani, V.; Moghadam, M.; Tangestaninejad, S.; Mohammadpoor-Baltork, I.; Mahdavi, M. *Monatsh. Chem.* **2009**, *140*, 1489-1494.
25. Ghorbani-Choghamarani, A.; Darvishnejad, Z.; Norouzi, M. *Appl. Organometal. Chem.* **2015**, *29*, 170-175.
26. Zarnegar, Z.; Safari, J. *New J. Chem.* **2014**, *38*, 4555-4565.
27. Firozabadi, H.; Iranpoor, N.; Gholinejad, M.; Akbari, S.; Jeddi, N. *RSC Adv.* **2014**, *4*, 17060-17070.
28. Kumar, M. R. A.; Shanmukhappa, S.; Rangaswamy, B. E.; Revanasiddappa, M. *J. Applicable. Chem.* **2014**, *3*, 1440-1446.
29. Katwal, R.; Kaur, H.; Kapur, B. K. *Sci. Revs. Chem. Com.* **2013**, *3*, 1-15.
30. Hiesh, S.; Huang, B. Y.; Hsieh, S. L.; Wu, C. C.; Wu, C. H.; Lin, P. Y.; Huang, Y. S.; Chang, C. W. *Nanotechnology* **2010**, *21*, 445601-445606.
31. Kalaivani, S. S.; Vidhyadevi, T.; Murugesan, A.; Thiruvengadaravi, K. V.; Anuradha, C. D.; Sivanesan, S.; Ravikumar, L. *Water. Resour. Ind.* **2014**, *5*, 21.
32. Zarghani, M.; Akhlaghinia, B. *Appl. Organometal. Chem.* **2015**, *29*, 683-689.
33. Saranya, M.; Subashini, A.; Arunagiri, C.; Muthiah, P. T. *Int. J. Innov. Res. Sci. Eng.* **2014**, 2347-3207.

34. Sonnekar, V. S.; Jadhav, W. N.; Dake, S. A.; Dhole, S. G.; Narwad, S. S.; Pawar, R. P. *Eur. Chem. Bull.* **2014**, *8*, 792-797.
35. Yadav, S.; Moheman, A.; Siddiqi, K. S. *Arab. J. Chem.* **2012**. DOI: 10.1016/j.arabjc.2012.04.045.
36. Yuvakkuma, R.; Hong, S. I. *Adv. Mater. Res.* **2014**, *1051*, 39-42.
37. Das, C. K.; Sudhakar, C. V. *J. Mater. Sci. Eng.* **2012**, *6*, 368-375.
38. Jegan, A.; Ramasubbu, A.; Saravanan, S.; Vasanthkumar, S. *Int. J. Nano. Dimens.* **2011**, *2*, 105-110.
39. Zarei, Z.; Akhlaghinia, B. *Chem. Pap.* **2015**, *69*, 1421-1437.
40. Safari, J.; Javadian, L. *RSC Adv.* **2014**, *4*, 48973-48979.
41. Kaboudian, B.; Mostafalu, R.; Yokomatsu, T. *Green Chem.* **2013**, *15*, 2266-2274.
42. Rezazadeh, S.; Akhlaghinia, B.; Razavi, N. *Aust. J. Chem.* **2015**, *68*, 145-155.
43. Zarghani, M.; Akhlaghinia, B. *RSC Adv.* **2015**, *5*, 87769-87780.
44. Razavi, N.; Akhlaghinia, B. *RSC Adv.* **2015**, *5*, 12372-12381.
45. Razavi, N.; Akhlaghinia, B. *New J. Chem.* **2016**, *40*, 447-457.
46. Ghodsinia, S. S. E.; Akhlaghinia, B. *RSC Adv.* **2015**, *5*, 49849-49860.
47. Jahanshahi, R.; Akhlaghinia, B. *RSC Adv.* **2015**, *5*, 104087-104094.
48. Jahanshahi, R.; Akhlaghinia, B. *RSC Adv.* **2016**, *6*, 29210-29219.
49. Zarghani, M.; Akhlaghinia, B. *RSC Adv.* **2016**, *6*, 31850-31860.
50. Zarghani, M.; Akhlaghinia, B. *RSC Adv.* **2016**, *6*, 38592-38601.
51. Siavashi, N. Y.; Akhlaghinia, B.; Zarghani, M. *Res. Chem. Intermed.* **2016**, *42*, 5789-5806.
52. Karimian, E.; Akhlaghinia, B.; Ghodsinia, S. S. E. *J. Chem. Sci.* **2016**, *128*, 429-439.
53. Zarghani, M.; Akhlaghinia, B. *B. Chem. Soc. Jpn.* **2016**, *89*, 1192-1200.
54. Ghodsinia, S. S. E.; Akhlaghinia, B.; Jahanshahi, R. *RSC Adv.* **2016**, *6*, 63613-63623.
55. Zarei, Z.; Akhlaghinia, B. *RSC Adv.* **2016**, *6*, 106473-106484.
56. Esmaielpour, M.; Akhlaghinia, B.; Jahanshahi, R. *J. Chem. Sci.* **2017**, *129*, 313-328.
57. Jahanshahi, R.; Akhlaghinia, B. *New J. Chem.* **2017**, *41*, 7203-7219.
58. Ghasemzadeh, M. S.; Akhlaghinia, B. *B. Chem. Soc. Jpn.* **2017**, *90*, 1119-1128.
59. Mohammadian, N.; Akhlaghinia, B. *Res. Chem. Intermed.* **2017**, *43*, 3225-3347.
60. Mohammadinezhad, A.; Akhlaghinia, B. *Aust. J. Chem.* **2017**. DOI: 10.1071/CH17093.
61. Jahanshahi, R.; Akhlaghinia, B. *Catal. Lett.* **2017**. DOI:10.1007/s10562-017-2170-x.
62. Nejatianfar, M.; Akhlaghinia, B.; Jahanshahi, R. *Appl. Organomet. Chem.* **2017**. DOI: 10.1002/aoc.4095.
63. Mohammadian, N.; Akhlaghinia, B. *Res. Chem. Intermed.* **2017**, in press.
64. Mohammadinezhad, A.; Akhlaghinia, B. *Green Chem.* **2017**. DOI: 10.1039/C7GC02647A.
65. Zarei, Z.; Akhlaghinia, B. *New J. Chem.* **2017**. DOI: 10.1039/C7NJ03281A.
66. An, S.; Yin, B.; Liu, P.; Li, X.; Li, C.; Li, J.; Shi, Z. *Synthesis* **2013**, *45*, 2525-2532.
67. Sun, M.; Wei, H. T.; Li, D.; Zheng, Y. G.; Cai, J.; Ji, M. *Synthetic. Commun.* **2008**, *38*, 3151-3158.
68. Nasr-Esfahani, M. N.; Montazerozohori, M.; Moghadam, M.; Akhlaghi, P. *Arkivoc* **2010**, *2010*, 97-109.
69. Zhang, J.; Wang, X.; Yang, M.; Wan, K.; Yin, B.; Wang,Y.; Li, J.; Shi, Z. *Tetrahedron Lett.* **2011**, *52*, 1578-1582.
70. Crane, L. J.; Anastassiadou, M.; Stigliani, J. L.; Baziard-Mouysset, G.; Payard, M. *Tetrahedron* **2004**, *60*, 5325-5330.

71. Pathan, M. Y.; Paike, V. V.; Pachmase, P. R.; More, S. P.; Ardhapure, S. S.; Pawar, R. P. *Arkivoc* **2006**, *2006*, 205-210.

72. Nasr-Esfahani, M.; Montazerozohori, M.; Mehrizi, S. *J. Heterocyclic Chem.* **2011**, *48*, 249-254.

73. Mohammadpoor-Baltork, I.; Khosropour, A. R; Hojati, S. F. *Catal. Commun.* **2007**, *8*, 200-204.

74. Mirkhani, V.; Moghadam, M.; Tangestaninejad, S.; Kargar, H. *Tetrahedron Lett.* **2006**, *47*, 2129-2132.

75. Manikandan, R.; Anitha, P.; Prakash, G.; Vijayan, P.; Viswanathamurthi, P.; Butcher, R. J.; Malecki, J. G. *J. Mol. Catal. A: Chem.* **2015**, *398*, 312-324.

76. Mohammadpoor-Baltork, I.; Moghadam, M.; Tangestaninejad, S.; Mirkhani, V.; Hojati, S. F. *Catal. Commun.* **2008**, *9*, 1153-1161.

77. Bazgir, A.; Amini, M. M.; Fazaeli, Y. *Tocat* **2009**, *2*, 163-165.

78. Hojati, S. F.; Nezhadaoseiny, S. A. *J. Serb. Chem. Soc.* **2012**, *77*, 1181-1189.

79. Mohammadpoor-Baltork, I.; Mirkhani, V.; Moghadam, M.; Tangestaninejad, S.; Zolfigol, M. A.; Abdollahi-Alibeik, M.; Khosropour, A. R.; Kargar, H.; Hojati, S. F. *Catal. Commun.* **2008**, *9*, 894-901.

80. Cao, X.; Zhu, J.; Wang, D.; Dai, G.; Wu, X. *Chin. J. Chem. Eng.* **1997**, *5*, 69-73.

Supplementary Information

General Experimental

All chemical reagents and solvents were purchased from Merck and Sigma-Aldrich chemical companies and were used as received without further purification.

The melting points of products were determined with an Electrothermal Type 9100 melting point apparatus. The FT-IR spectra were provided on pressed KBr pellets using an AVATAR 370 FT-IR spectrometer (Therma Nicolet spectrometer, USA) at room temperature in the range between 4000 and 400 cm^{-1}. The NMR spectra were obtained in Bruker Avance 300 MHz instruments (Germany) in $CDCl_3$. Elemental analysis was performed using a Thermo Finnigan Flash EA 1112 Series instrument. Mass spectra were recorded with a CH7A Varianmat Bremem instrument (Germany) at 70 eV electron impact ionization, in m/z (rel %). All of the products were known compounds and characterized by mass spectrometry and comparison of their melting points with those of known compounds. The structure of selected products was further confirmed by FT-IR, ^{1}H NMR, and ^{13}C NMR spectroscopy. All yields refer to isolated products after purification by recrystallization or thin layer chromatography.

2-(Phenyl) imidazoline (1a). White solid, mp 98–100 °C (Lit. [1]101.5–102 °C). ν_{max} (KBr)/cm^{-1} 3204 (NH), 2974 (CH_2), 2929 (CH_2), 1611 (C=N). *m/z* (ESI)146 (44%, M^+). δ_H ($CDCl_3$, 300 MHz) 7.79 (dd, *J* 6 Hz, 1.8 Hz, 2H, Ph), 7.48–7.43 (m, 1H, Ph), 7.42 (d, *J* 7.5 Hz, 1H, Ph), 7.37 (d, *J* 1.8 Hz, 1H, Ph),4.36 (brs, 1H, NH), 3.78 (s, 4H, $2CH_2$).

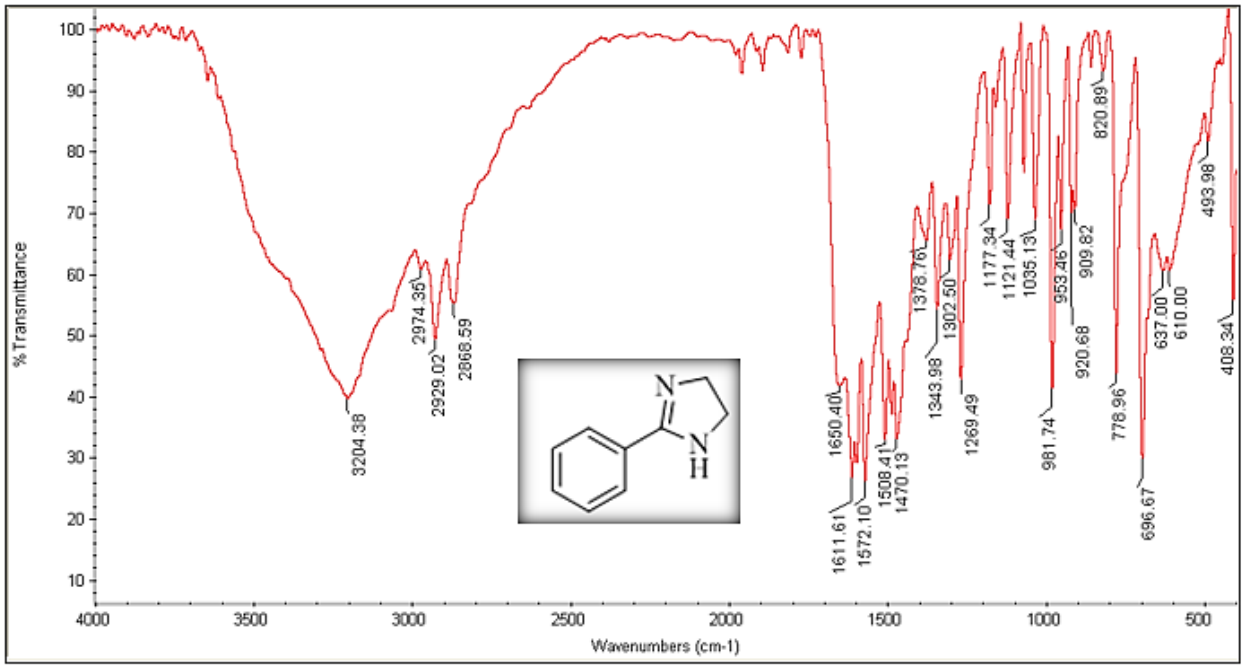

Figure 1. FT-IR (KBr) spectrum of 2-(Phenyl) imidazoline (**1a**).

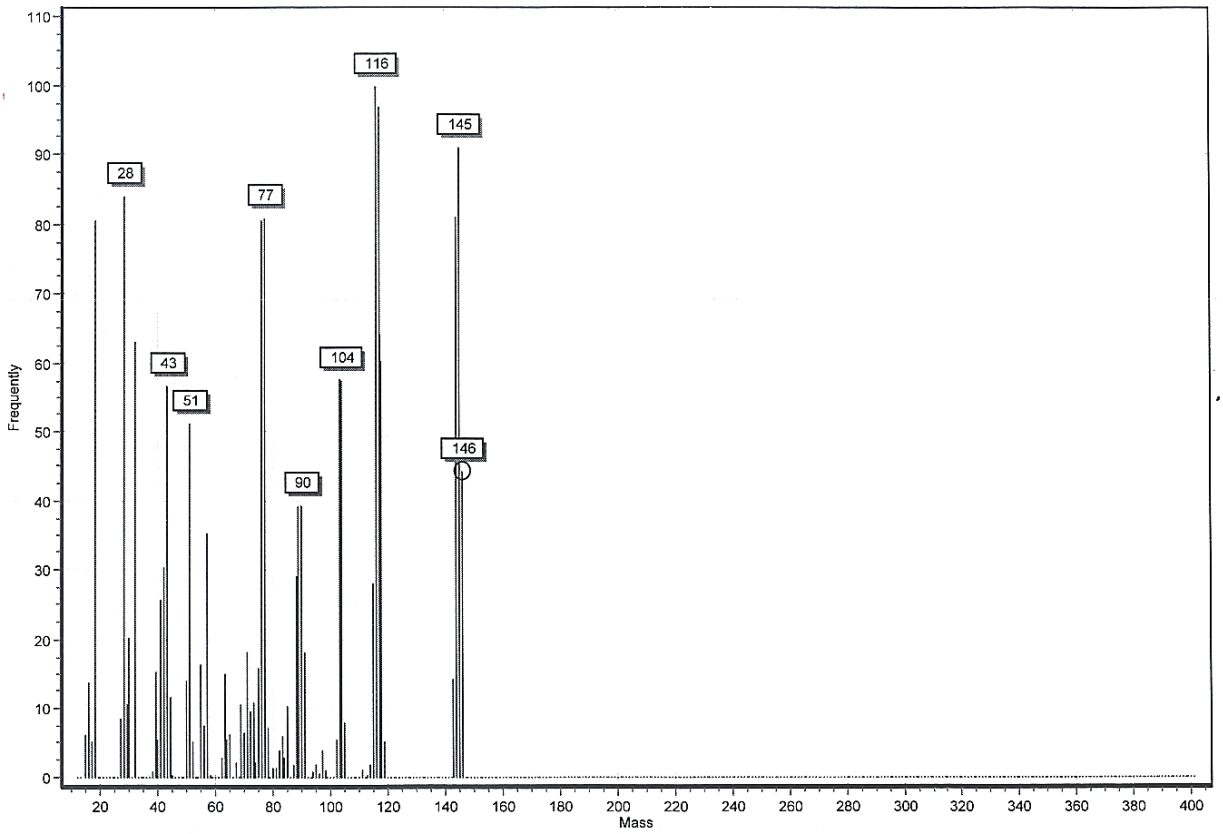

Figure 2. Mass spectrum of 2-(Phenyl) imidazoline (**1a**).

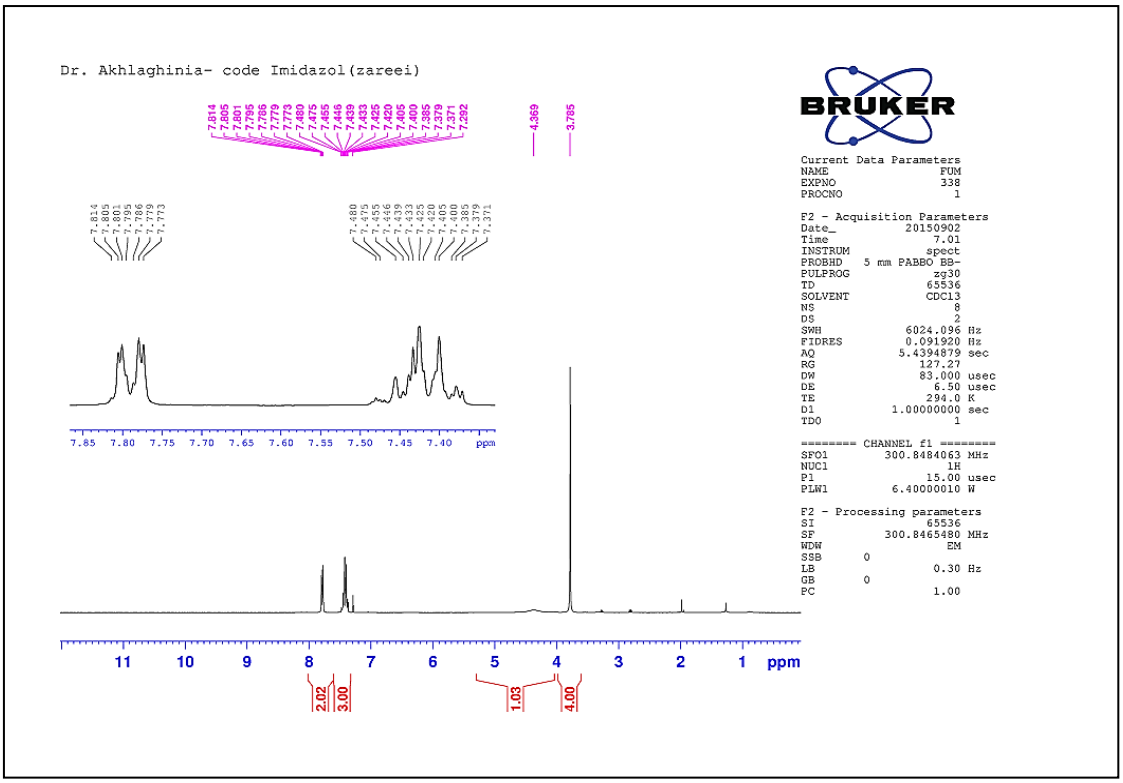

Figure 3. ^{1}H NMR (300 MHz, $CDCl_3$) spectrum of 2-(Phenyl) imidazoline (**1a**).

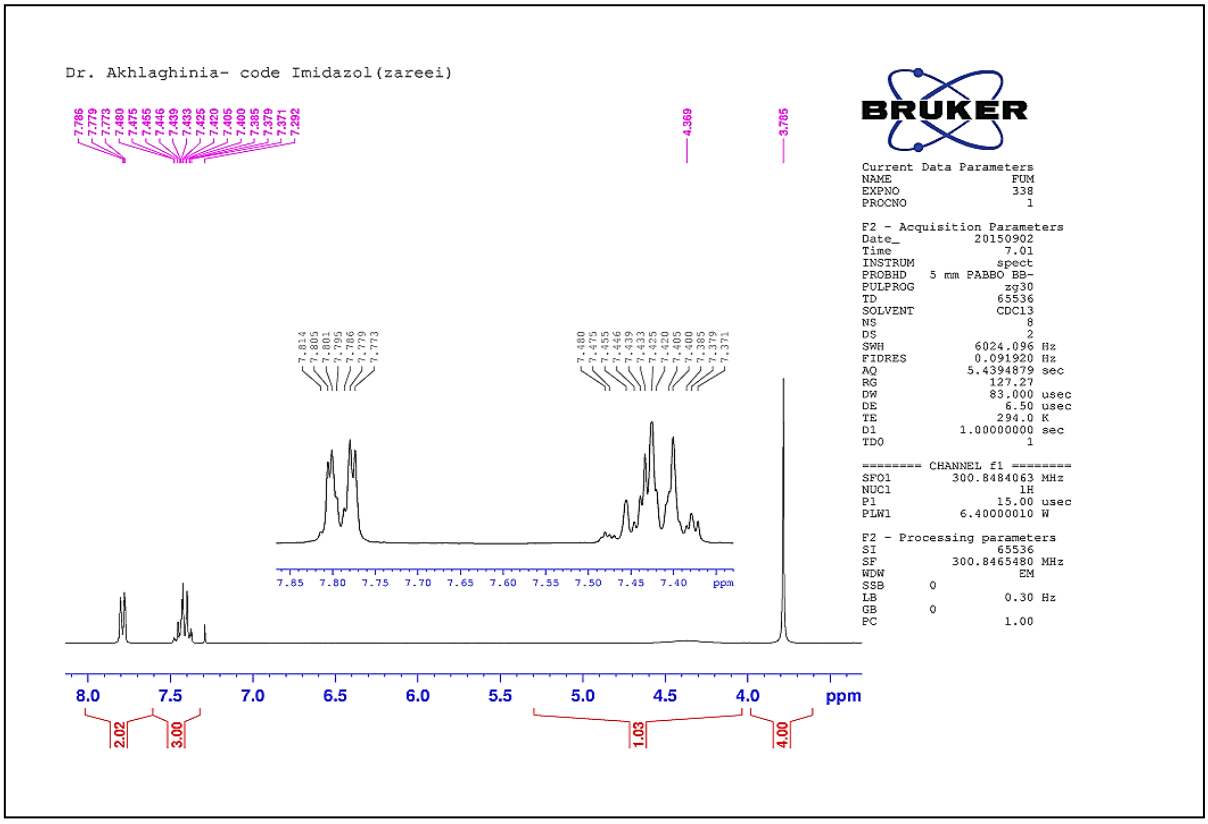

Figure 4. ^{1}H NMR (300 MHz, $CDCl_3$) spectrum of 2-(Phenyl) imidazoline (**1a**) expanded.

2-(Phenyl) oxazoline (1b). Oily light liquid. ν_{max} (neat)/cm^{-1} 2953 (CH_2), 2924 (CH_2), 2854 (CH_2), 1649 (C=N), 1360, 1260, 1063, 777, 694.[1] *m/z* (ESI) 147 (87%, M^+).

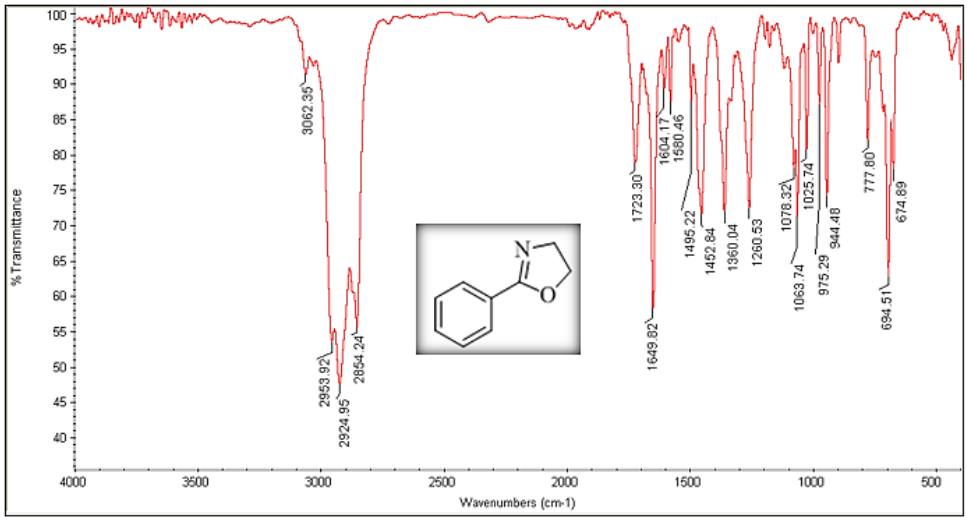

Figure 5. FT-IR (neat) spectrum of 2-(Phenyl) oxazoline (**1b**).

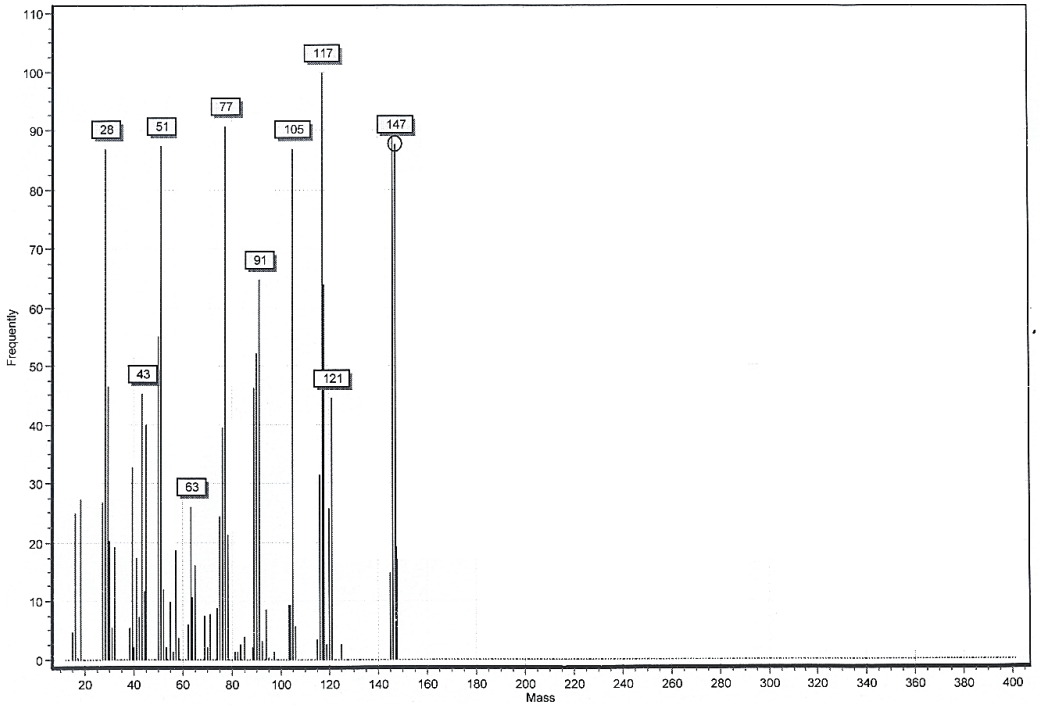

Figure 6. Mass spectrum of 2-(Phenyl) oxazoline (**1b**).

2-(Phenyl) thiazoline (1c). Light solid, mp 125–127 °C (Lit. [2] 126–128 °C). *m/z* (ESI) 164 (8%, M^+). δ_H ($CDCl_3$, 300 MHz) 7.76 (dd, *J* 7.8 Hz, 1.5 Hz, 2H, Ph), 7.48–7.36 (m, 1H, Ph), 7.31 (d, *J* 6 Hz, 1H, Ph), 7.28 (d, *J* 1.8 Hz, 1H, Ph),4.37 (t, *J* 8.4 Hz, 2H, CH_2), 3.31 (t, *J* 8.4 Hz, 2H, CH_2). δ_C ($CDCl_3$, 75 MHz) 168.7, 133.2, 131.1, 128.5, 128.3, 65.1, 33.6.

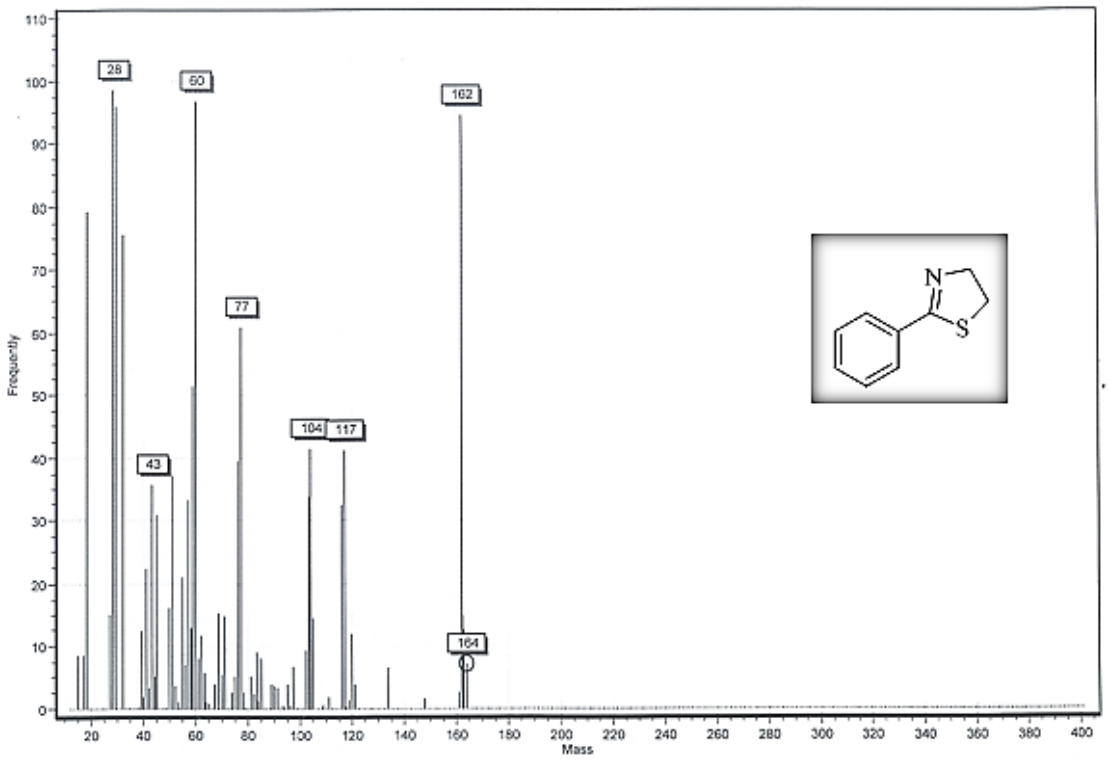

Figure 7. Mass spectrum of 2-(Phenyl) thiazoline (**1c**).

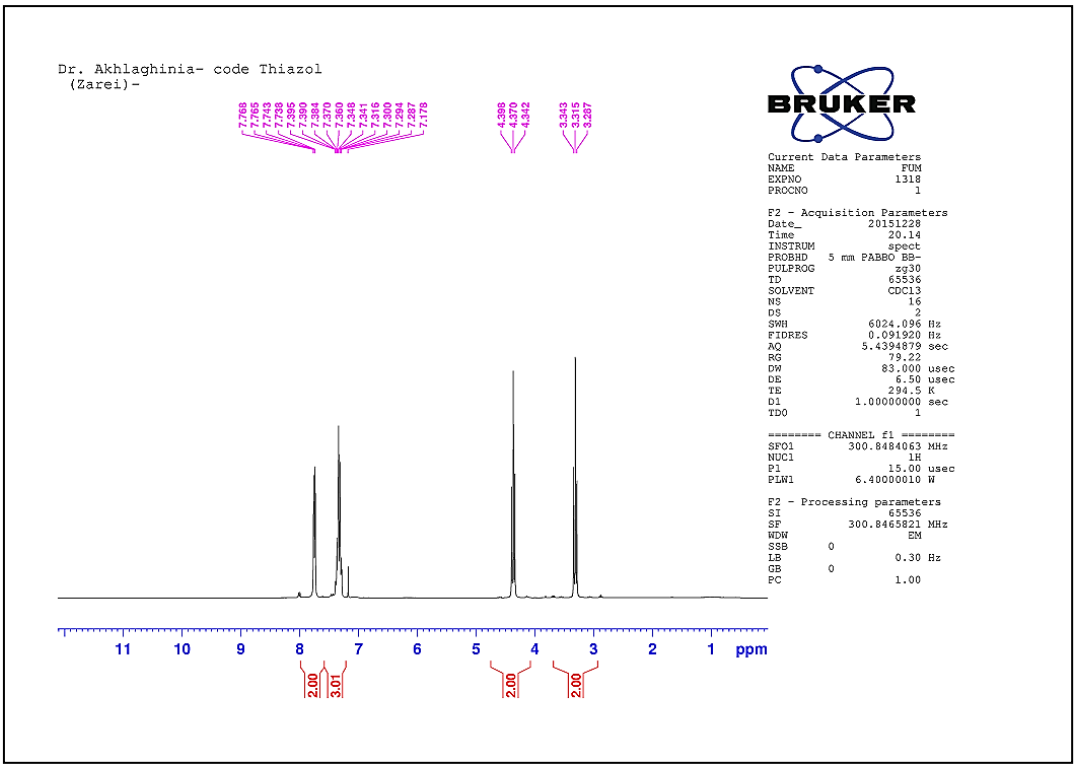

Figure 8. ^{1}H NMR (300 MHz, $CDCl_3$) spectrum of 2-(Phenyl) thiazoline (**1c**).

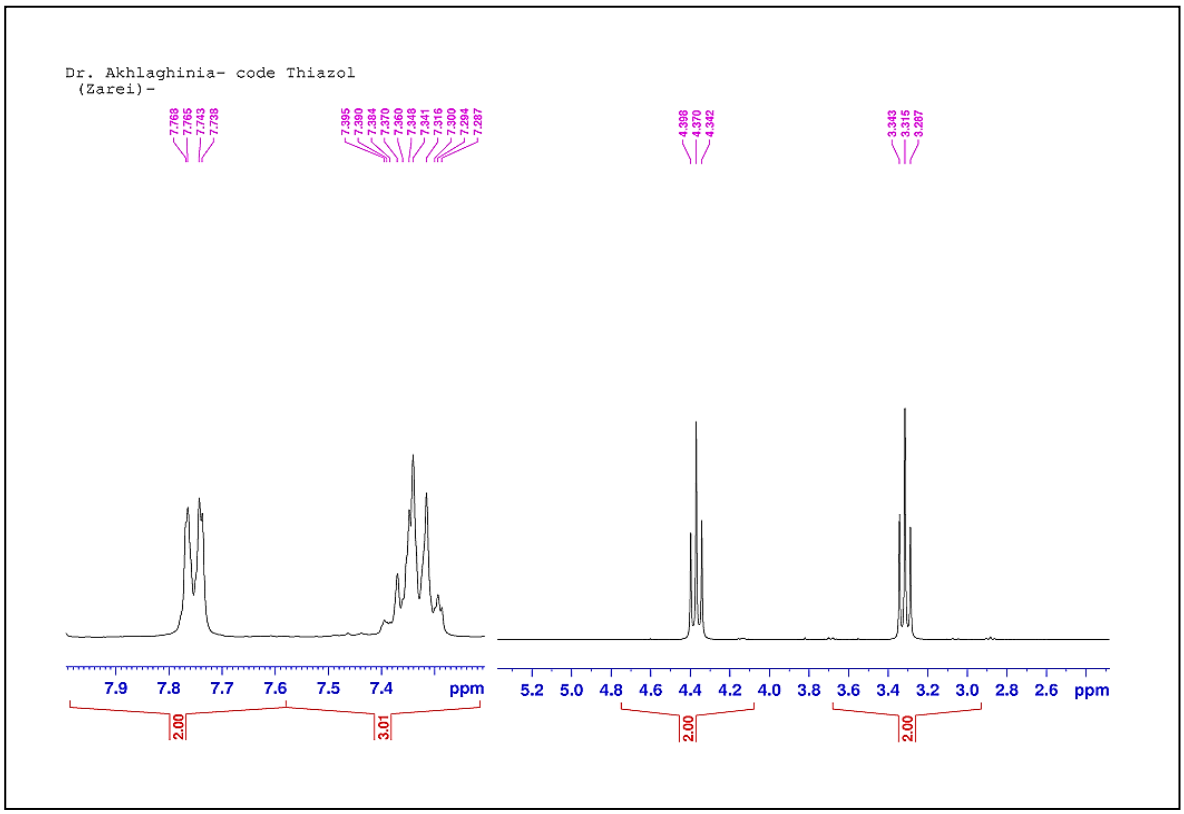

Figure 9. ^{1}H NMR (300 MHz, $CDCl_3$) spectrum of 2-(Phenyl) thiazoline (**1c**) expanded.

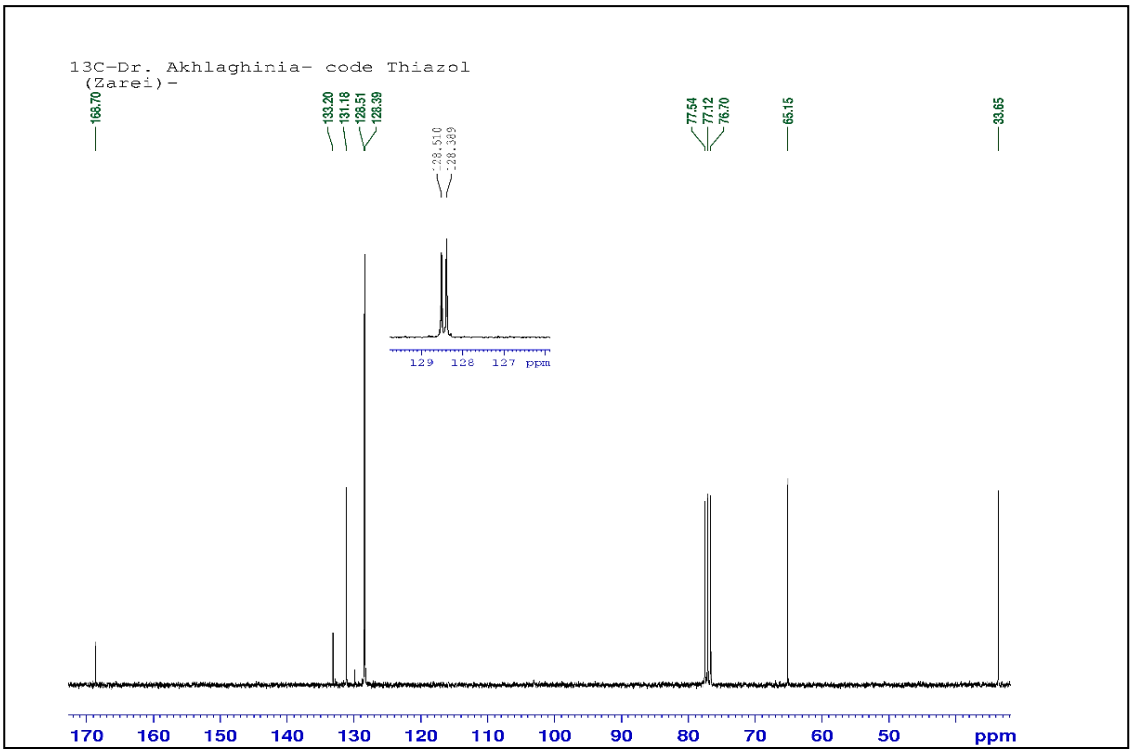

Figure 10. ^{13}C NMR (75 MHz, $CDCl_3$) spectrum of 2-(Phenyl) thiazoline (**1c**).

2-(4-Chlorophenyl) imidazoline (2a). White solid, mp 185–187 °C (Lit. [2] 186–188 °C). ν_{max} (KBr)/cm^{-1} 3141 (NH), 3027 (Ph), 2971 (CH_2), 2925 (CH_2), 1606 (C=N), 838 (C–Cl). *m/z* (ESI)182 (8%, $M^+ + 2$), 180 (68%, M^+). δ_H ($CDCl_3$, 300 MHz) 7.74 (d, *J* 8.4 Hz, 2H, Ph), 7.39 (d, *J* 8.4 Hz, 2H, ph), 3.82 (s, 4H, $2CH_2$), 3.46 (brs, 1H, NH).

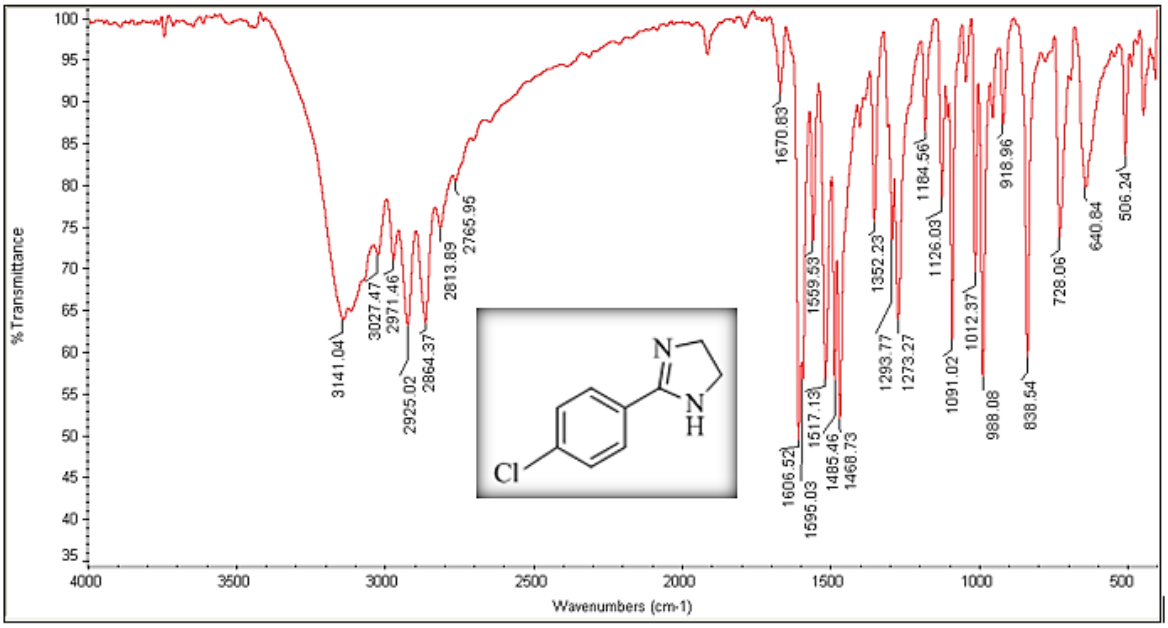

Figure 11. FT-IR (KBr) spectrum of 2-(4-Chlorophenyl) imidazoline (**2a**).

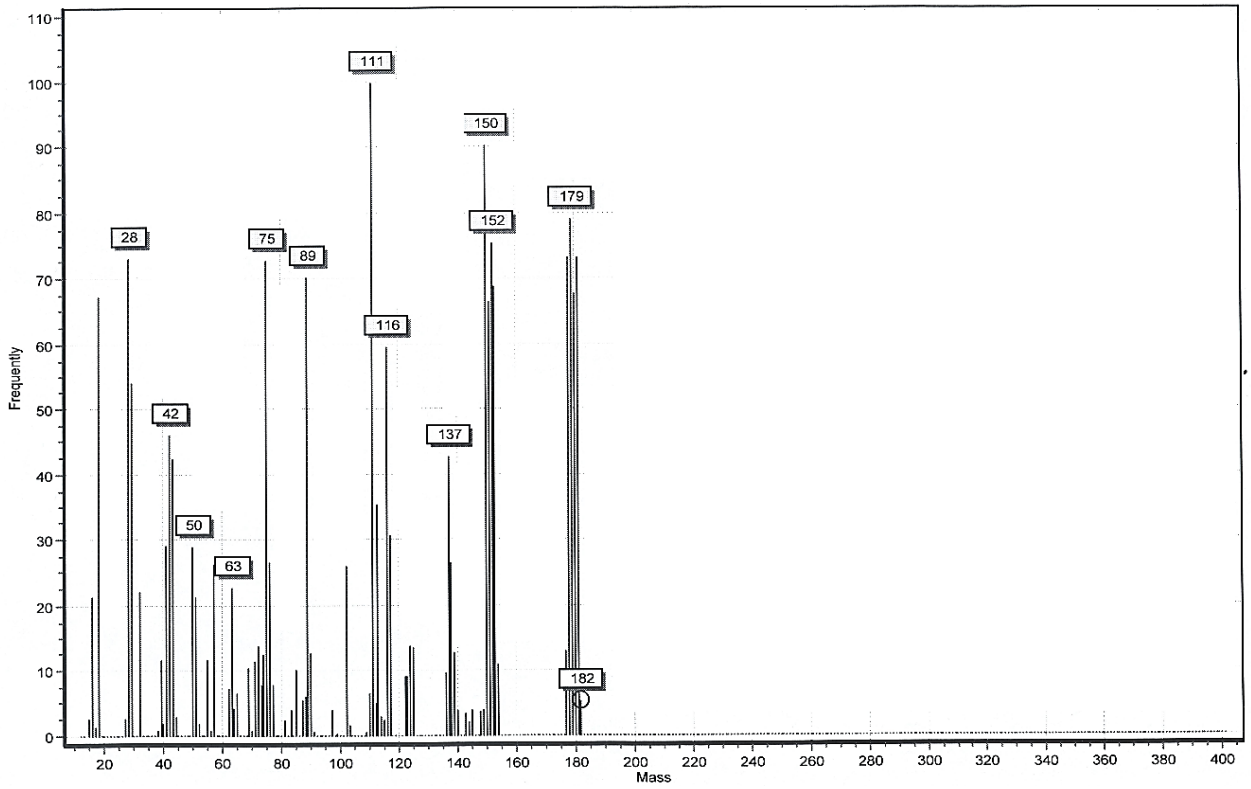

Figure 12. Mass spectrum of 2-(4-Chlorophenyl) imidazoline (**2a**).

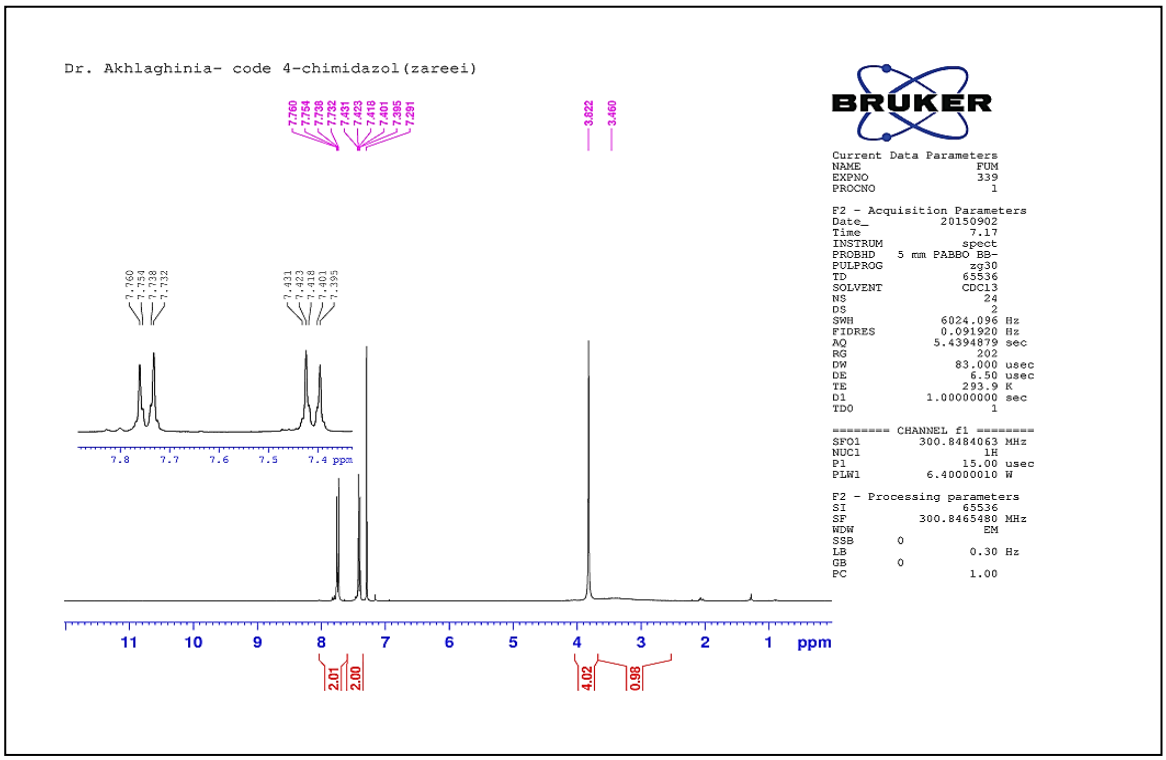

Figure 13. ^{1}H NMR (300 MHz, $CDCl_3$) spectrum of 2-(4-Chlorophenyl) imidazoline (**2a**).

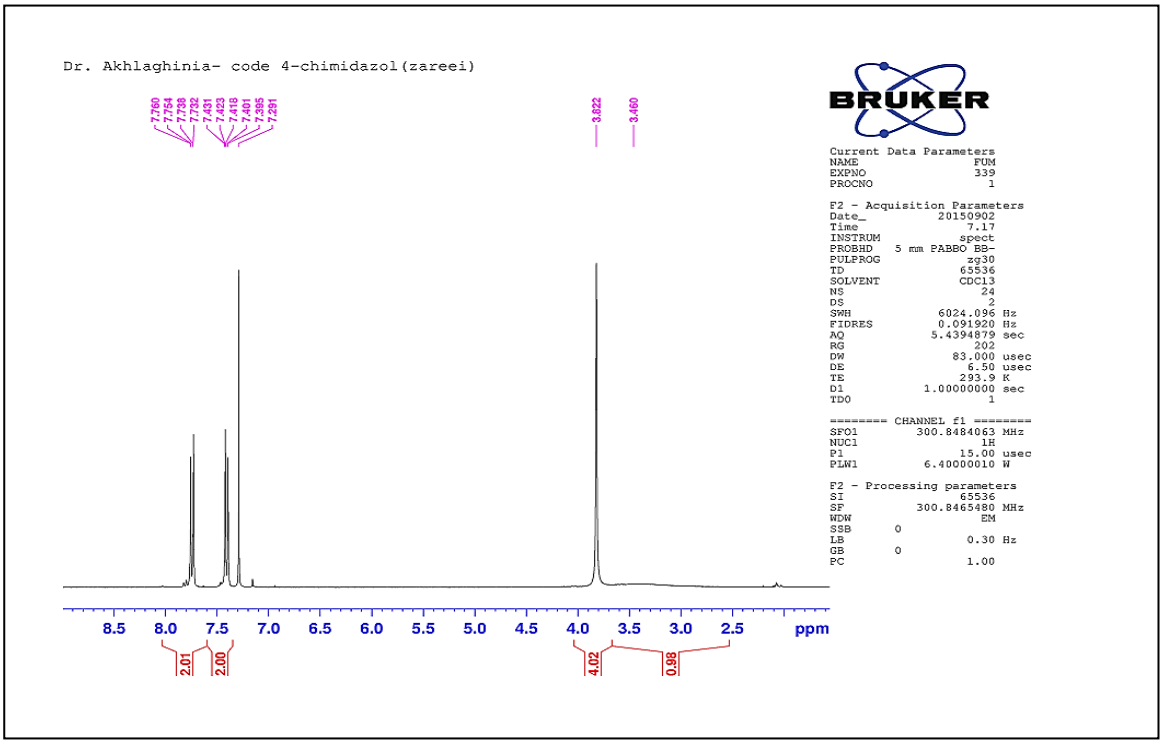

Figure 14. ^{1}H NMR (300 MHz, $CDCl_3$) spectrum of 2-(4-Chlorophenyl) imidazoline (**2a**) expanded.

2-(4-Chlorophenyl) oxazoline (2b). Light yellow solid, mp 76–78 °C (Lit. [2] 77–79 °C). *m/z* (ESI)182 (78%, $M^+ + 2$), 180 (82%, M^+). δ_H ($CDCl_3$, 300 MHz) 7.89 (d, *J* 8.4 Hz, 2H, Ph), 7.40 (d, *J* 8.4 Hz, 2H, Ph), 4.44 (t, *J* 9.3 Hz, 2H, CH_2), 4.07 (t, *J* 9.3 Hz, 2H, CH_2). δ_C ($CDCl_3$, 75 MHz) 163.7, 137.4, 129.5, 128.6, 126.2, 67.7, 54.9.

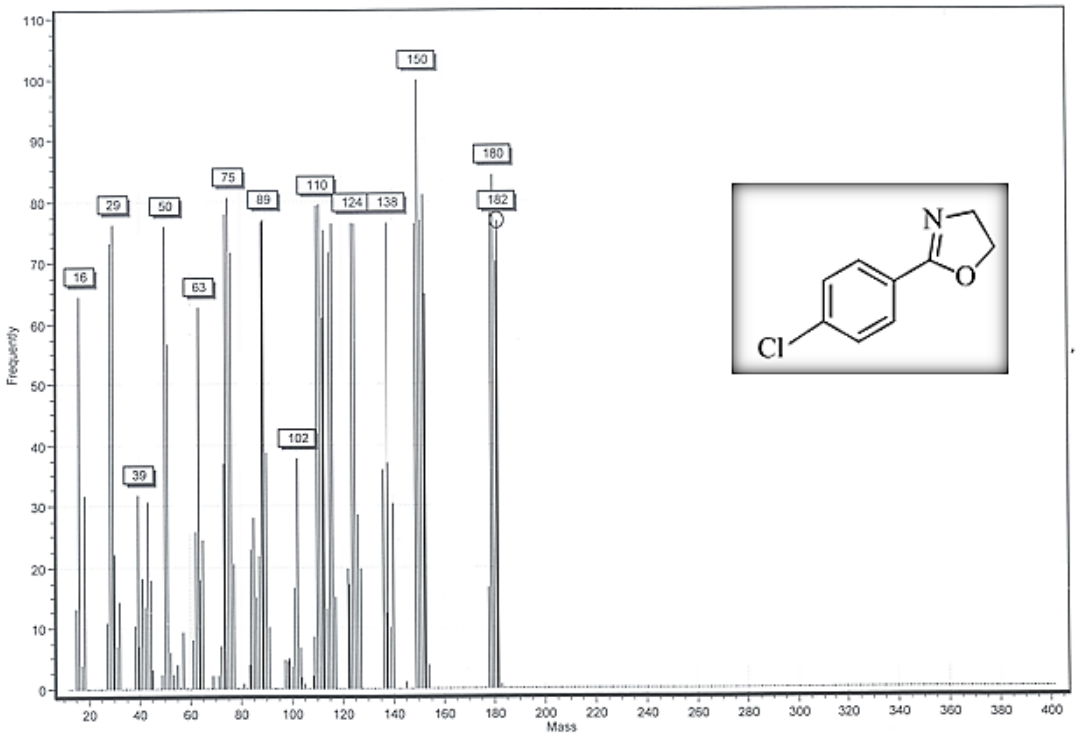

Figure 15. Mass spectrum of 2-(4-Chlorophenyl) oxazoline (**2b**).

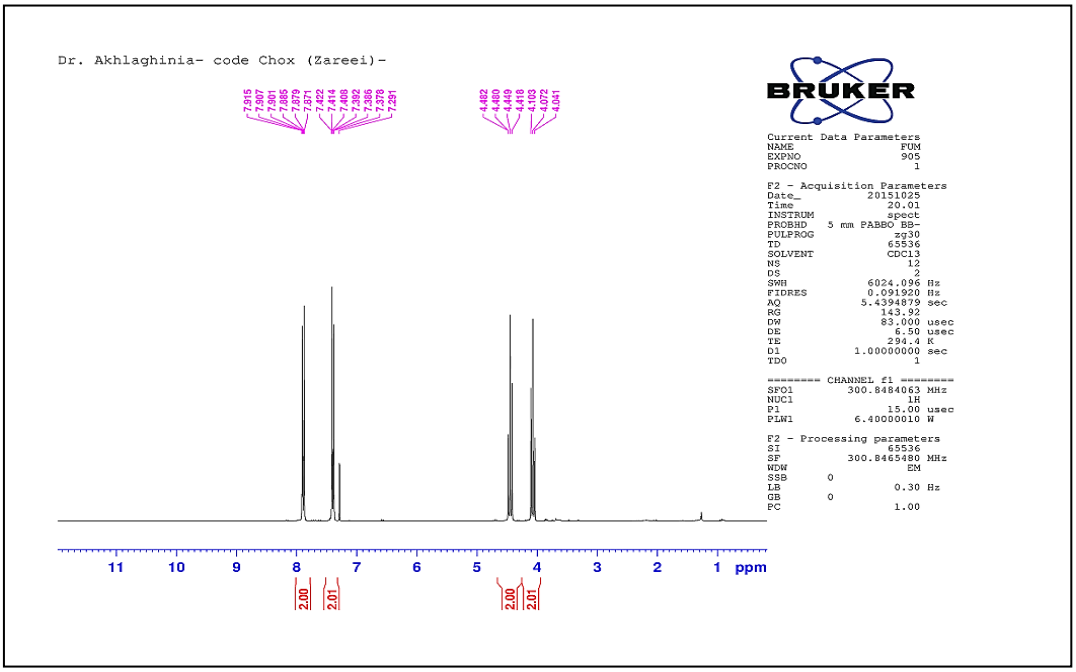

Figure 16. ^{1}H NMR (300 MHz, $CDCl_3$) spectrum of 2-(4-Chlorophenyl) oxazoline (**2b**).

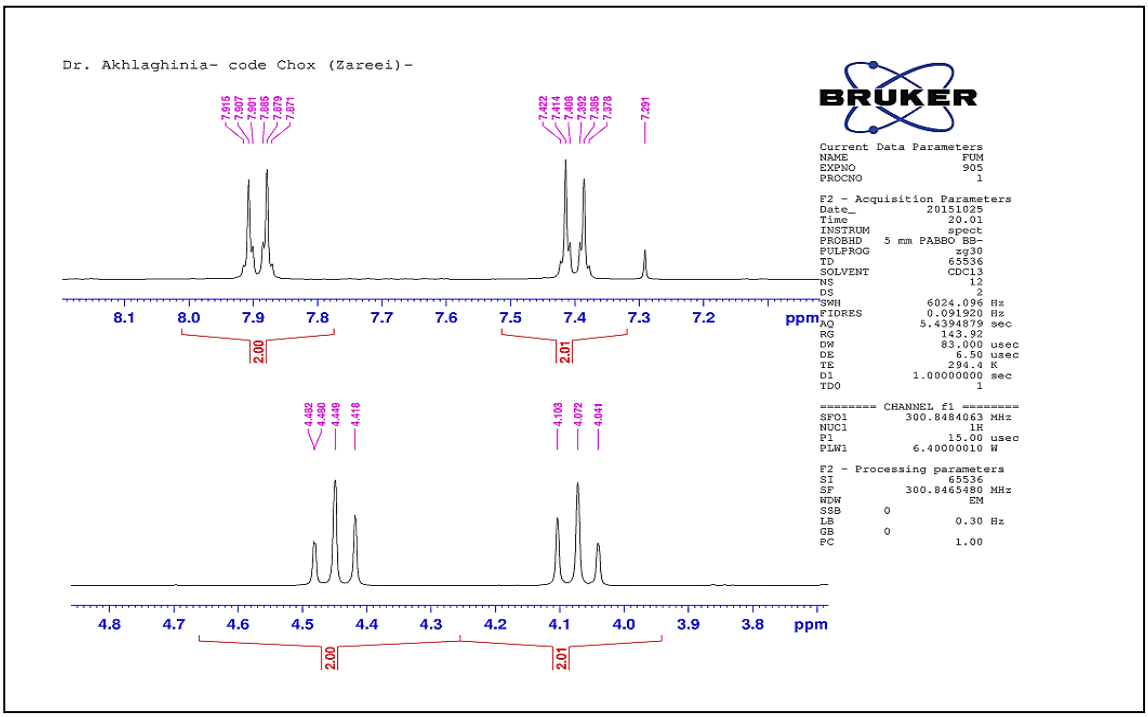

Figure 17. ^{1}H NMR (300 MHz, $CDCl_3$) spectrum of 2-(4-Chlorophenyl)oxazoline (**2b**) expanded.

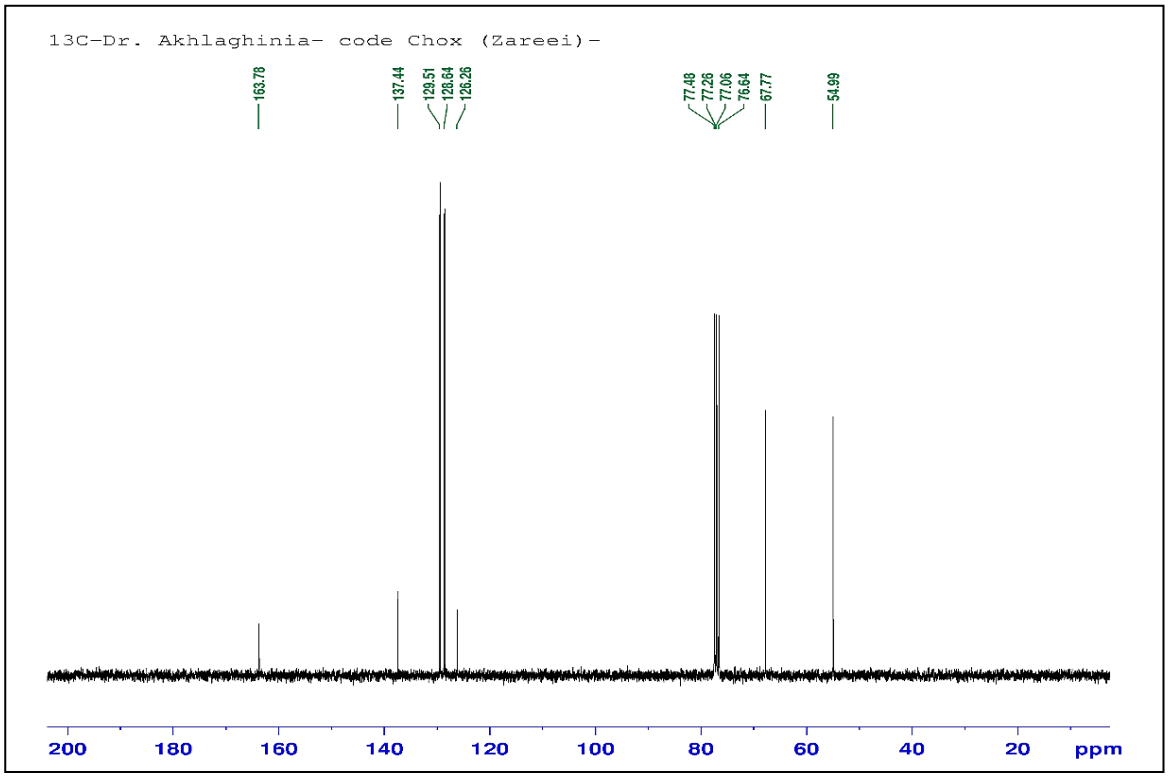

Figure 18. ^{13}C NMR (75 MHz, $CDCl_3$) spectrum of 2-(4-Chlorophenyl) oxazoline (**2b**).

2-(4-Chlorophenyl) thiazoline (2c). White solid, mp 50–52 °C (Lit.[2] 53–55 °C). *m/z* (ESI) 199 (50%, $M^+ + 2$), 197 (72%, M^+). δ_H ($CDCl_3$, 300 MHz) 7.66 (d, *J* 8.4 Hz, 2H, Ph), 7.47 (d, *J* 8.4 Hz, 2H, Ph), 4.34 (t, *J* 8.4 Hz, 2H, CH_2), 3.31 (t, *J* 8.4 Hz, 2H, CH_2). δ_C ($CDCl_3$, 75 MHz) 167.2, 137.1, 131.7, 129.6, 128.7, 65.2, 33.9.

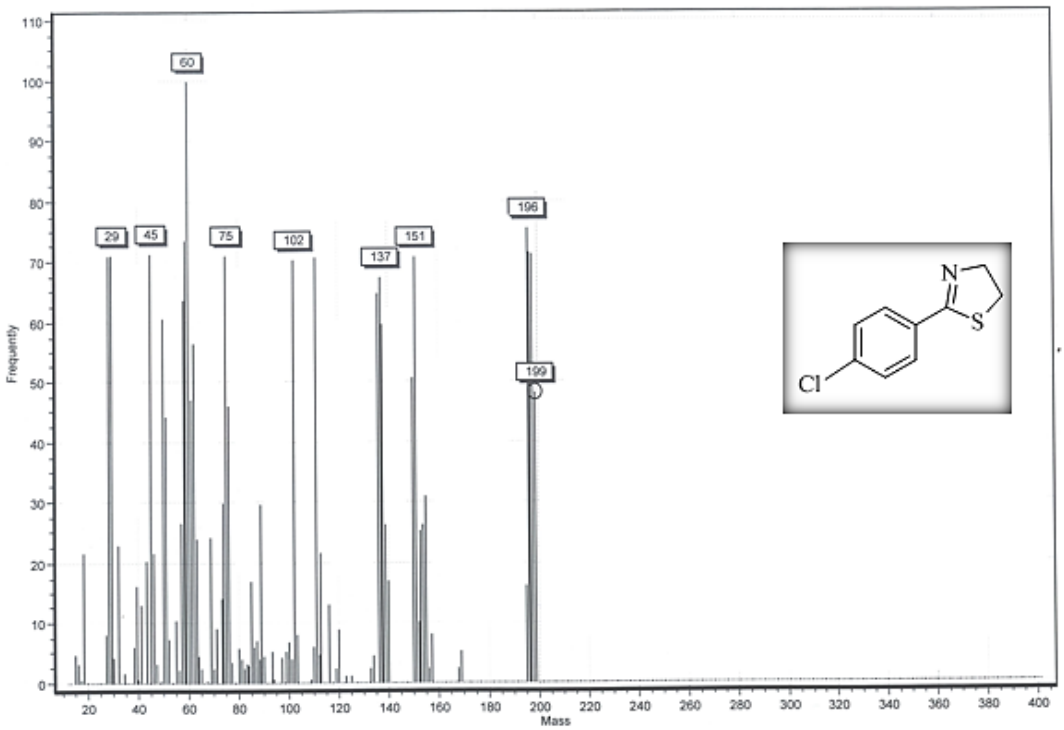

Figure 19. Mass spectrum of 2-(4-Chlorophenyl) thiazoline (**2c**).

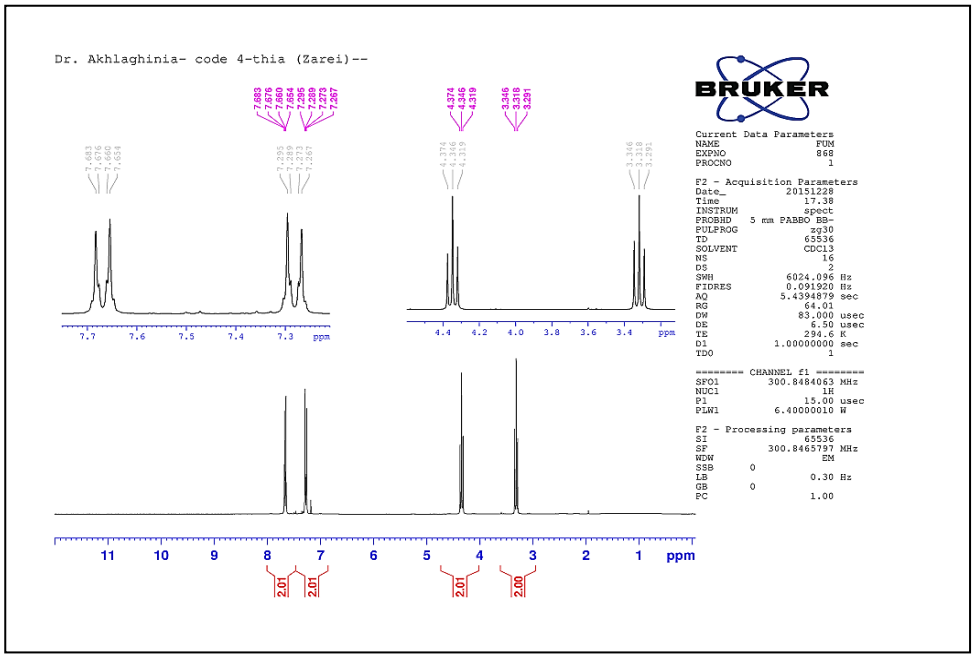

Figure 20. ^1H NMR (300 MHz, $CDCl_3$) spectrum of 2-(4-Chlorophenyl) thiazoline (**2c**).

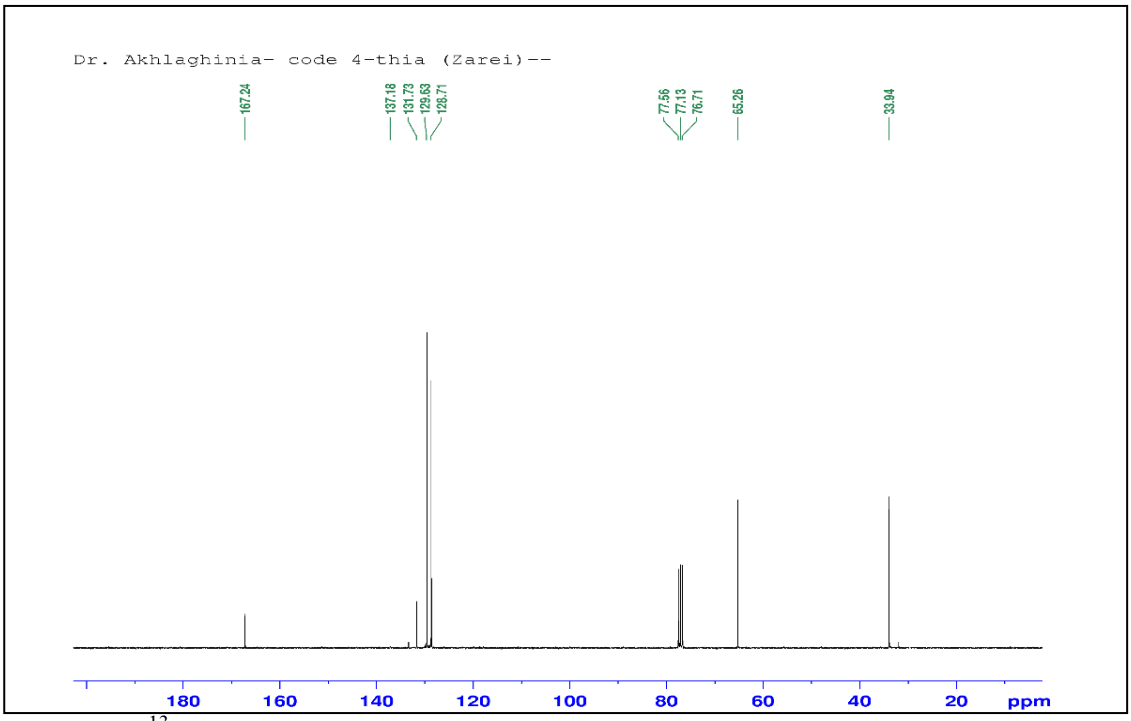

Figure 21. ^{13}C NMR (75 MHz, $CDCl_3$) spectrum of 2-(4-Chlorophenyl) thiazoline (**2c**).

2-(4-Bromophenyl) imidazoline (3a). White solid, mp 176–177 °C (Lit.[1] 177–177.5 °C). ν_{max} (KBr)/cm^{-1} 3248 (NH), 3190 (NH), 3062 (Ph), 2975 (CH_2), 2899 (CH_2), 2810 (CH_2), 2485 (Overlaps of C–H), 1605 (C=N). *m/z* (ESI)146 (70%, M^+-Br).

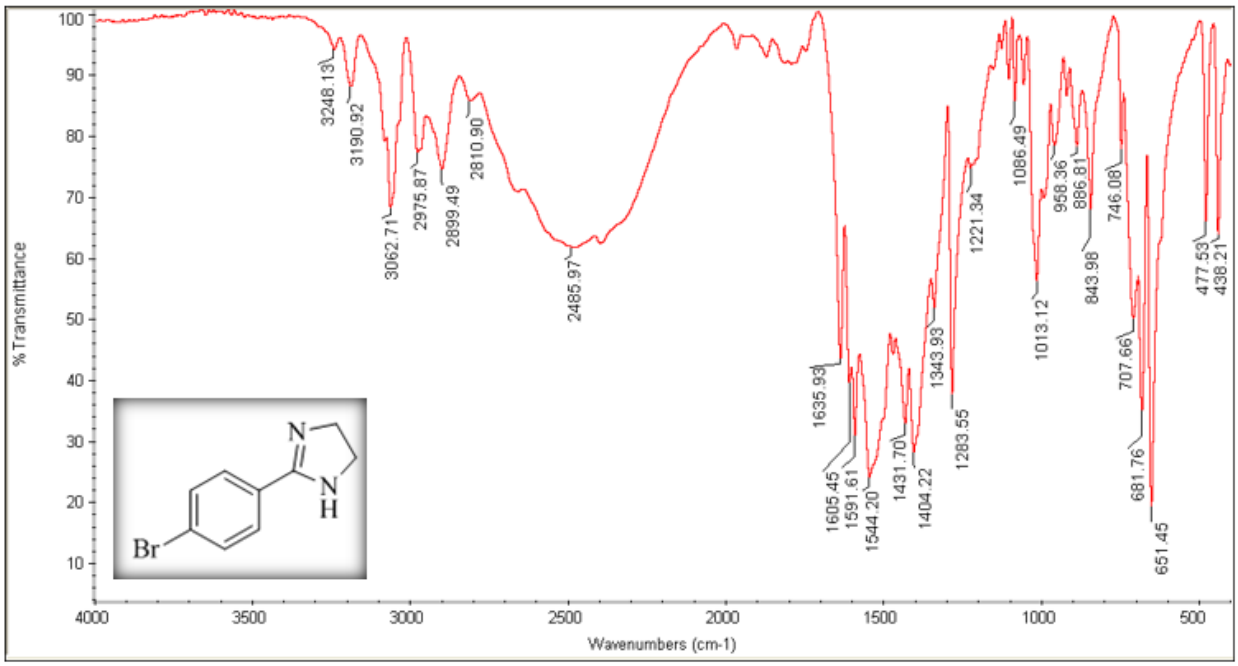

Figure 22. FT-IR (KBr) spectrum of 2-(4-Bromophenyl) imidazoline (**3a**).

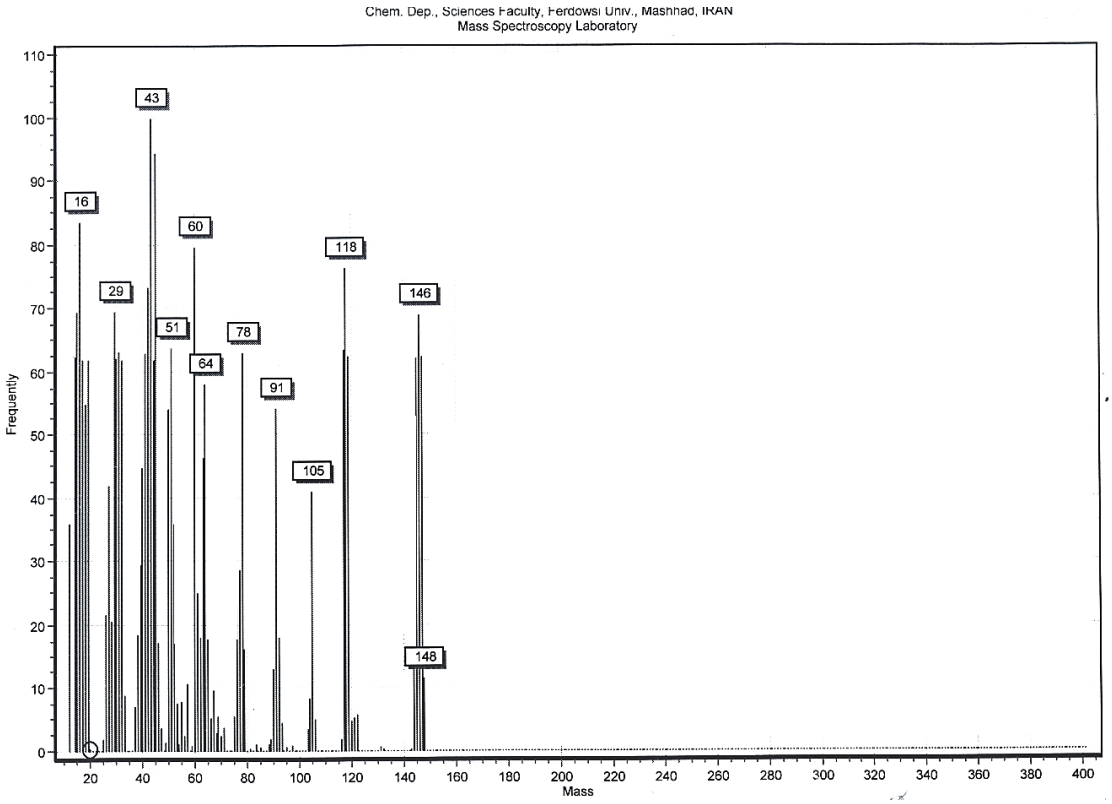

Figure 23. Mass spectrum of 2-(4-Bromophenyl) imidazoline (**3a**).

2-(4-Nitrophenyl) thiazoline (4c). Yellowish solid, mp 151–152 °C (Lit.[2] 150–152 °C). ν_{max} (KBr)/cm^{-1} 3072 (Ph), 2953 (CH_2), 2922 (CH_2), 2851 (CH_2), 1591 (C=N), 1343 (NO_2). *m/z* (ESI) 209 (10%, M^+).

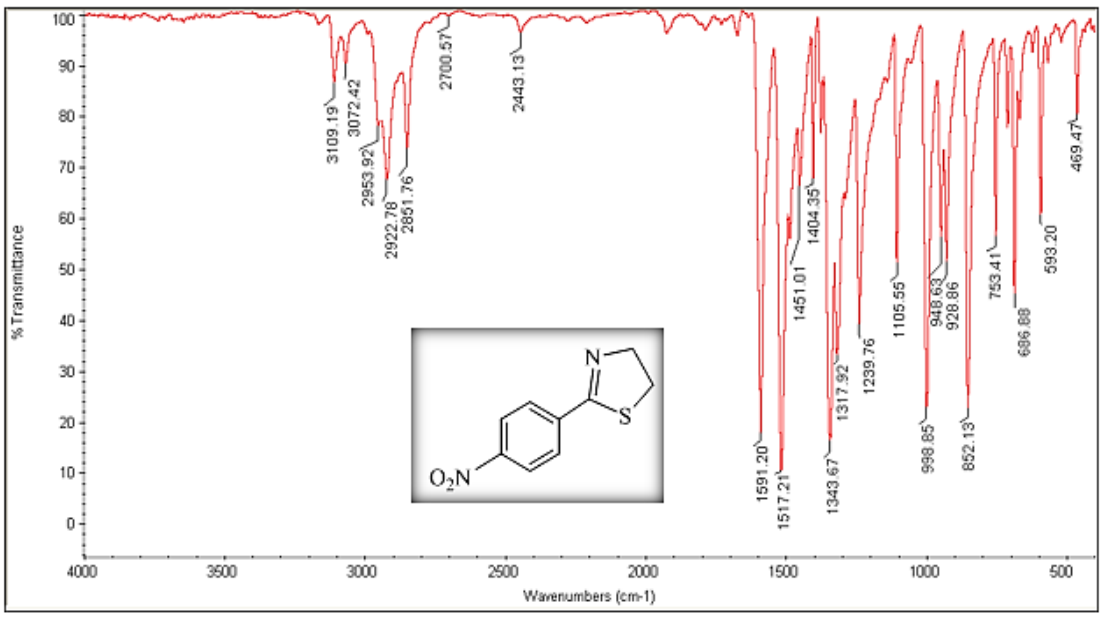

Figure 24. FT-IR (KBr) spectrum of 2-(4-Nitrophenyl) thiazoline (**4c**).

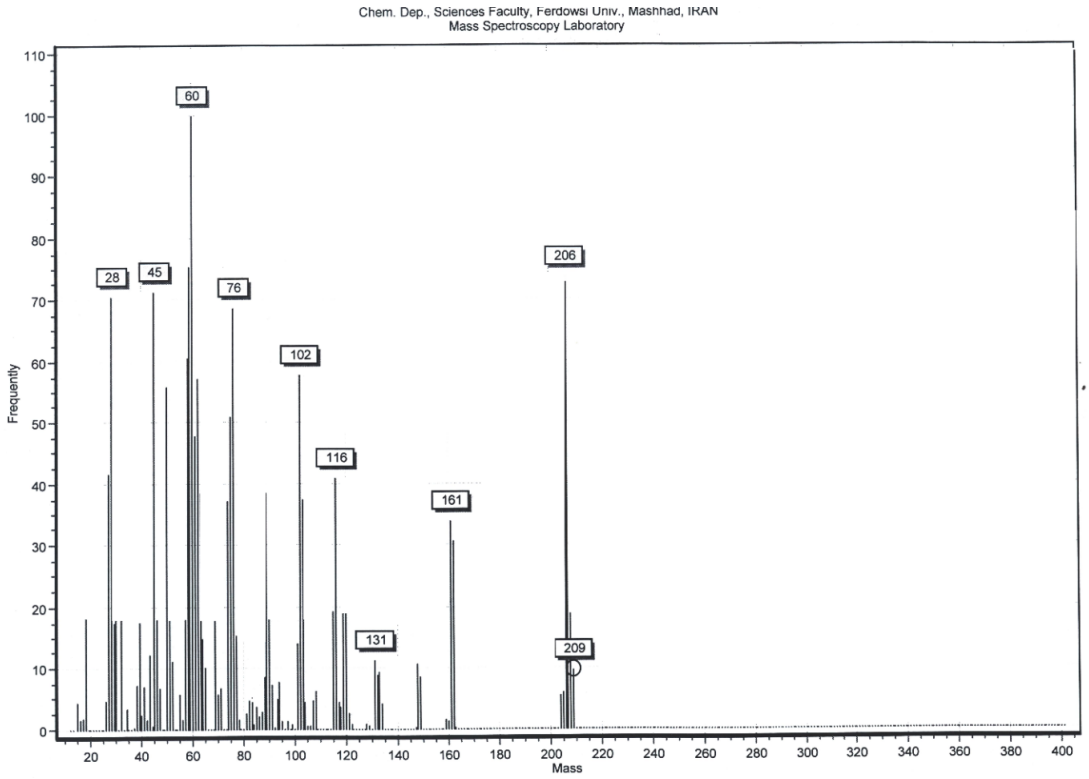

Figure 25. Mass spectrum of 2-(4-Nitrophenyl) thiazoline (**4c**).

1,4-Bis (4, 5-dihydroimidazol-2-yl) benzene (5a). White solid, mp 311–313 °C (Lit.[3] 312–314 °C). ν_{max} (KBr)/cm^{-1} 3186 (NH), 2925 (CH_2), 2885 (CH_2), 1606 (C=N). *m/z* (ESI) 214 (23%, M^+).

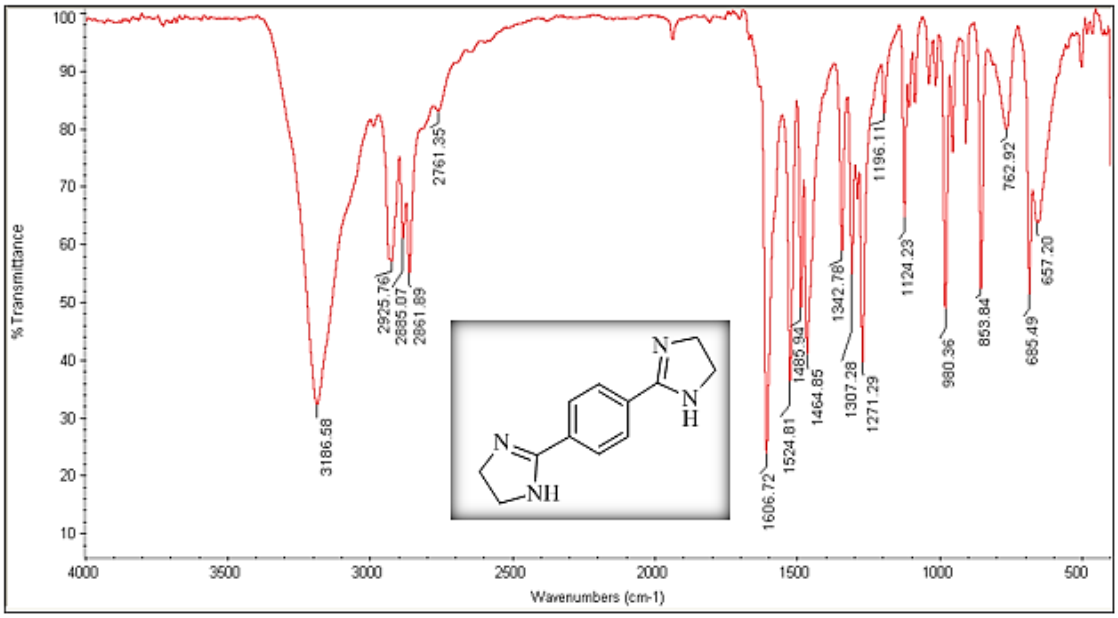

Figure 26. FT-IR (KBr) spectrum of 1,4-Bis (4,5-dihydroimidazol-2-yl) benzene (**5a**).

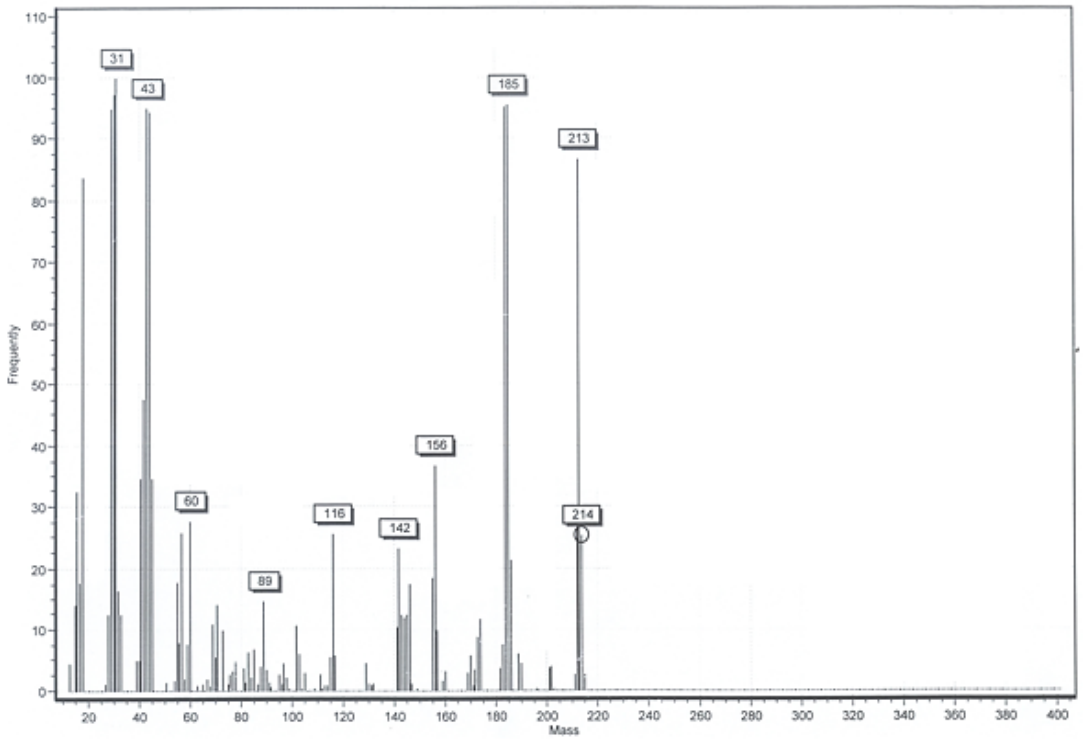

Figure 27. Mass spectrum of 1,4-Bis (4,5-dihydroimidazol-2-yl) benzene (**5a**).

2-(3-Methylphenyl) imidazoline (6a). Light yellow solid, mp 176–178 °C (Lit.[4] 178–179 °C). *m/z* (ESI) 160 (20%, M^+). ν_{max} (KBr)/cm^{-1} 3296 (NH), 3060 (Ph), 2939 (CH_2), 2872 (CH_2), 1660 (C=N). δ_C ($CDCl_3$, 75 MHz) 7.66 (s, 1H, Ph), 7.55 (d, *J* 6 Hz, 1H, Ph), 7.29–7.27 (m, 2H, Ph), 5.16 (s, 1H, NH), 3.78 (s, 4H, $2CH_2$), 2.38 (s, 3H, CH_3).

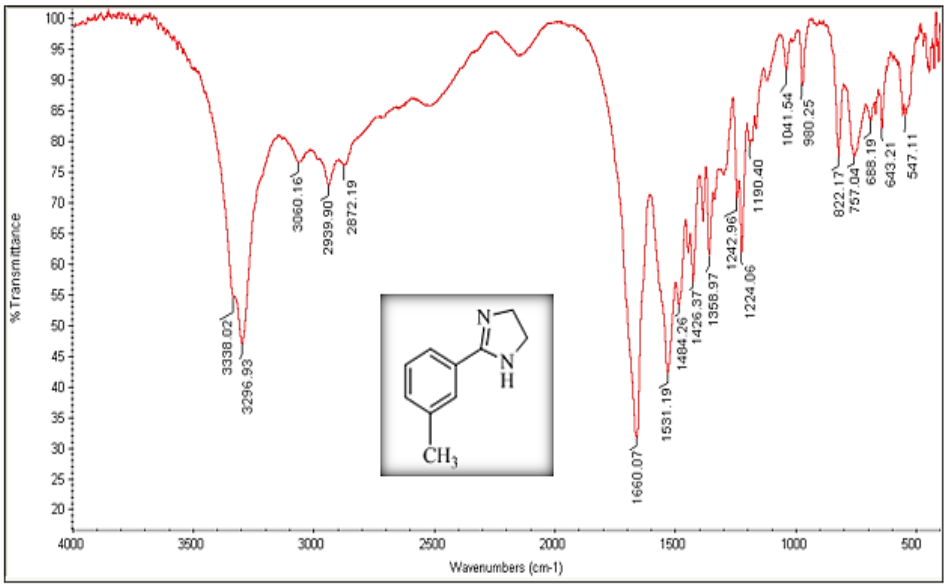

Figure 28. FT-IR (KBr) spectrum of 2-(3-Methylphenyl) imidazoline (**6a**).

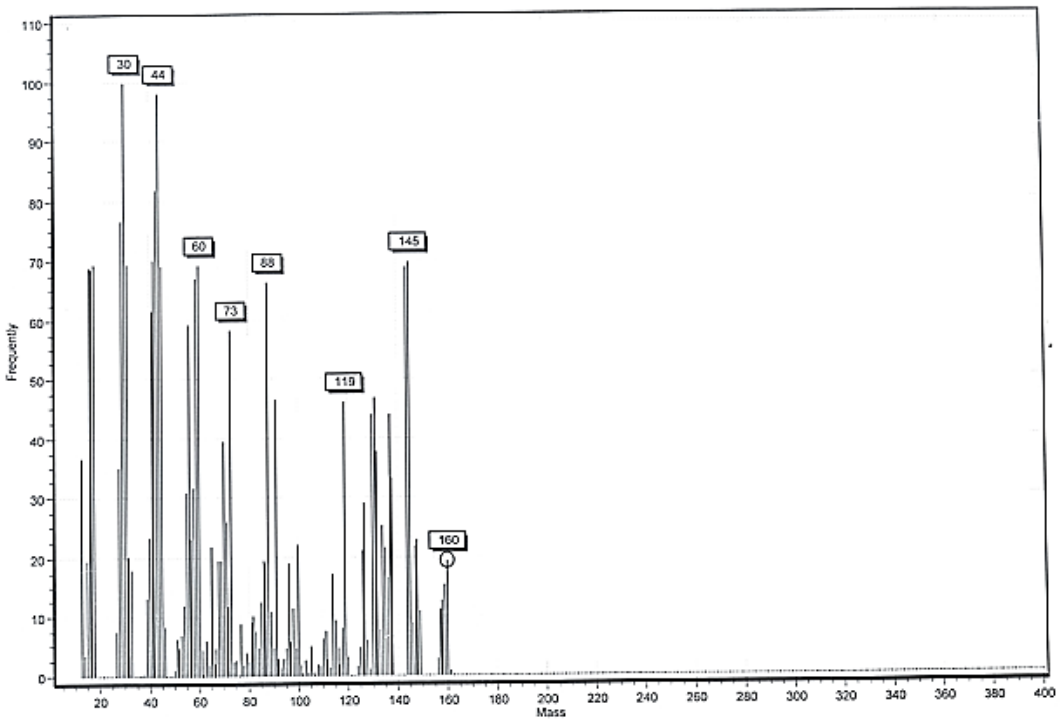

Figure 29. Mass spectrum of 2-(3-Methylphenyl) imidazoline (**6a**).

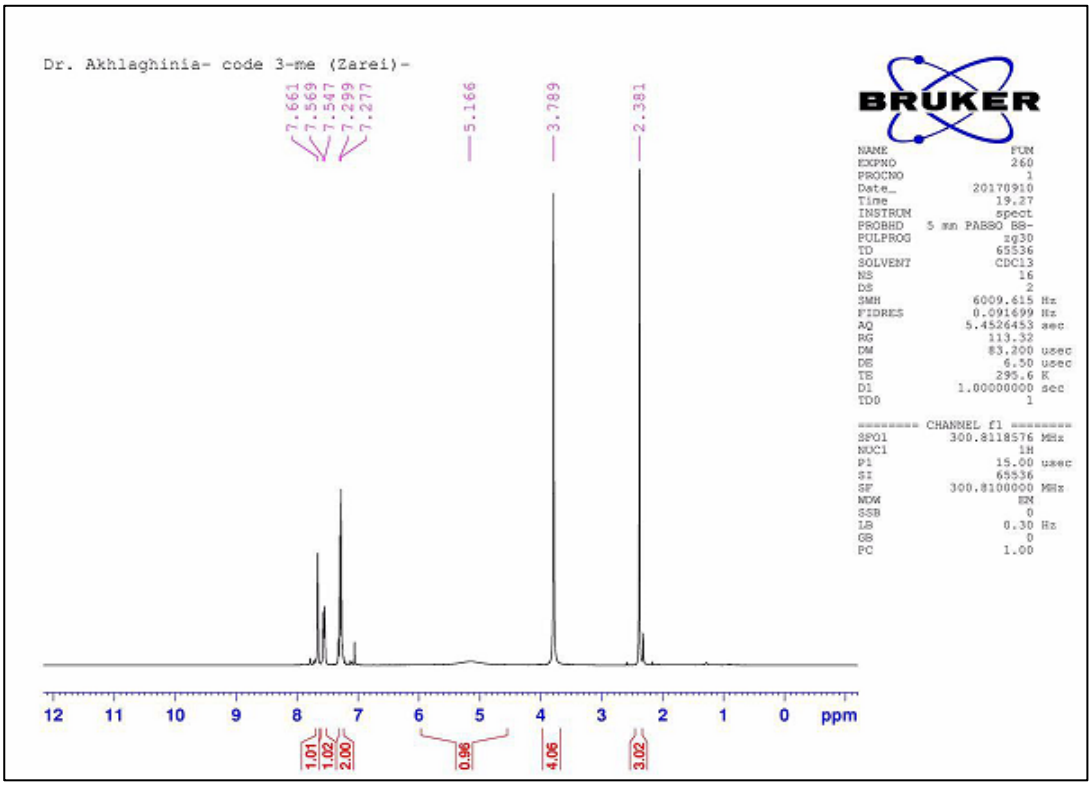

Figure 30. ^{1}H NMR (300 MHz, $CDCl_3$) spectrum 2-(3-Methylphenyl) imidazoline (**6a**).

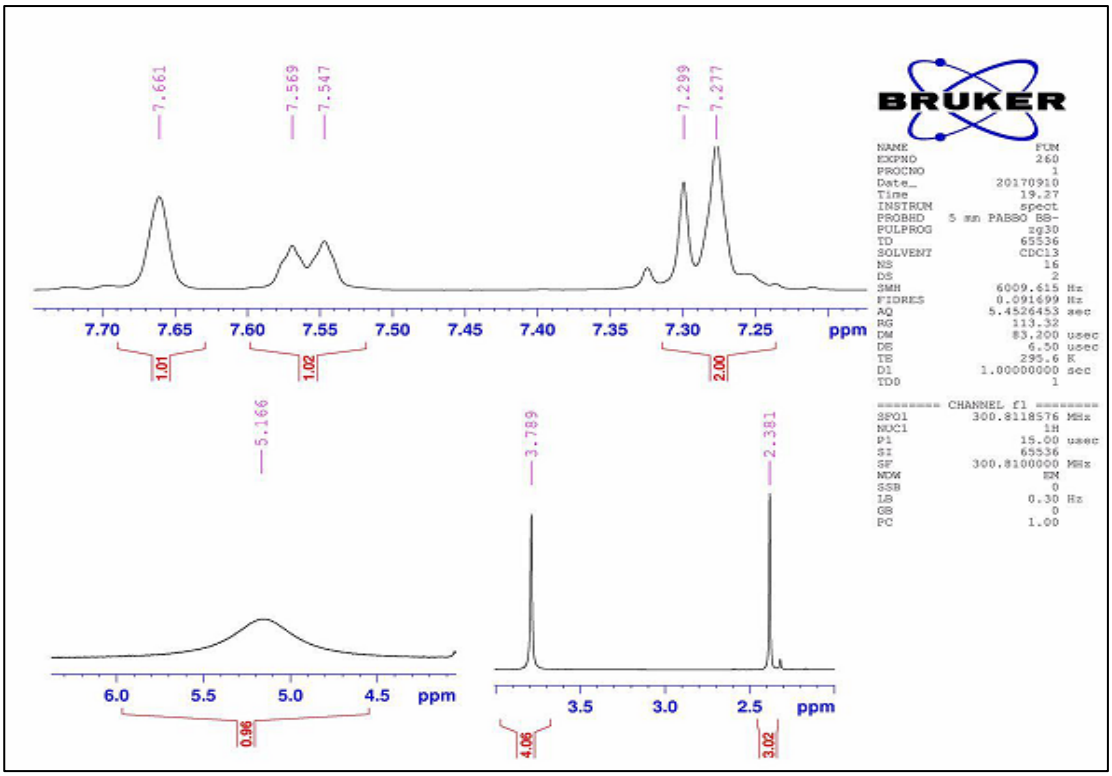

Figure 31. ^{1}H NMR (300 MHz, $CDCl_3$) spectrum 2-(3-Methylphenyl) imidazoline (**6a**) expanded.

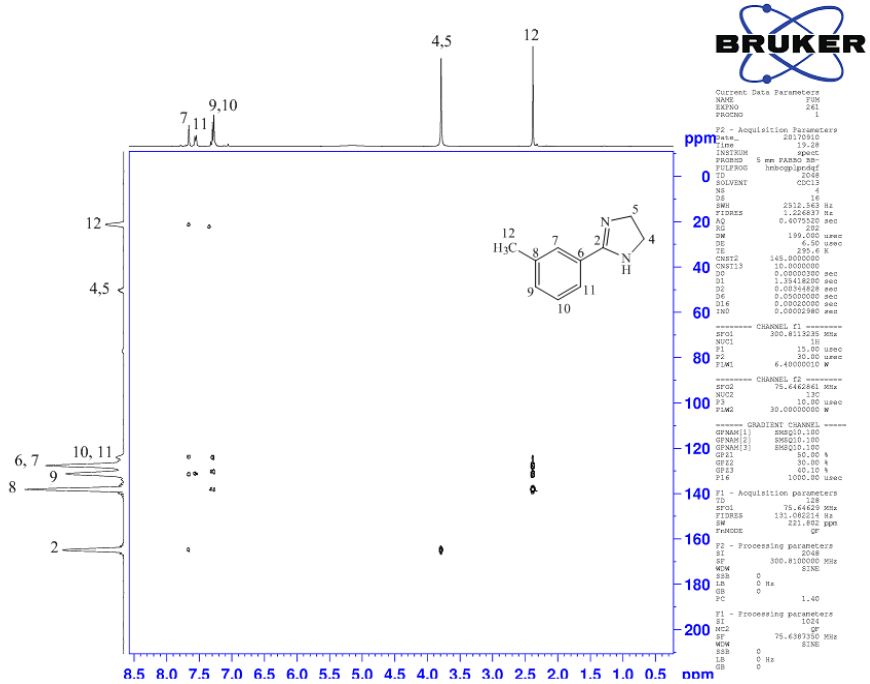

Figure 32. HMBC spectrum of 2-(3-Methylphenyl) imidazoline (**6a**).

2-(3-Methylphenyl) oxazoline (6b). Yellow oily liquid. *m/z* (ESI) 162 (4%, M^+). δ_H ($CDCl_3$, 300 MHz) 7.80–7.74 (m, 2H, Ph), 7.36–7.29 (m, 2H, Ph), 4.45 (t, *J* 9.6 Hz, 2H, CH_2), 4.06 (t, *J* 9.6 Hz, 2H, CH_2), 2.40 (s, 3H, CH_3).[5]

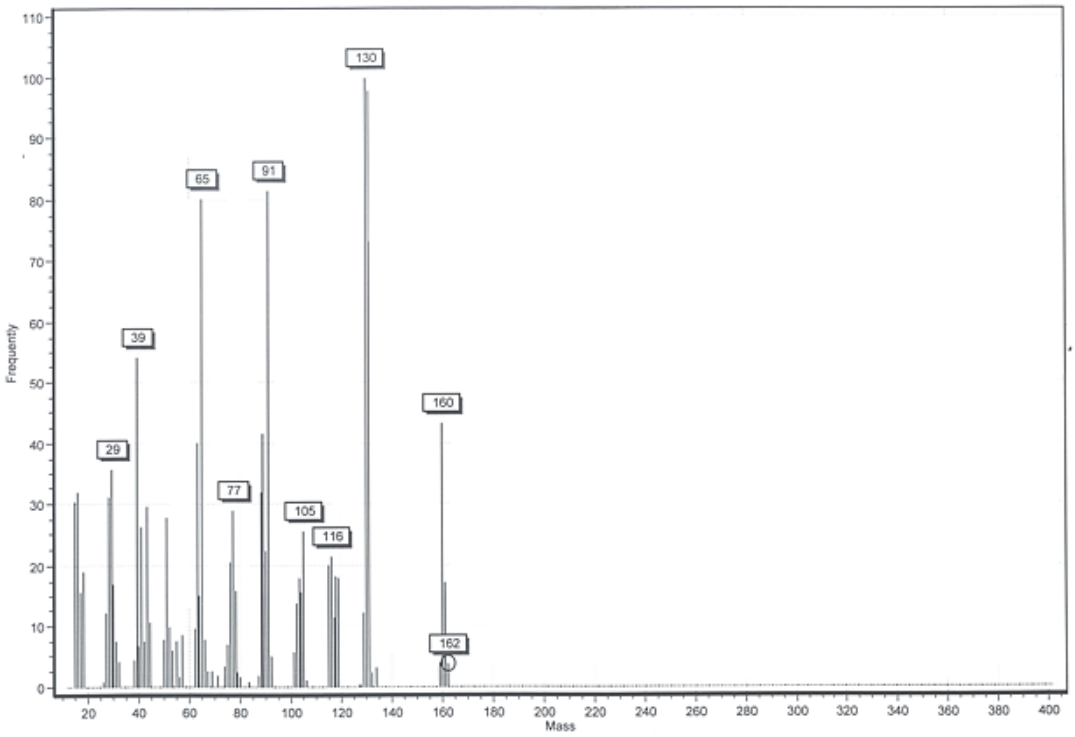

Figure 33. Mass spectrum of 2-(3-Methylphenyl) oxazoline (**6b**).

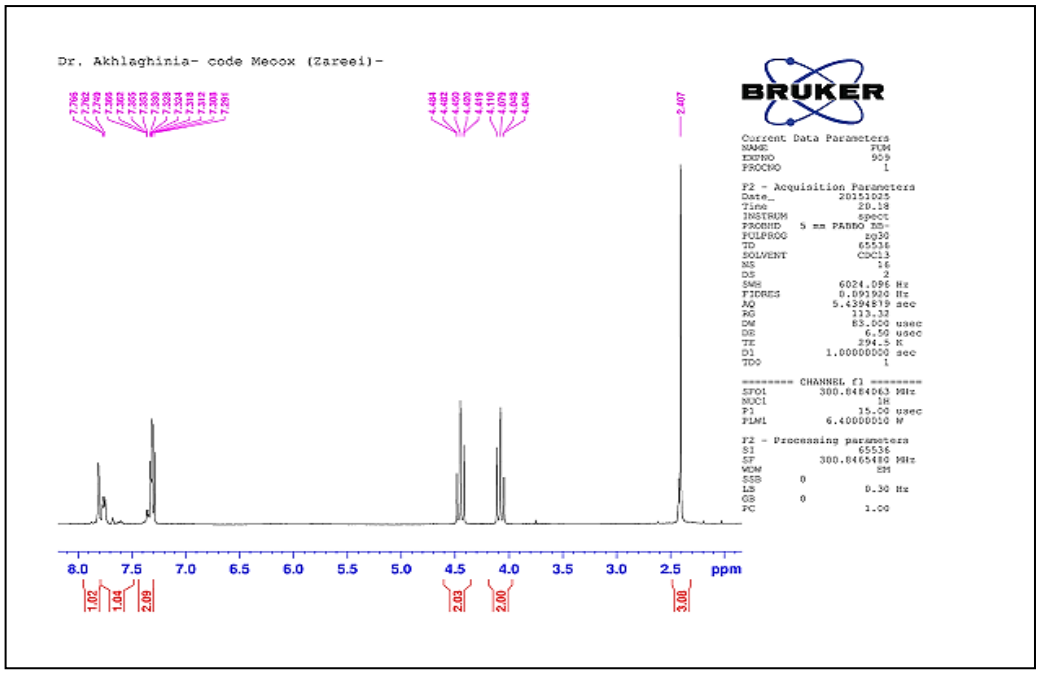

Figure 34. ^1H NMR (300 MHz, $CDCl_3$) spectrum of 2-(3-Methylphenyl) oxazoline (**6b**).

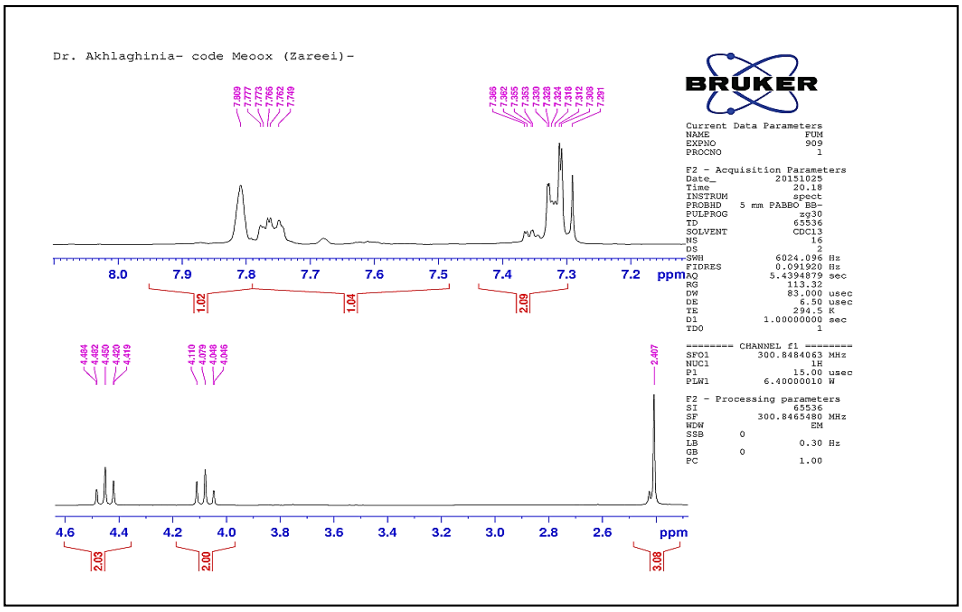

Figure 35. ^{1}H NMR (300 MHz, $CDCl_3$) spectrum of 2-(3-Methylphenyl) oxazoline (**6b**) expanded.

2-(3-Methylphenyl) thiazoline (6c). Yellow oily liquid. *m/z* (ESI) 178 (48%, M^+). δ_H ($CDCl_3$, 300 MHz) 7.58 (s, 1H, Ph), 7.53 (d, *J* 6 Hz, 1H, Ph), 7.22–7.15 (m, 2H, Ph), 4.35 (t, *J* 8.4 Hz, 2H, CH_2), 3.29 (t, *J* 8.4 Hz, 2H, CH_2), 2.29 (s, 3H, CH_3). $^{6}\delta_C$ ($CDCl_3$, 75 MHz) 168.7, 138.2, 133.1, 131.9, 128.8, 128.4, 125.6, 65.1, 33.5, 21.2.

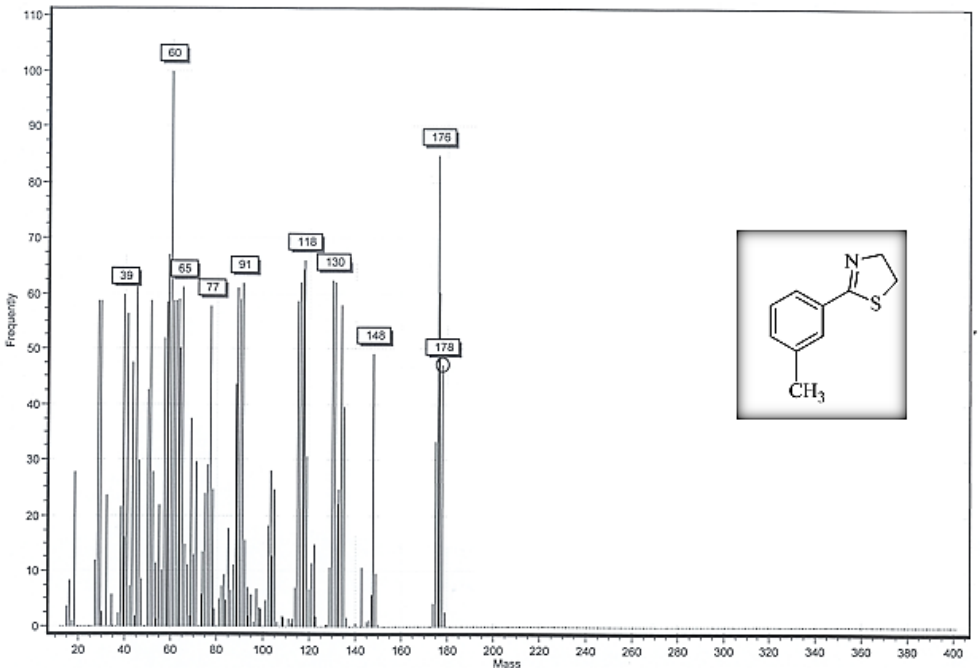

Figure 36. Mass spectrum of 2-(3-Methylphenyl) thiazoline (**6c**).

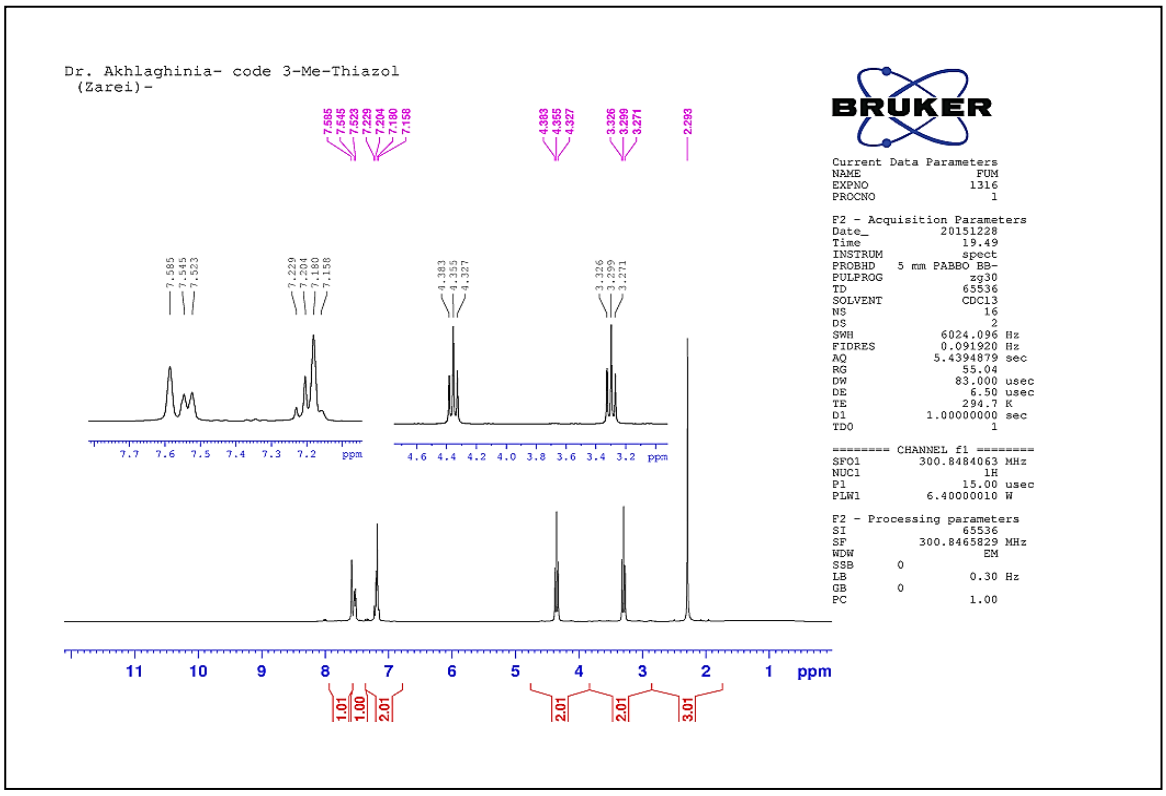

Figure 37. ^{1}H NMR (300 MHz, $CDCl_3$) spectrum of 2-(3-Methylphenyl) thiazoline (**6c**).

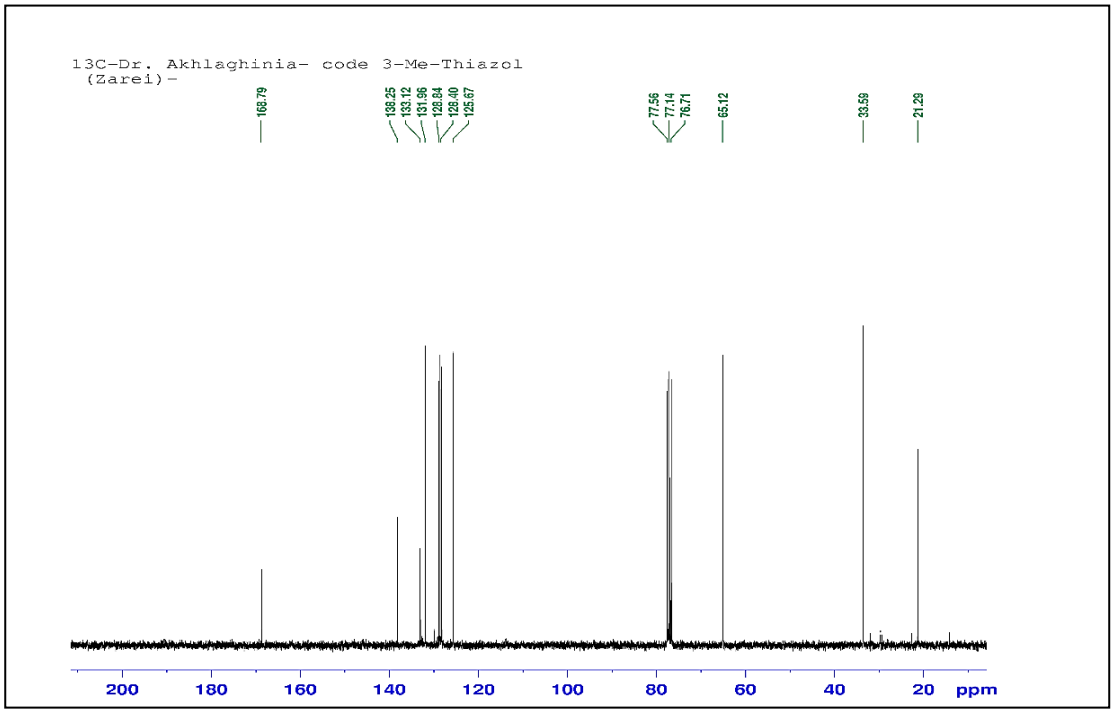

Figure 38. ^{13}C NMR (75 MHz, $CDCl_3$) spectrum of 2-(3-Methylphenyl) thiazoline (**6c**).

2-(4-Ethoxyphenyl) imidazoline (7a). White solid, mp 176–178 °C (Lit.[7] 177.4–179 °C). ν_{max} (KBr)/cm^{-1} 3186 (NH), 3055 (Ph), 2973 (CH_2), 2929 (CH_2), 1619 (C=N). *m/z* (ESI) 190 (74%, M^+). δ_H ($CDCl_3$ + DMSO, 300 MHz) 7.73 (d, *J* 9 Hz, 2H, Ph), 6.67 (d, *J* 9 Hz, 2H, Ph), 4.02 (q, *J* 6.9 Hz, 2H, CH_2), 3.85 (brs, 1H, NH), 3.60 (s, 4H, $2CH_2$), 1.33 (t, *J* 9 Hz, 3H, CH_3). δ_C ($CDCl_3$ + DMSO, 75 MHz) 168.8, 165.5, 133.9, 127.3, 118.9, 68.3, 54.3, 19.7.

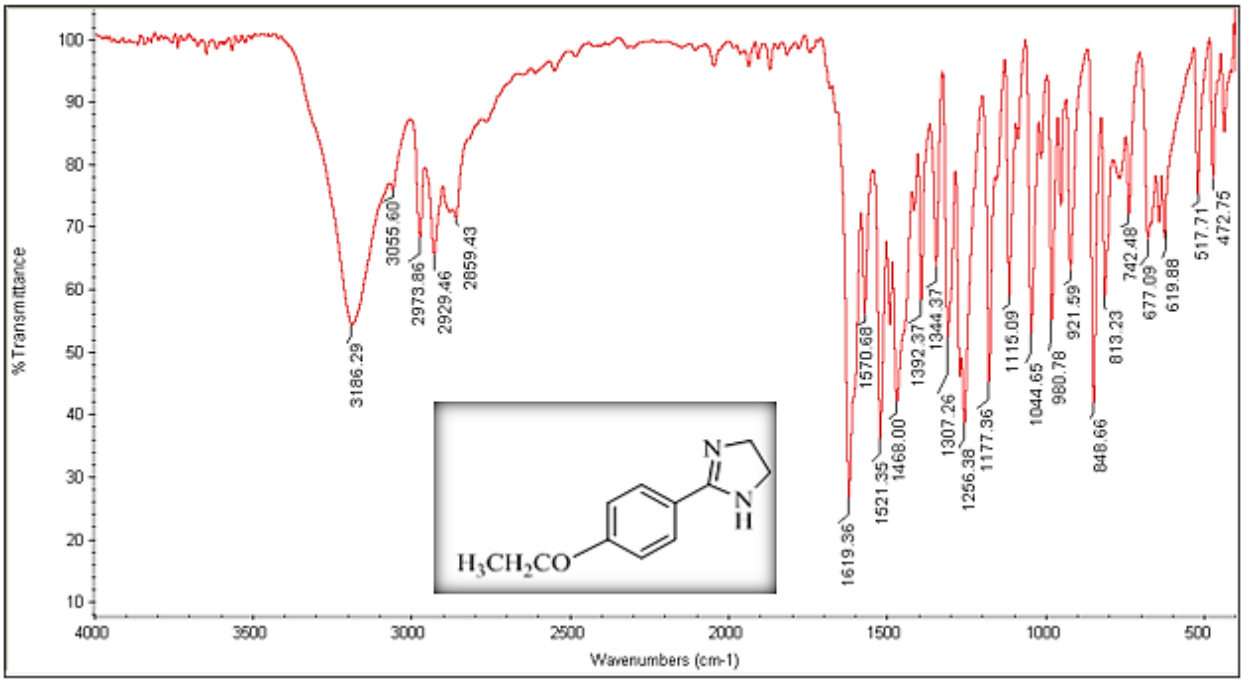

Figure 39. FT-IR (KBr) spectrum of 2-(4-Ethoxyphenyl) imidazoline (**7a**).

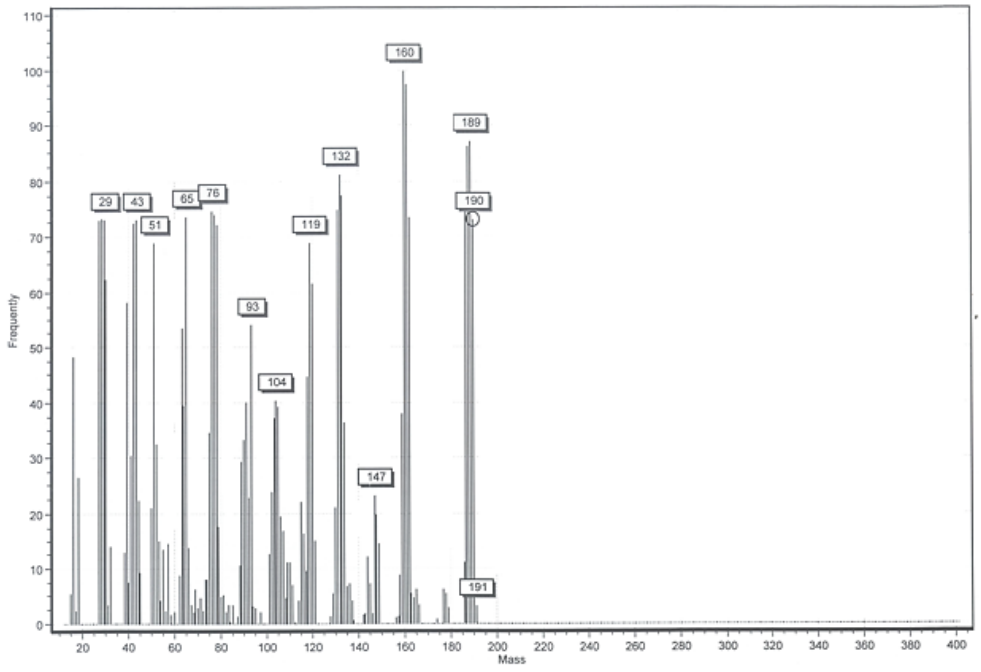

Figure 40. Mass spectrum of 2-(4-Ethoxyphenyl) imidazoline (**7a**).

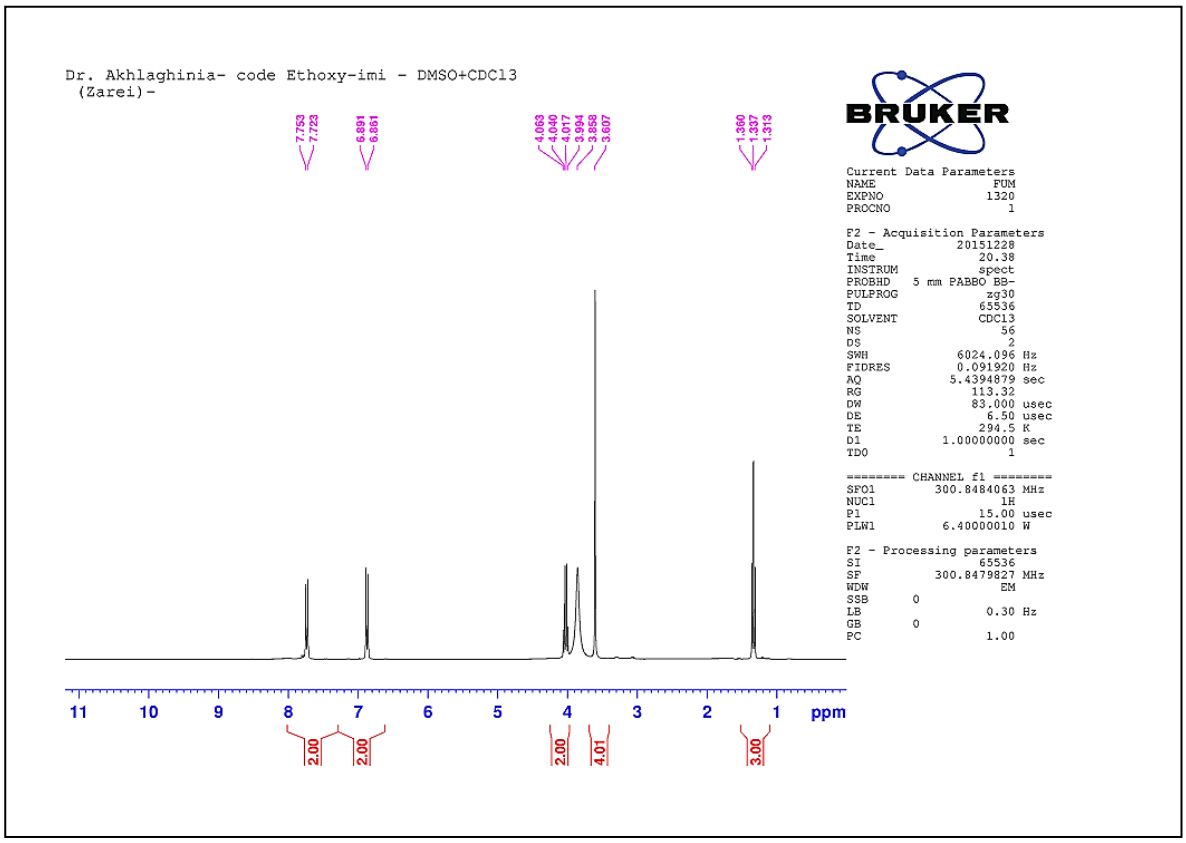

Figure 41. ^{1}H NMR (300 MHz, $CDCl_3$) spectrum of 2-(4-Ethoxyphenyl) imidazoline (**7a**).

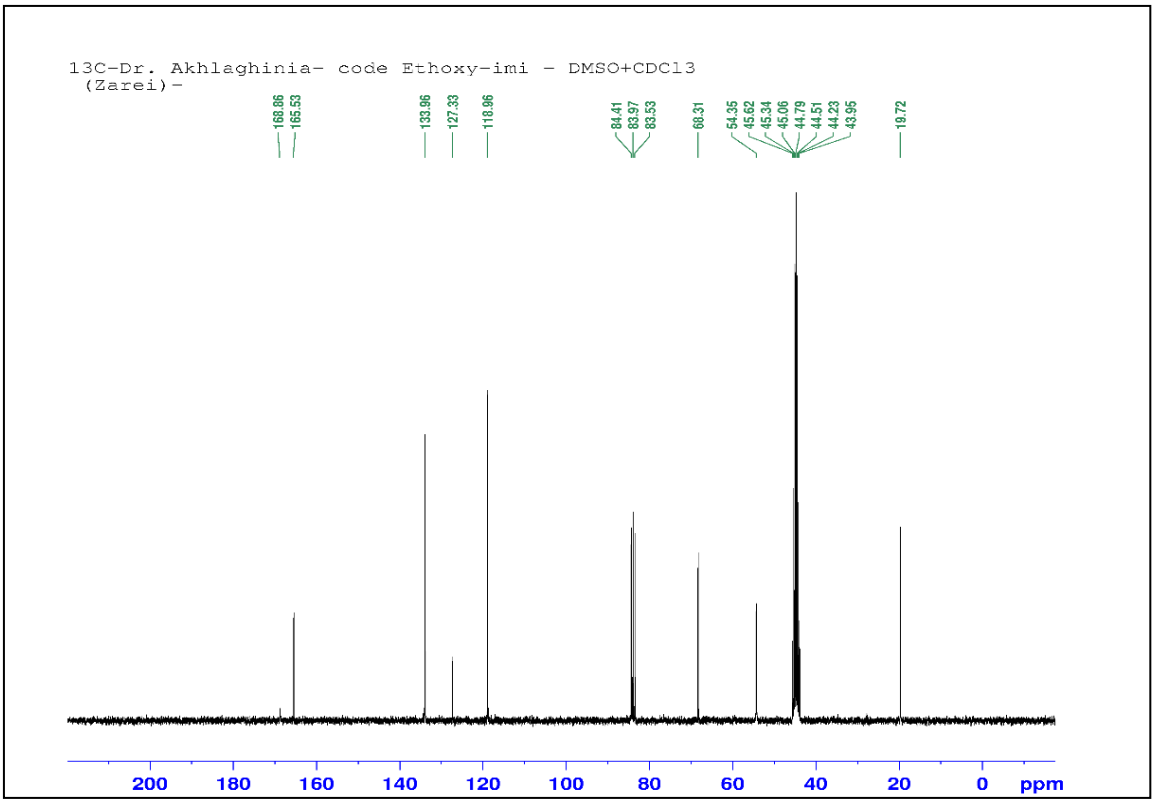

Figure 42. ^{13}C NMR (75 MHz, $CDCl_3$) spectrum of 2-(4-Ethoxyphenyl) imidazoline (**7a**).

2-(4-Ethoxyphenyl) oxazoline (7b). White solid, mp 120–122 °C (Lit.[8] 122–123 °C). *m/z* (ESI) 192 (38%, M^+). δ_H ($CDCl_3$, 300 MHz) 7.88 (d, *J* 9 Hz, 2H, Ph), 6.90 (d, *J* 9 Hz, 2H, Ph), 4.41 (q, *J* 9 Hz, 2H, CH_2), 4.11–4.01 (m, 4H, $2CH_2$), 1.44 (t, *J* 9 Hz, 3H, CH_3).

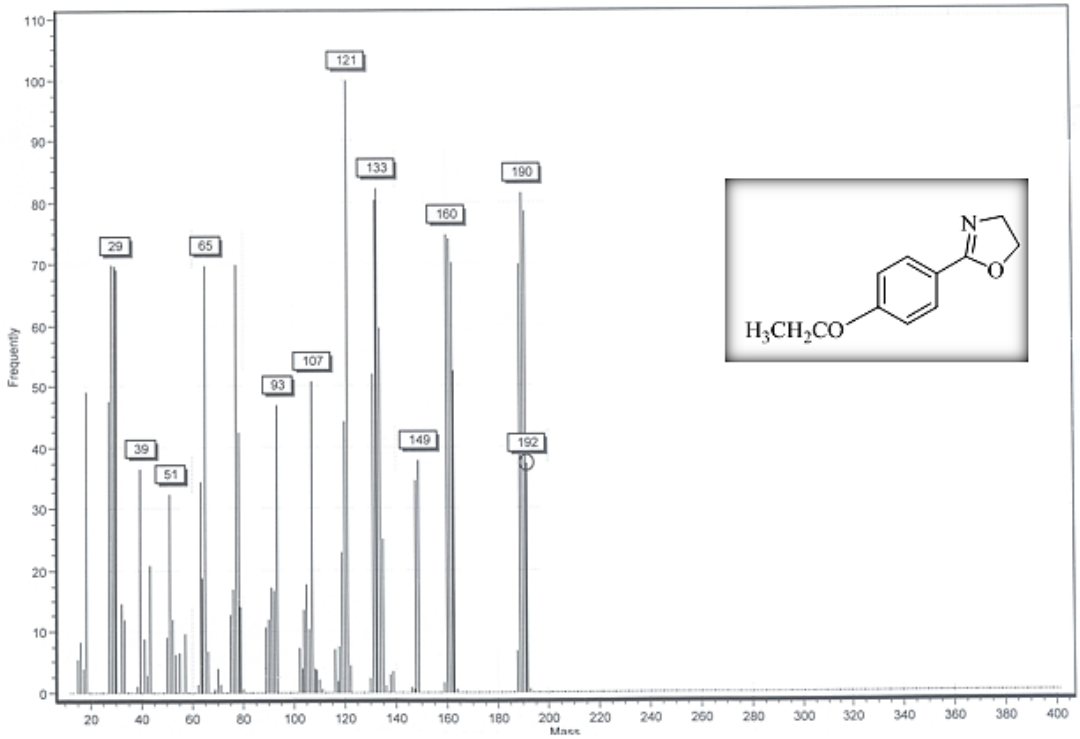

Figure 43. Mass spectrum of 2-(4-Ethoxyphenyl) oxazoline (**7b**).

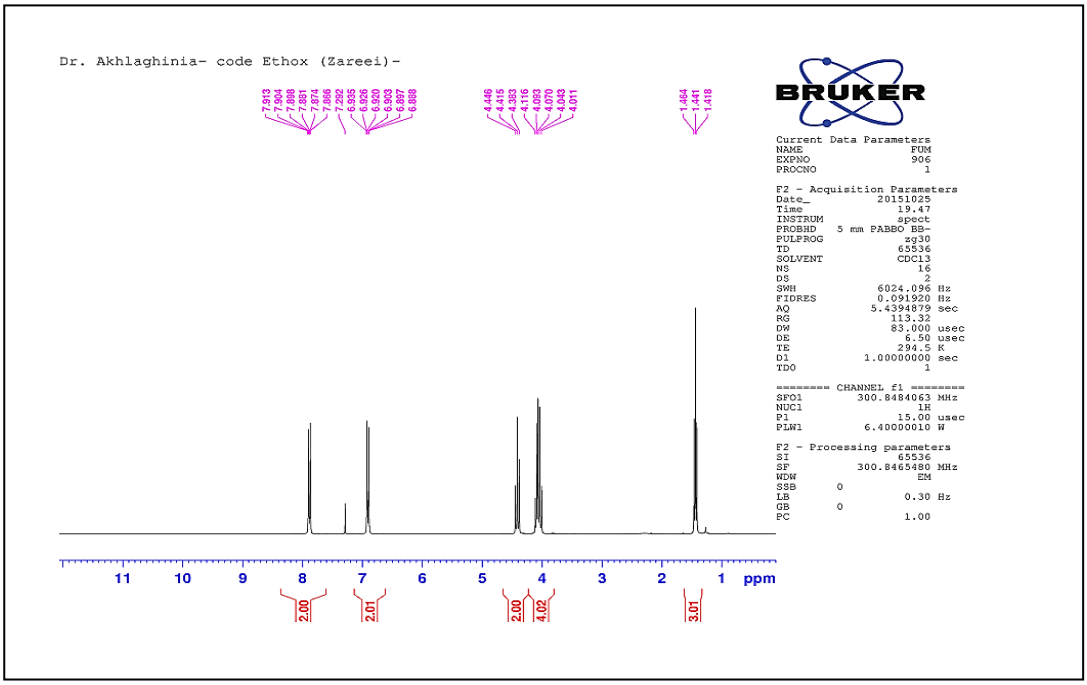

Figure 44. ^1H NMR (300 MHz, $CDCl_3$) spectrum of 2-(4-Ethoxyphenyl) oxazoline (**7b**).

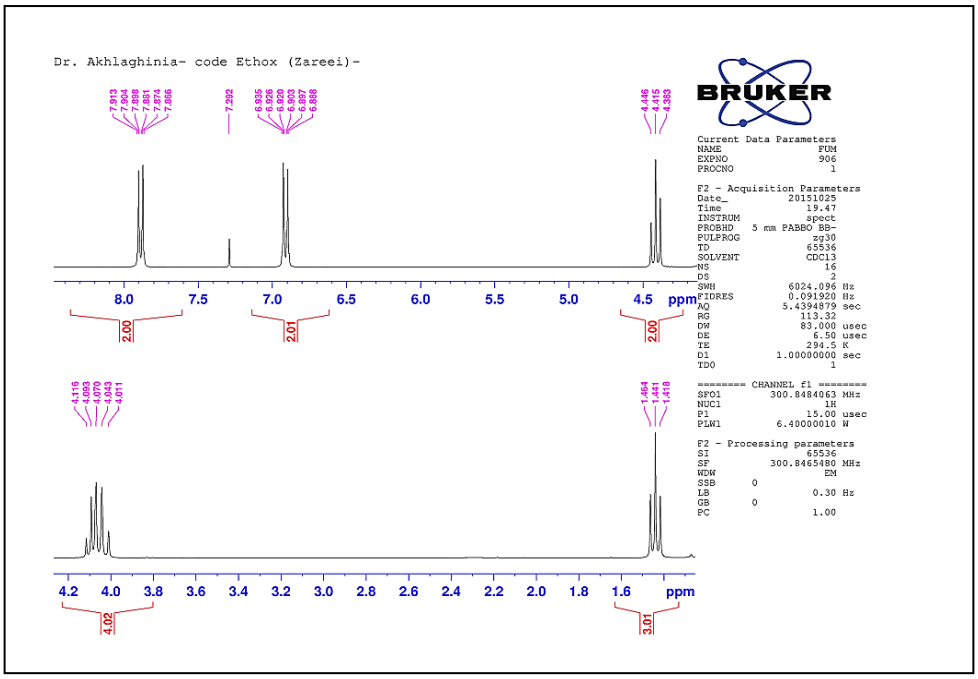

Figure 45. ^{1}H NMR (300 MHz, $CDCl_3$) spectrum of 2-(4-Ethoxyphenyl) oxazoline (**7b**) expanded.

2-(3,4,5-Trimethoxyphenyl)imidazoline (8a). Cream solid, mp 182 °C. ν_{max} (KBr)/cm^{-1} 3118 (NH), 2998 (CH_2), 2864 (CH_2), 2843 (CH_2), 1606 (C=N). [9] *m/z* (ESI) 236 (38%, M^+). δ_H ($CDCl_3$, 300 MHz) 7.29 (s, 2H, Ph), 3.90 (s, 4H, $2CH_2$), 3.61 (s, 9H, $3OCH_3$). δ_C ($CDCl_3$, 75 MHz) 164.7, 153.2, 141.1, 122.4, 105.4, 60.9, 56.1, 48.0. Anal. Calc. for $C_{12}H_{16}N_2O_3$: C 61.00, H 6.83, N 11.86. Found: C 60.52, H 6.53, N 11.92%.

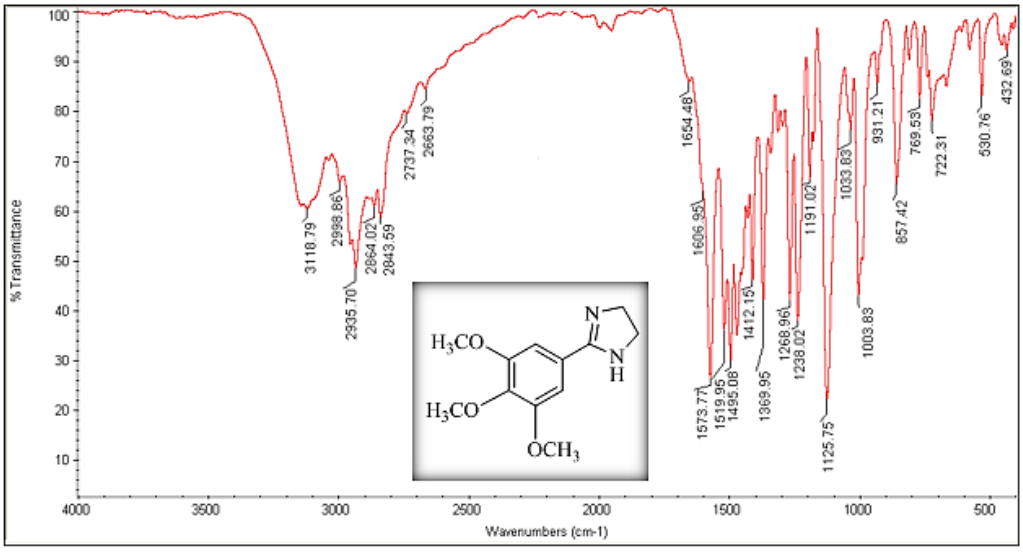

Figure 46. FT-IR (KBr) spectrum of 2-(3,4,5-Trimethoxyphenyl) imidazoline (**8a**).

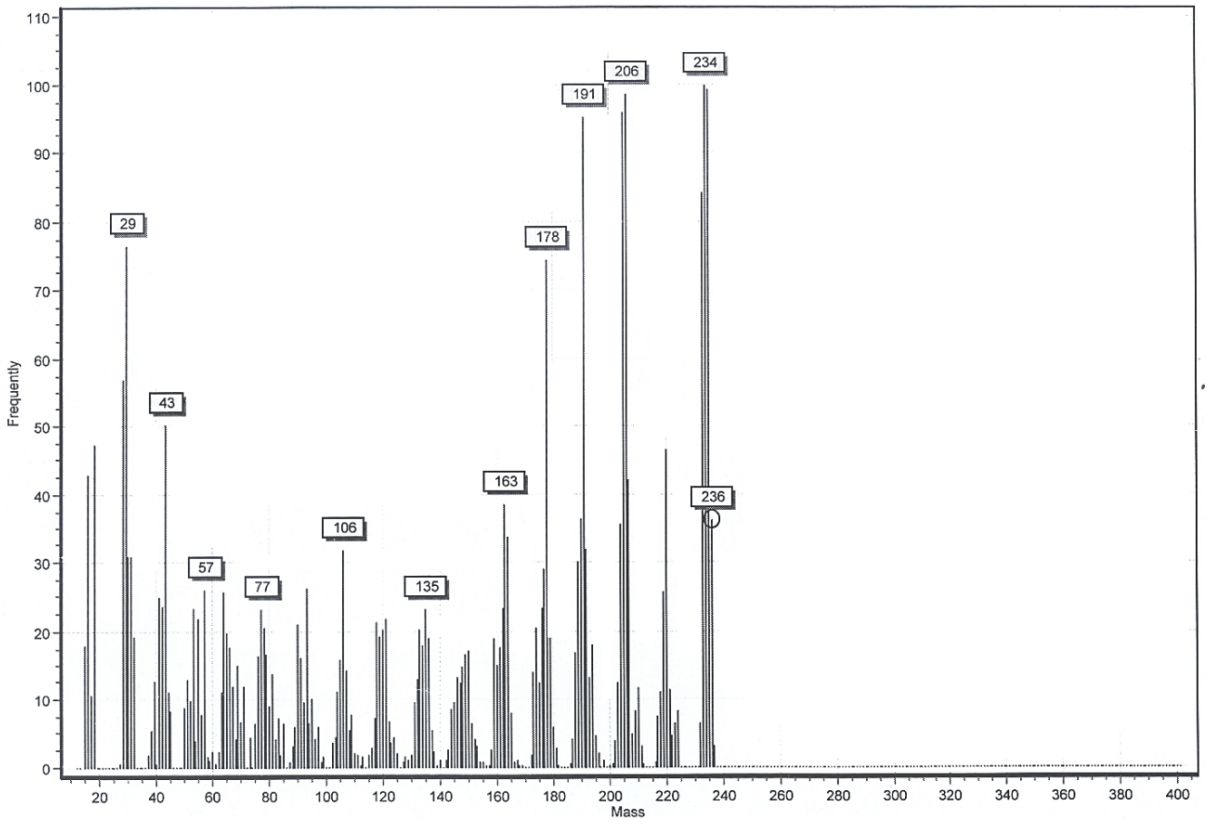

Figure 47. Mass spectrum of 2-(3,4,5-Trimethoxyphenyl) imidazoline (**8a**).

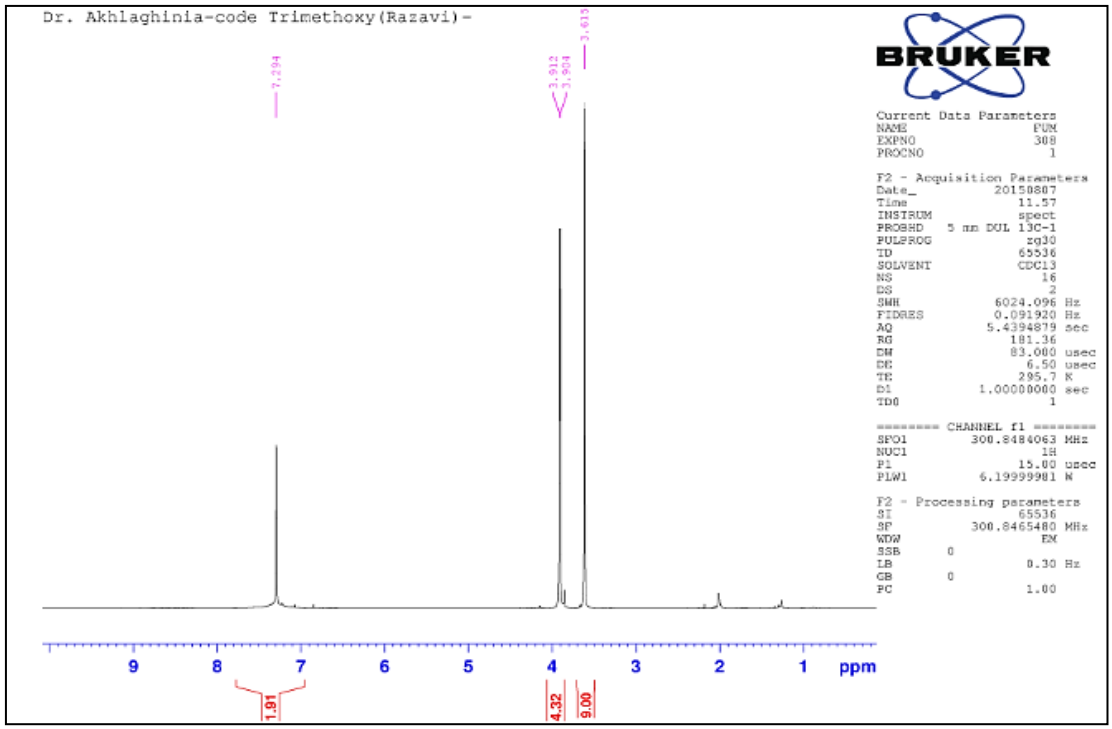

Figure 48. ^{1}H NMR (300 MHz, $CDCl_3$) spectrum of 2-(3,4,5-Trimethoxyphenyl) imidazoline (**8a**).

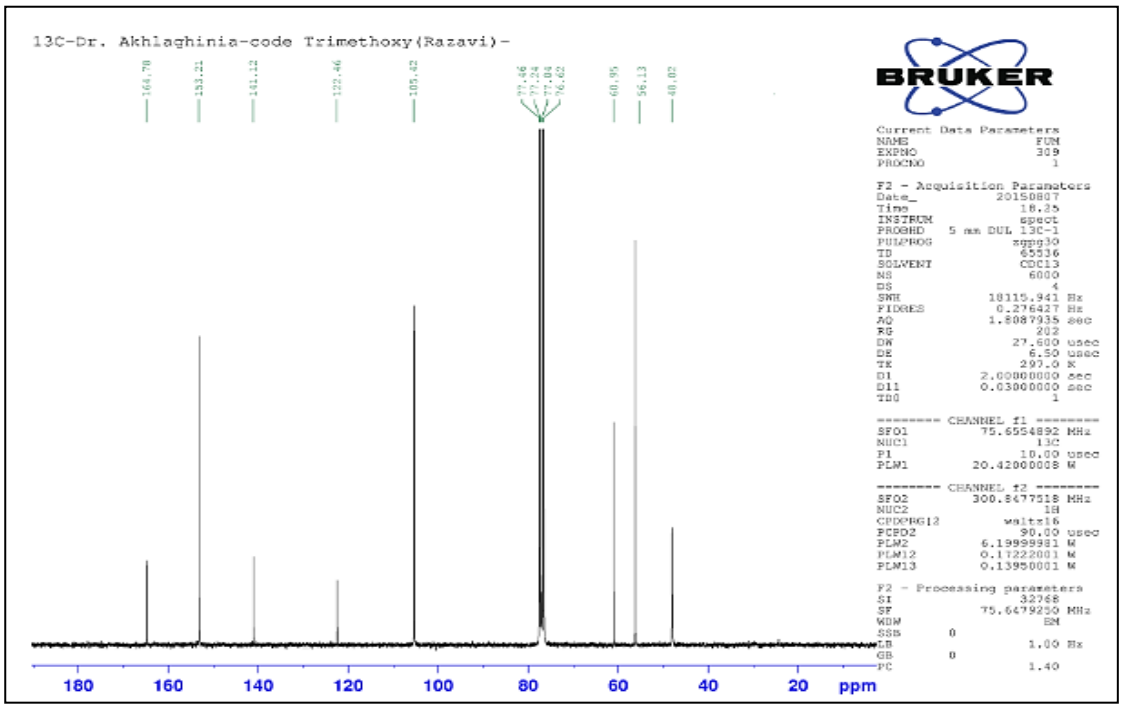

Figure 49. ^{13}C NMR (75 MHz, $CDCl_3$) spectrum of 2-(3,4,5-Trimethoxyphenyl) imidazoline (**8a**).

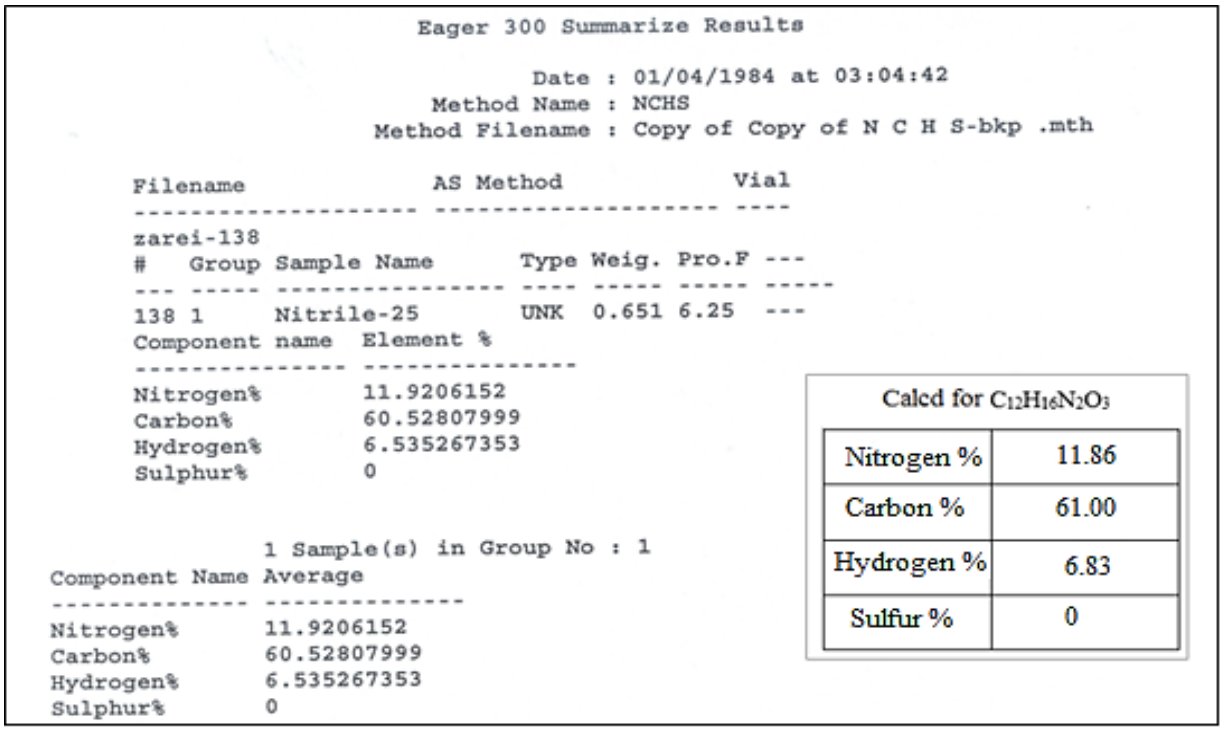

Eager 300 Summarize Results

Date : 01/04/1984 at 03:04:42
Method Name : NCHS
Method Filename : Copy of Copy of N C H S-bkp .mth

Filename	AS Method	Vial
zarei-138		

#	Group	Sample Name	Type	Weig.	Pro.F		
138	1	Nitrile-25	UNK	0.651	6.25	---	

Component name	Element %
Nitrogen%	11.9206152
Carbon%	60.52807999
Hydrogen%	6.535267353
Sulphur%	0

1 Sample(s) in Group No : 1

Component Name	Average
Nitrogen%	11.9206152
Carbon%	60.52807999
Hydrogen%	6.535267353
Sulphur%	0

Calcd for $C_{12}H_{16}N_2O_3$

Nitrogen %	11.86
Carbon %	61.00
Hydrogen %	6.83
Sulfur %	0

Figure 50. CHN analysis data of 2-(3,4,5-Trimethoxyphenyl) imidazoline (**8a**).

2-(3-Pyridyl) imidazoline (9a). Yellow solid, mp 105–107 °C (Lit.[2] 106–108 °C). *m/z* (ESI)147 (92%, M^+). δ_H ($CDCl_3$, 300 MHz) 8.96 (d, *J* 2.1 Hz, 1H, Pyridine), 8.65 (dd, *J* 4.8

Hz, *J* 1.5 Hz, 1H, Pyridine), 8.11 (dt, *J* 7.8 Hz, *J* 2.1 Hz, 1H, Pyridine), 7.35–7.29 (m, 1H, pyridine), 4.82 (brs, 1H, NH), 3.80 (s, 4H, $2CH_2$).

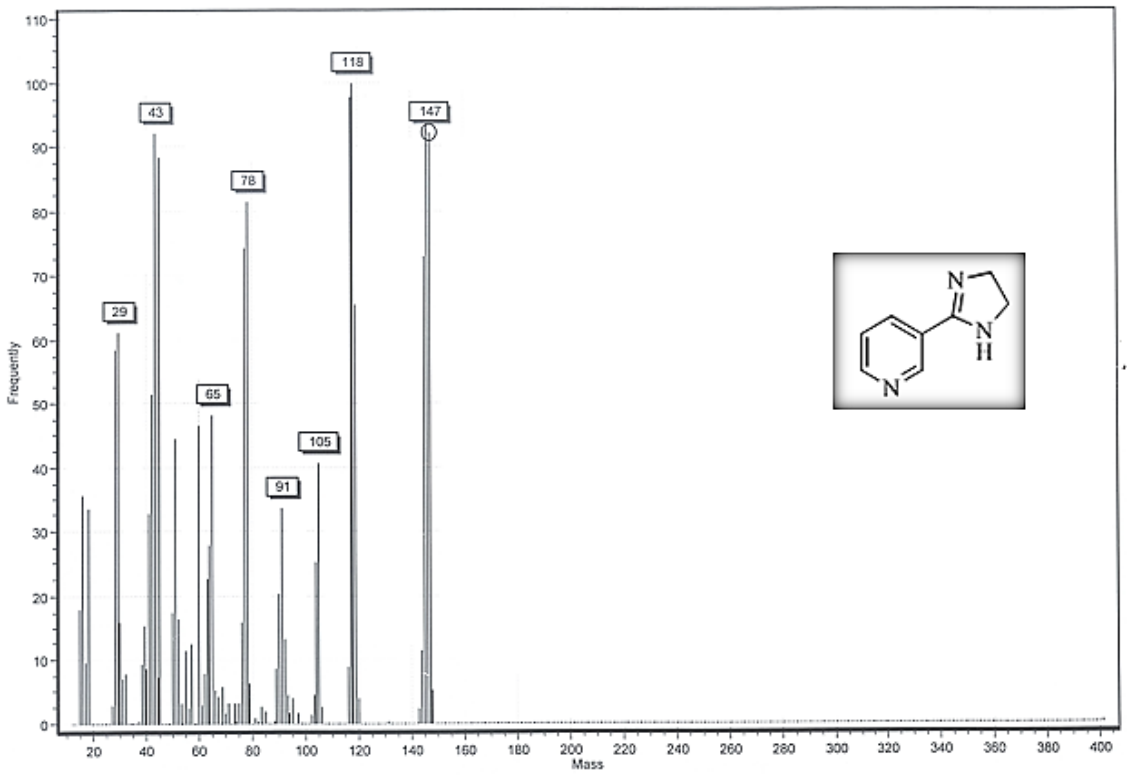

Figure 51. Mass spectrum of 2-(3-Pyridyl) imidazoline (**9a**).

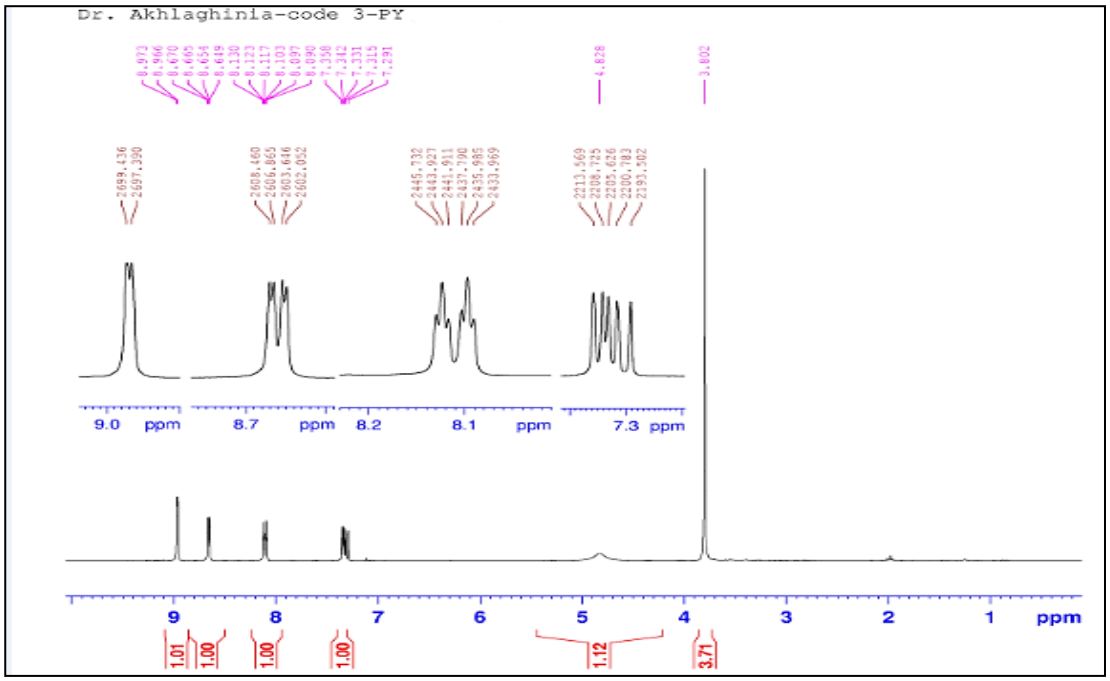

Figure 52. ^1H NMR (300 MHz, $CDCl_3$) spectrum of 2-(3-Pyridyl) imidazoline (**9a**).

2-(3-Pyridyl) oxazoline (9b). Cream solid, mp 65–67 °C (Lit.[2] 66–68 °C). *m/z* (ESI) 149 (24%, M^+). δ_H ($CDCl_3$, 300 MHz) 9.15 (d, *J* 1.5 Hz, 1H, Pyridine), 8.70 (dd, *J* 4.8 Hz, *J* 1.5 Hz, 1H, Pyridine), 8.21 (dt, *J* 7.8 Hz, *J* 1.8 Hz, 1H, Pyridine), 7.38–7.33 (m, 1H, Pyridine), 4.47 (t, *J* 9.6 Hz, 2H, CH_2), 4.09 (t, *J* 9.6 Hz, 2H, CH_2).

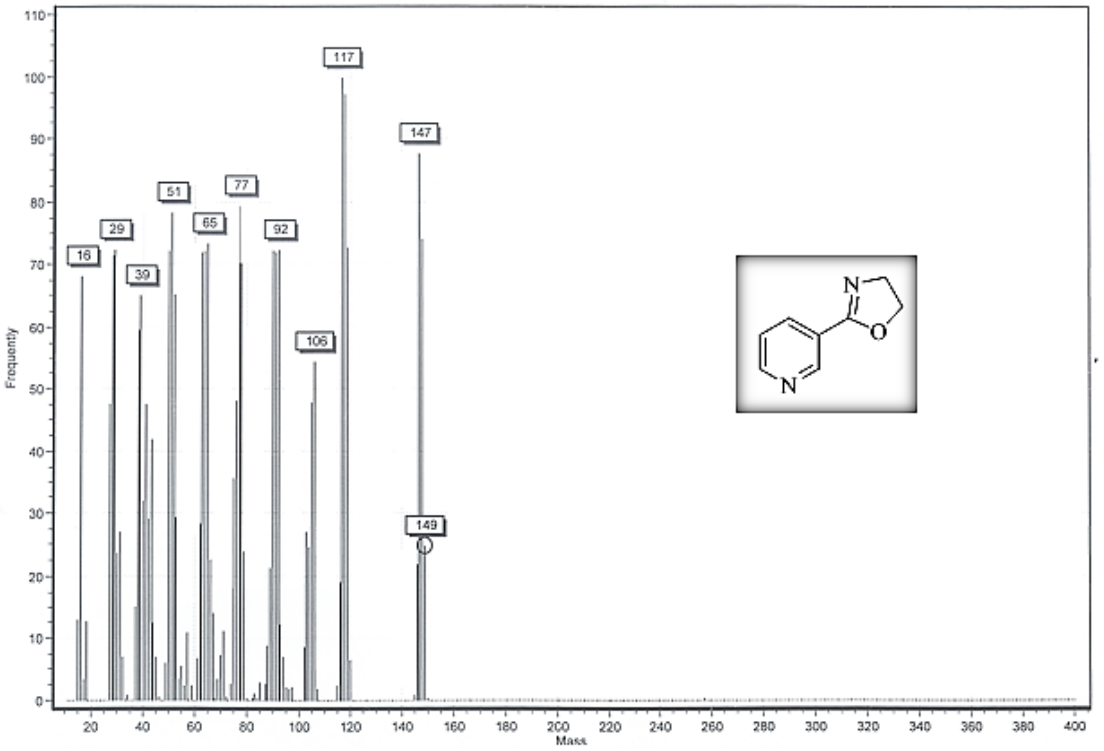

Figure 53. Mass spectrum of 2-(3-Pyridyl) oxazoline (**9b**).

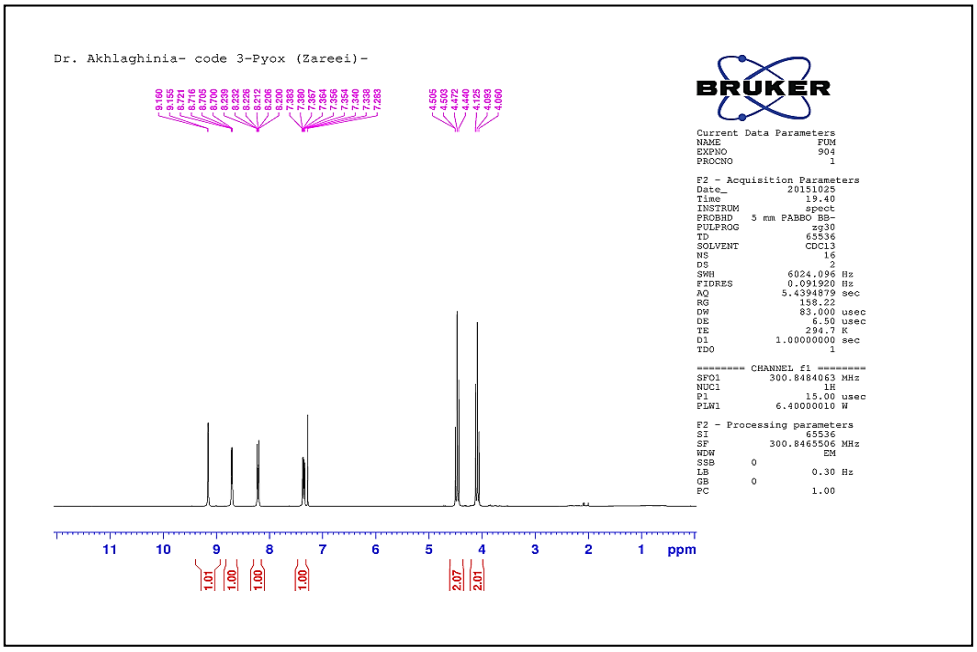

Figure 54. ^{1}H NMR (300 MHz, $CDCl_3$) spectrum of 2-(3-Pyridyl) oxazoline (**9b**).

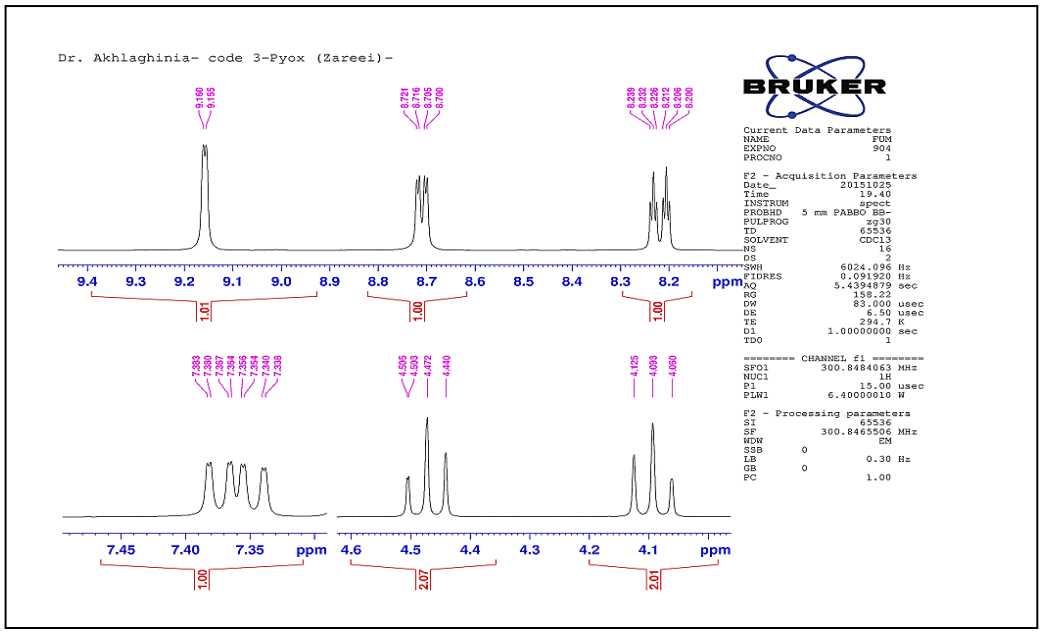

Figure 55. ^{1}H NMR (300 MHz, $CDCl_3$) spectrum of 2-(3-Pyridyl) oxazoline (**9b**) expanded.

2-(3-Pyridyl) thiazoline (9c). Yellow solid, mp 110–112 °C (Lit.[2] 111–113 °C). *m/z* (ESI) 165 (30%, M^+). δ_H ($CDCl_3$, 300 MHz) 8.96 (d, *J* 1.8 Hz, 1H, Pyridine), 8.60 (dd, *J* 4.9 Hz, *J* 1.8 Hz, 1H, Pyridine), 8.04 (dt, *J* 8.1 Hz, *J* 1.8 Hz, 1H, Pyridine), 7.31–7.28 (m, 1H, Pyridine), 4.40 (t, *J* 8.4 Hz, 2H, CH_2), 3.38 (t, *J* 8.4 Hz, 2H, CH_2). δ_C ($CDCl_3$, 75 MHz) 165.8, 151.7, 149.3, 135.5, 129.1, 123.3, 65.1, 33.8.

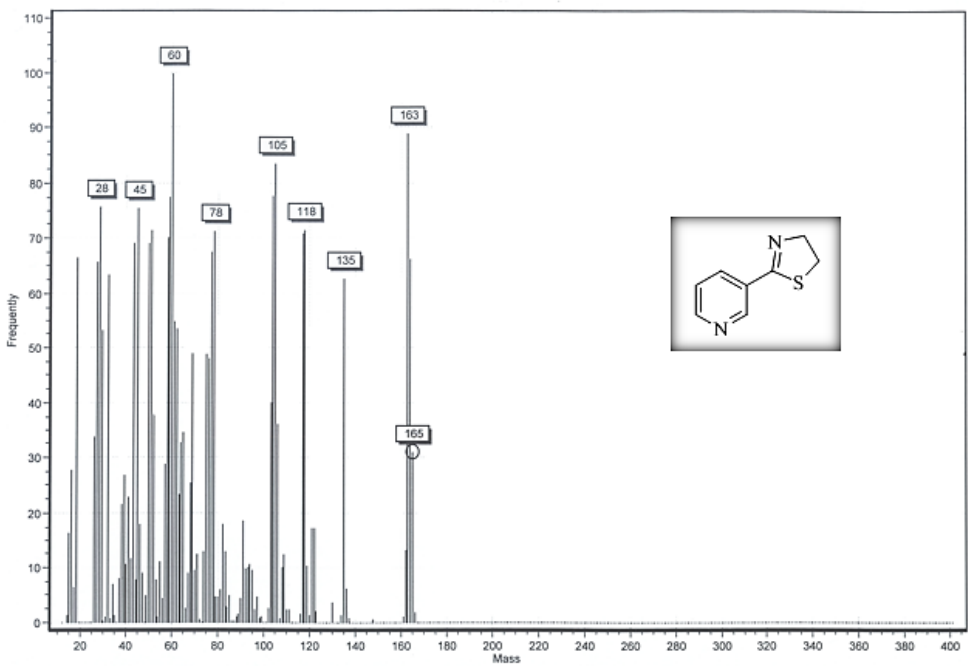

Figure 56. Mass spectrum of 2-(3-Pyridyl) thiazoline (**9c**).

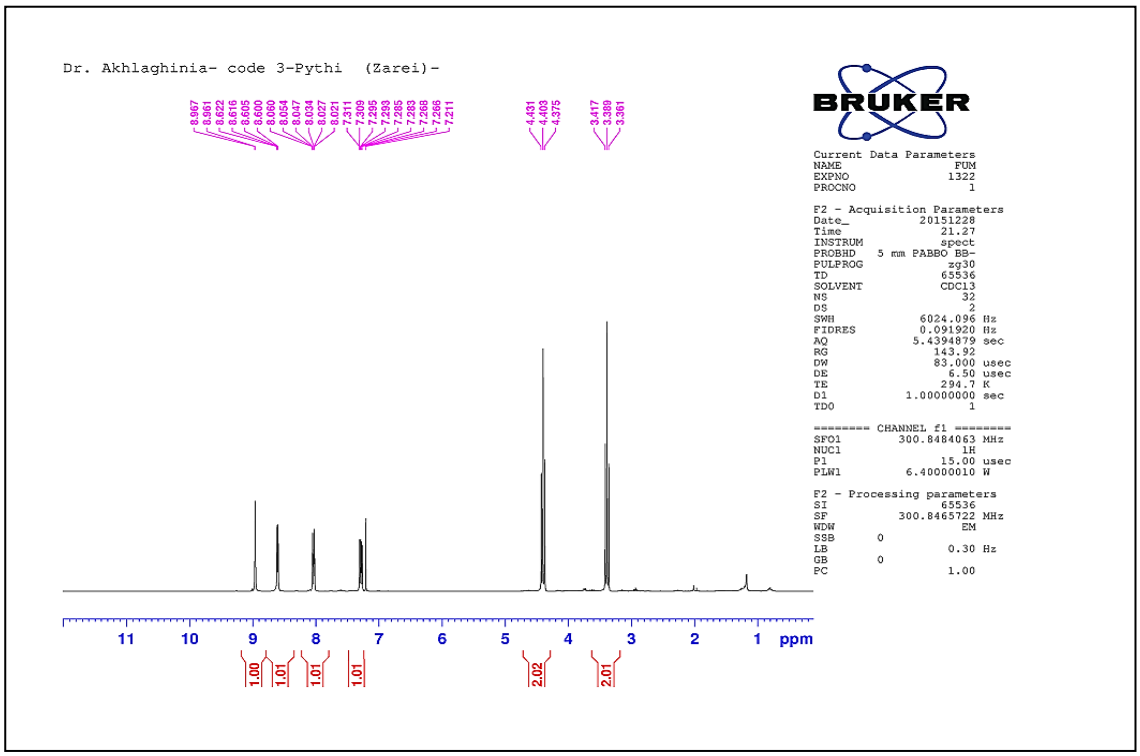

Figure 57. ^{1}H NMR (300 MHz, $CDCl_3$) spectrum of 2-(3-Pyridyl) thiazoline (**9c**).

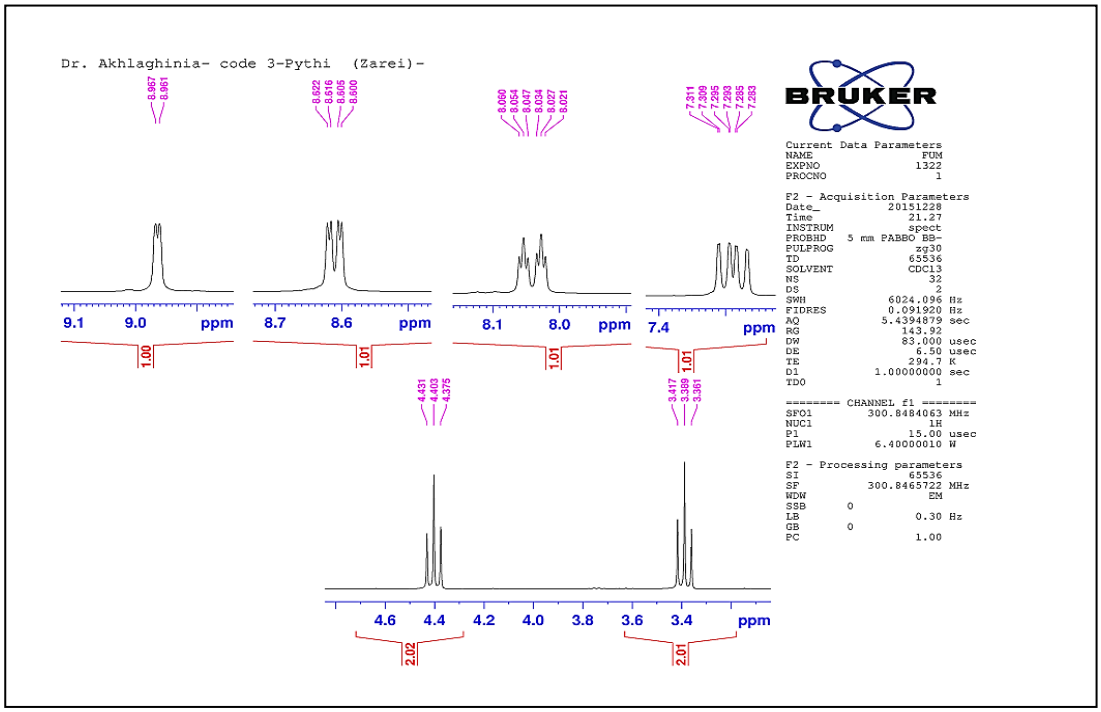

Figure 58. ^{1}H NMR (300 MHz, $CDCl_3$) spectrum of 2-(3-Pyridyl) thiazoline (**9c**) expanded.

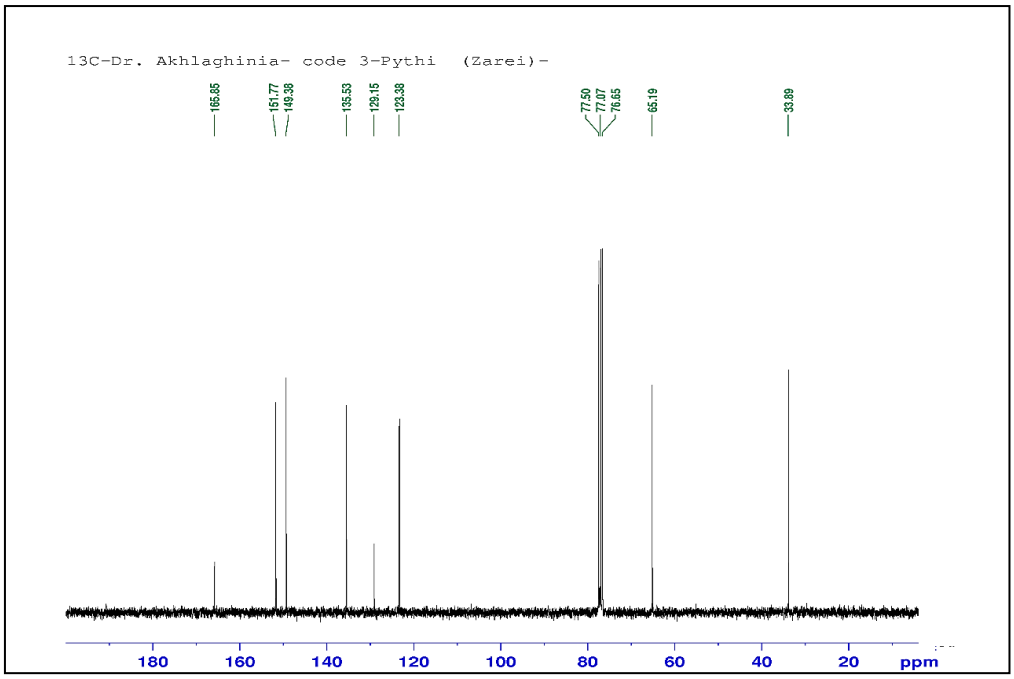

Figure 59. ^{13}C NMR (75 MHz, $CDCl_3$) spectrum of 2-(3-Pyridyl) thiazoline (**9c**).

2-(4-Pyridyl) imidazoline (10a). White solid, mp 134–136 °C (Lit.[2] 133–135 °C). ν_{max} (KBr)/cm^{-1} 3198 (NH), 3034 (Ph), 2934 (CH_2), 2868 (CH_2), 1611 (C=N). *m/z* (ESI) 147 (39 %, M^+). δ_H ($CDCl_3$, 300 MHz) 8.72 (d, *J* 6 Hz, 2H, Pyridine), 7.66 (d, *J* 6 Hz, 2H, Pyridine), 4.83 (brs, 1H, NH), 3.85 (s, 4H, $2CH_2$). δ_C ($CDCl_3$, 75 MHz) 162.8, 150.3, 137.7, 121.0, 50.3.

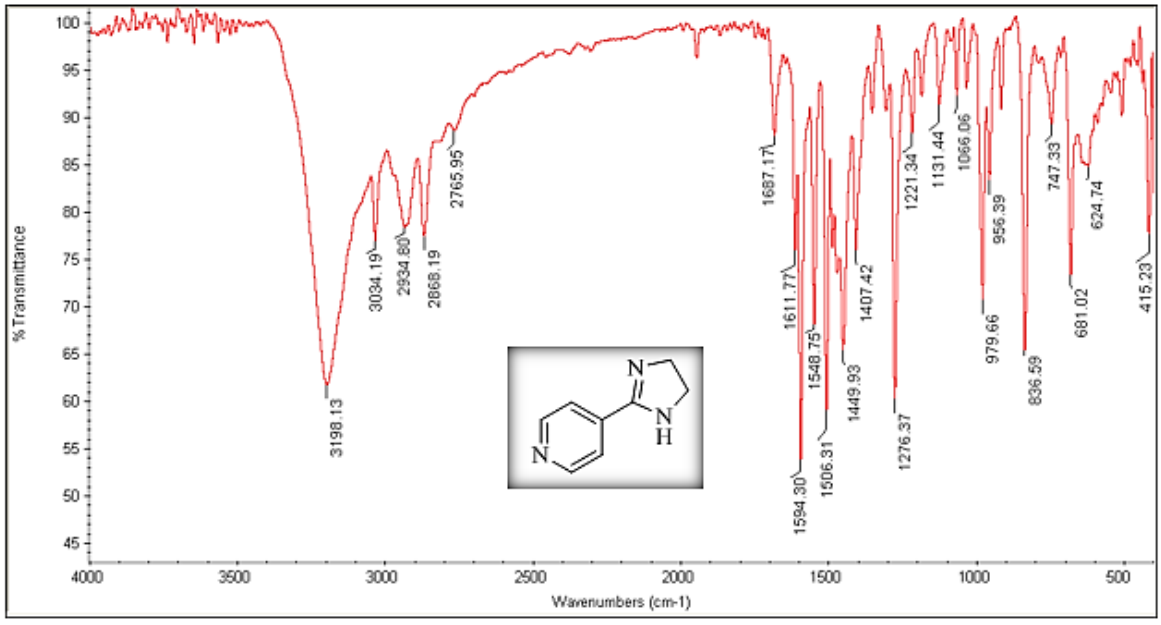

Figure 60. FT-IR (KBr) spectrum of 2-(4-Pyridyl) imidazoline (**10a**).

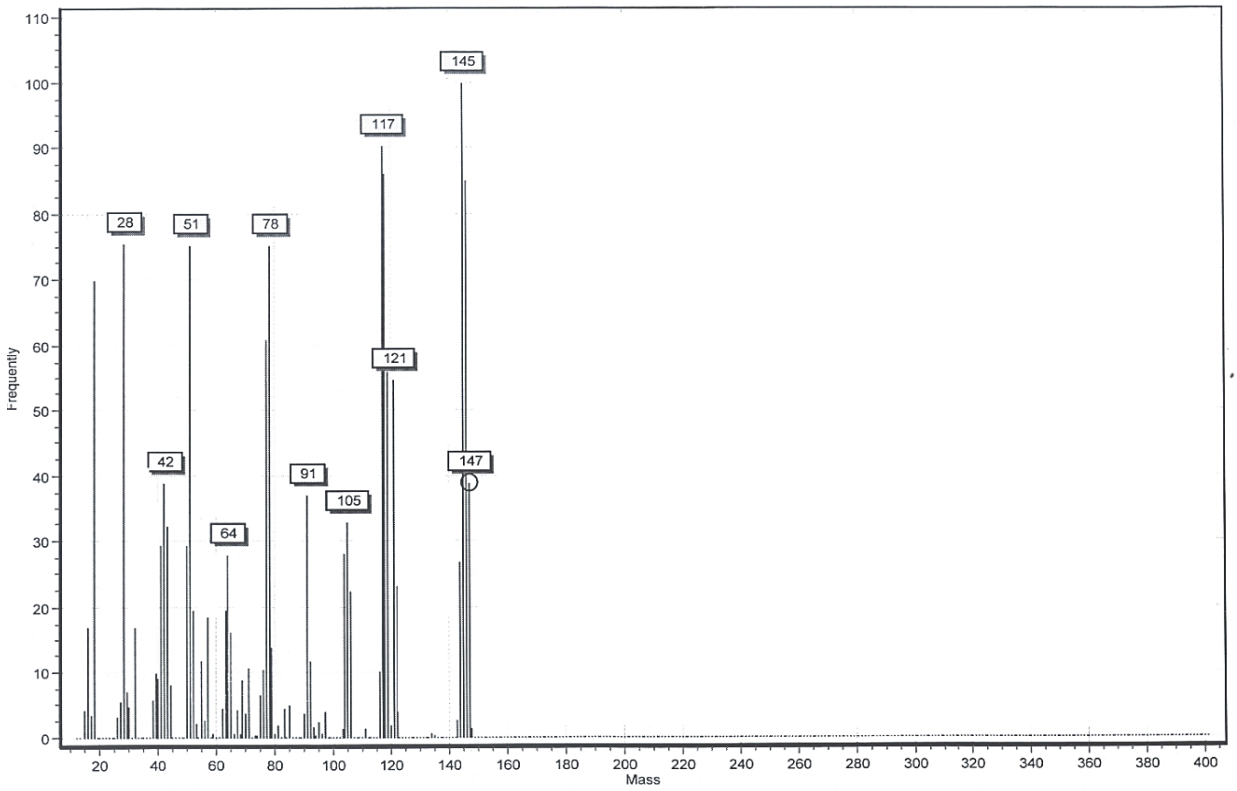

Figure 61. Mass spectrum of 2-(4-Pyridyl) imidazoline (**10a**).

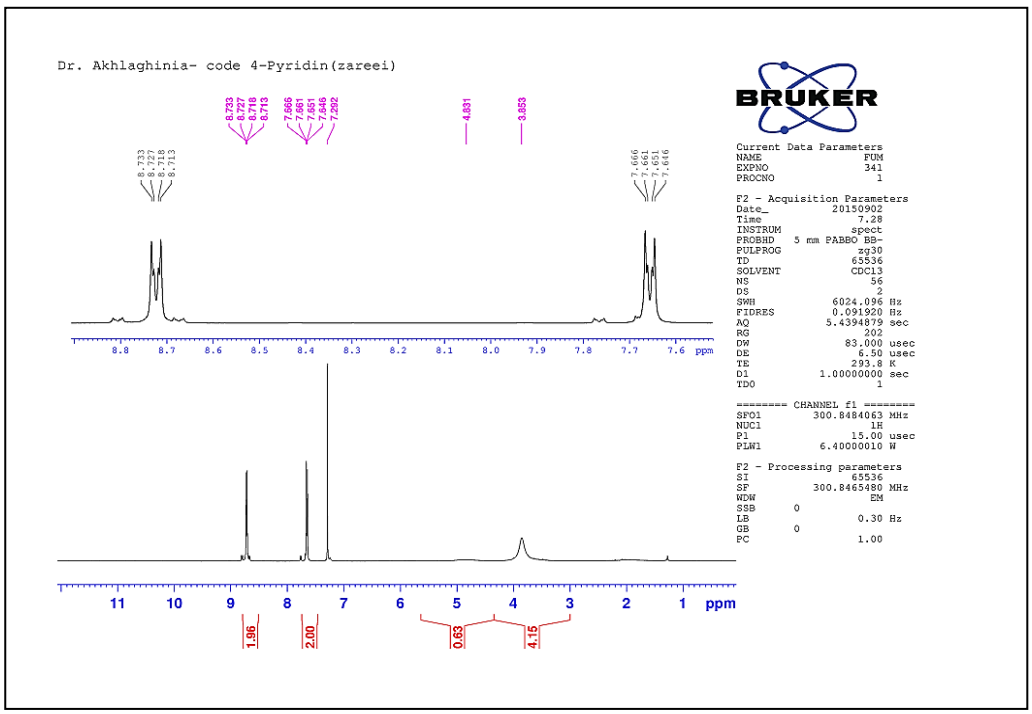

Figure 62. ^{1}H NMR (300 MHz, $CDCl_3$) spectrum of 2-(4-Pyridyl) imidazoline (**10a**).

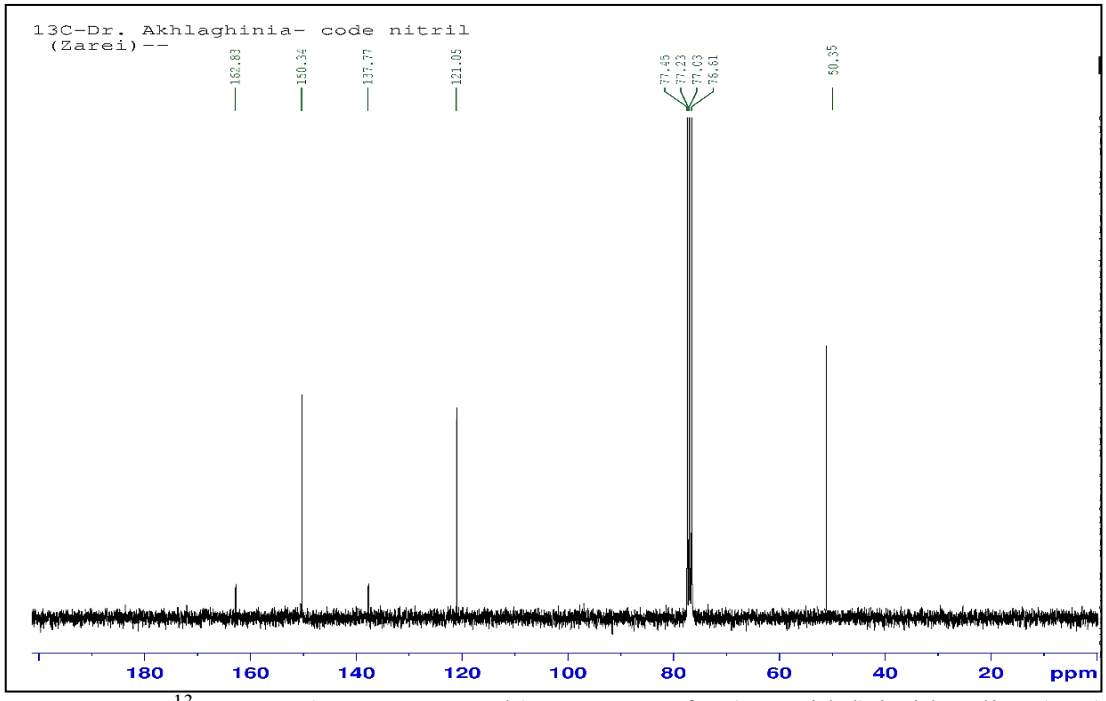

Figure 63. ^{13}C NMR (75 MHz, $CDCl_3$) spectrum of 2-(4-Pyridyl) imidazoline (**10a**).

2-(4-Pyridyl) oxazoline (10b). Yellow solid, mp 109–110 °C (Lit.[2] 109–111 °C). ν_{max} (KBr)/cm^{-1} 3080 (Ph), 3032 (Ph), 2982 (CH_2), 2919 (CH_2), 1650 (C=N). *m/z* (ESI) 149 (39%, M^+).

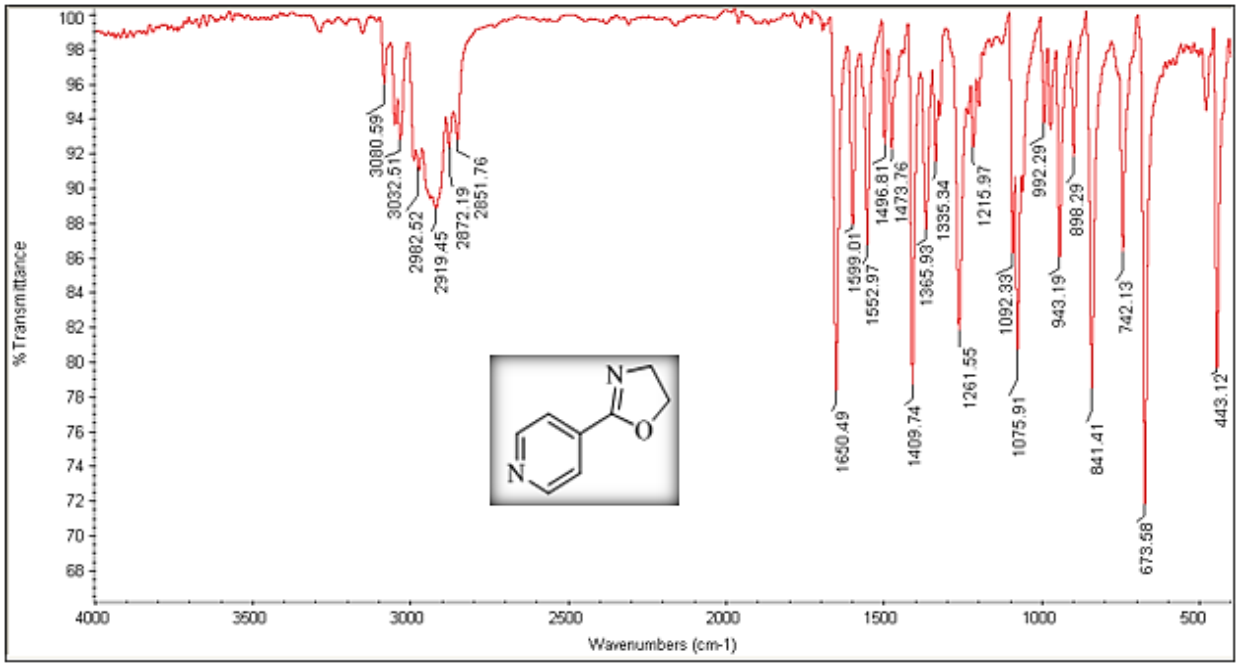

Figure 64. FT-IR (KBr) spectrum of 2-(4-Pyridyl) oxazoline (**10b**).

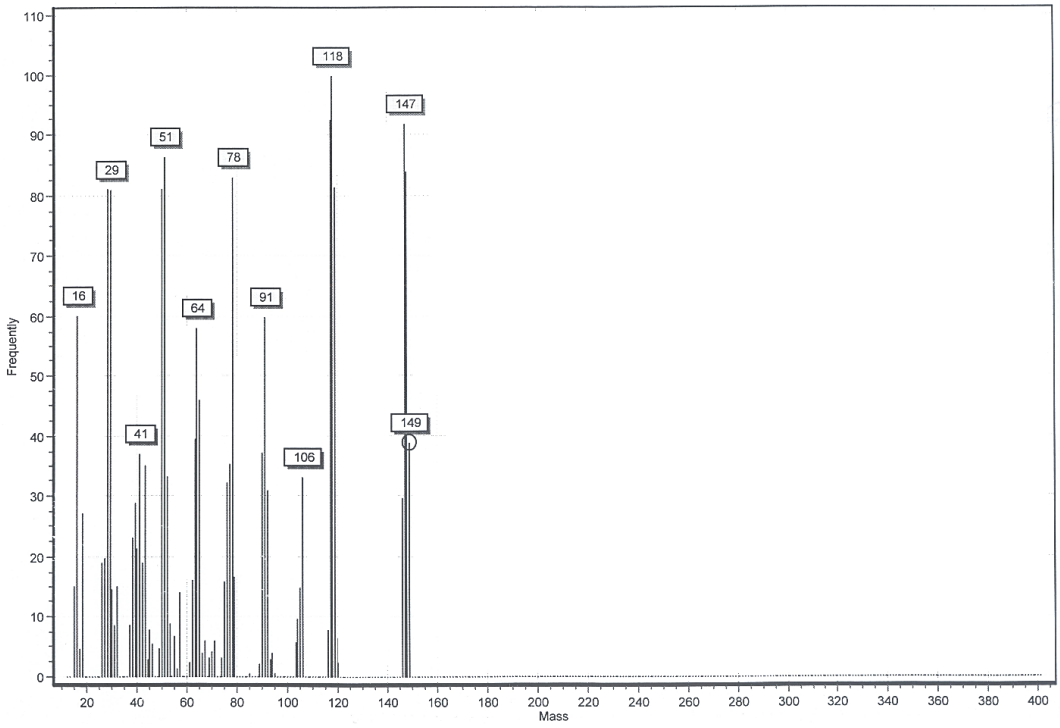

Figure 65. Mass spectrum of 2-(4-Pyridyl) oxazoline (**10b**).

2-(4-Pyridyl) thiazoline (10c). Yellow solid, mp 73–75 °C (Lit.[2] 74–76 °C). *m/z* (ESI) 165 (40%, M^+). δ_H ($CDCl_3$, 300 MHz) 8.62 (d, *J* 6 Hz, 2H, Pyridine), 7.58 (dd, *J* 6 Hz, 1.5 Hz, 2H, Pyridine), 4.41 (t, *J* 8.4 Hz, 2H, CH_2), 3.38 (t, *J* 8.4 Hz, 2H, CH_2). δ_C ($CDCl_3$, 75 MHz) 166.9, 150.0, 140.0, 122.0, 65.4, 33.8.

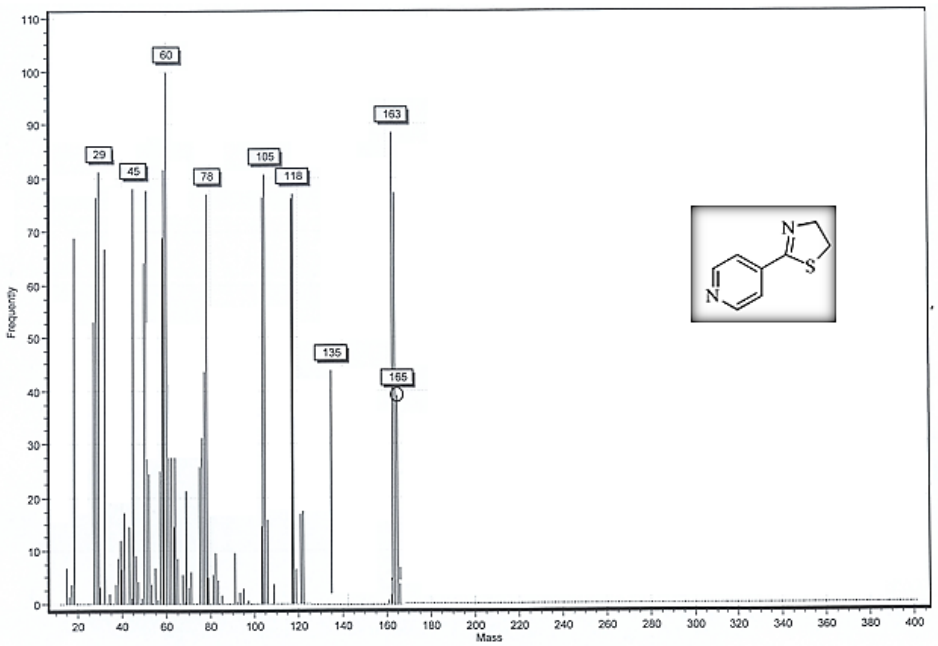

Figure 66. Mass spectrum of 2-(4-Pyridyl) thiazoline (**10c**).

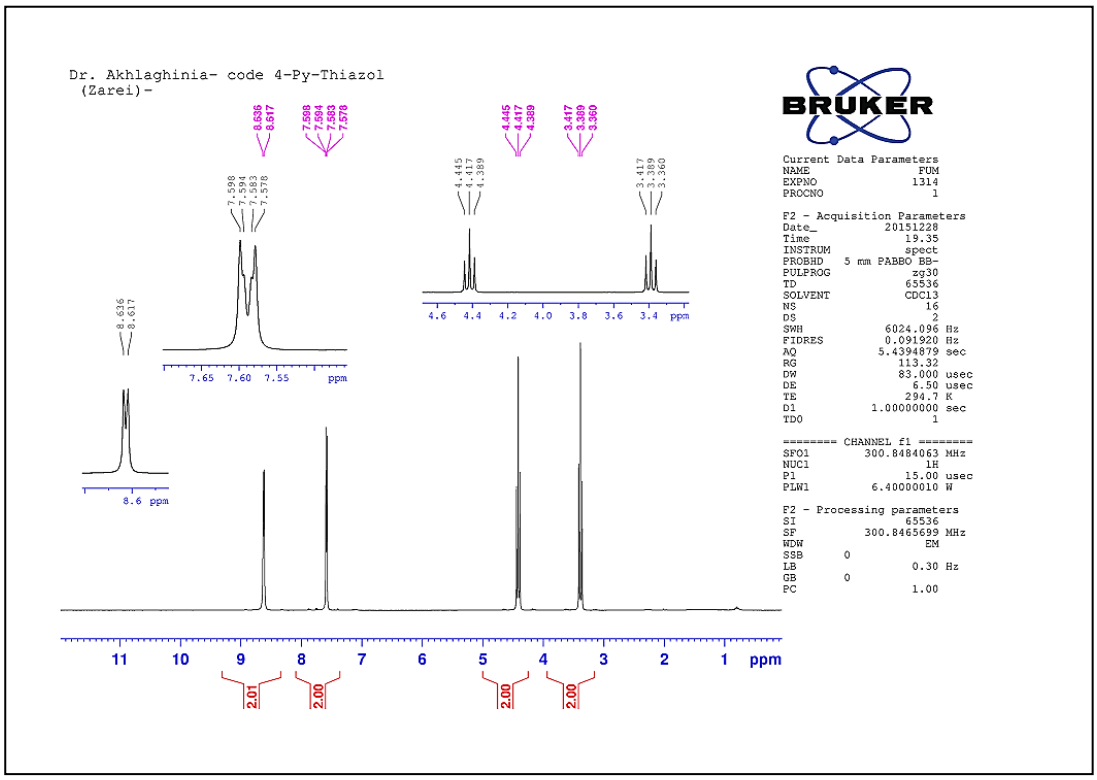

Figure 67. ^{1}H NMR (300 MHz, $CDCl_3$) spectrum of 2-(4-Pyridyl) thiazoline (**10c**).

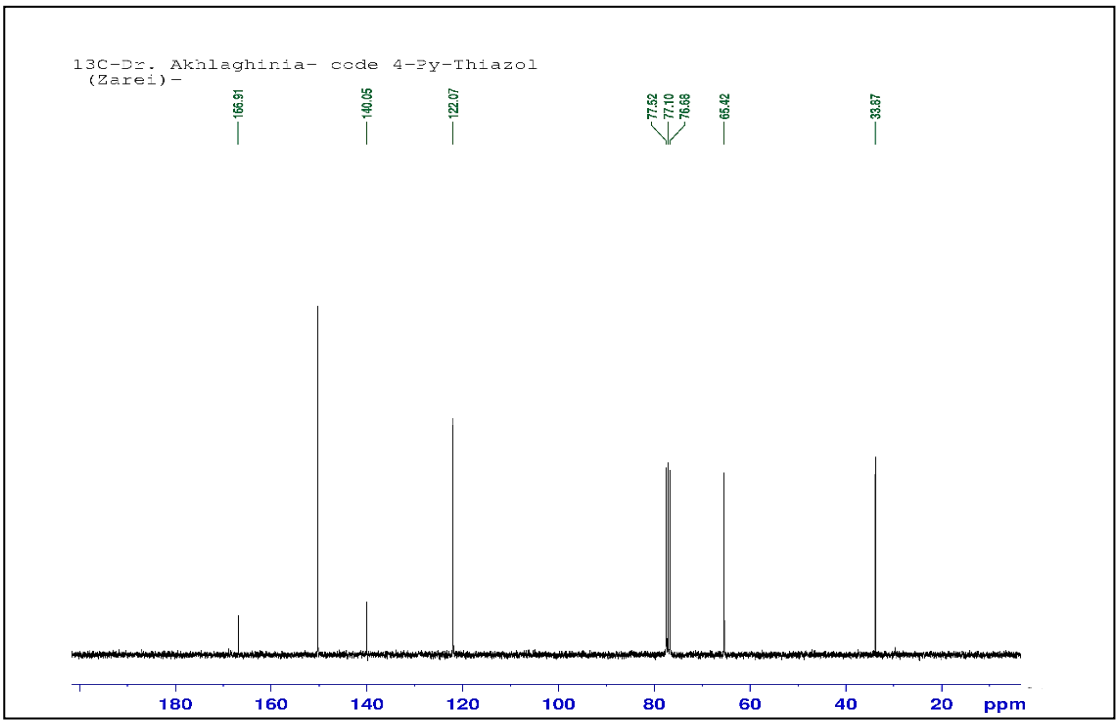

Figure 68. ^{13}C NMR (75 MHz, $CDCl_3$) spectrum of 2-(4-Pyridyl) thiazoline (**10c**).

2-(2-Thionyl)imidazoline (11a). White solid, mp 174–176 °C (Lit.[1] 175–177 °C). ν_{max} (KBr)/cm^{-1} 3297 (NH), 3064 (Ph), 2938 (CH_2), 2868 (CH_2), 1661 (C=N). *m/z* (ESI) 153 (3%, M^+). δ_H ($CDCl_3$, 300 MHz) 7.41–7.36 (m, 1H, Thiophene), 7.29 (s, 1H, Thiophene), 7.06 (t, *J* 4.2 Hz, 1H, Thiophene), 4.79 (brs, 1H, NH), 3.78 (s, 4H, $2CH_2$).

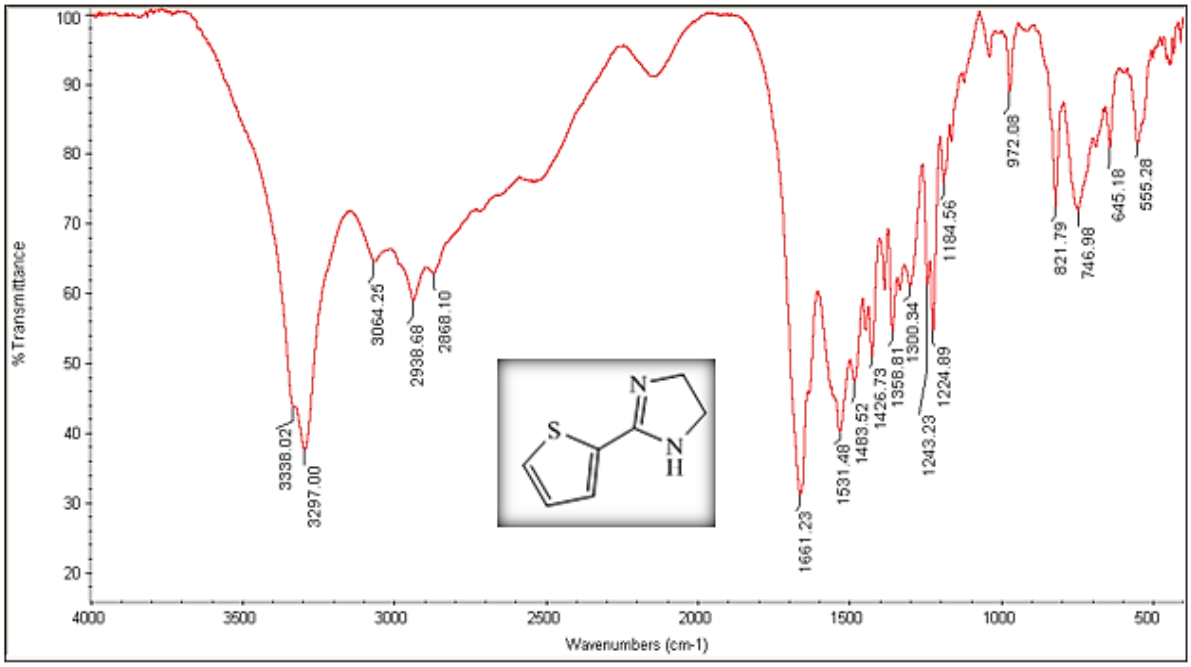

Figure 69. FT-IR (KBr) spectrum of 2-(2-Thionyl) imidazoline (**11a**).

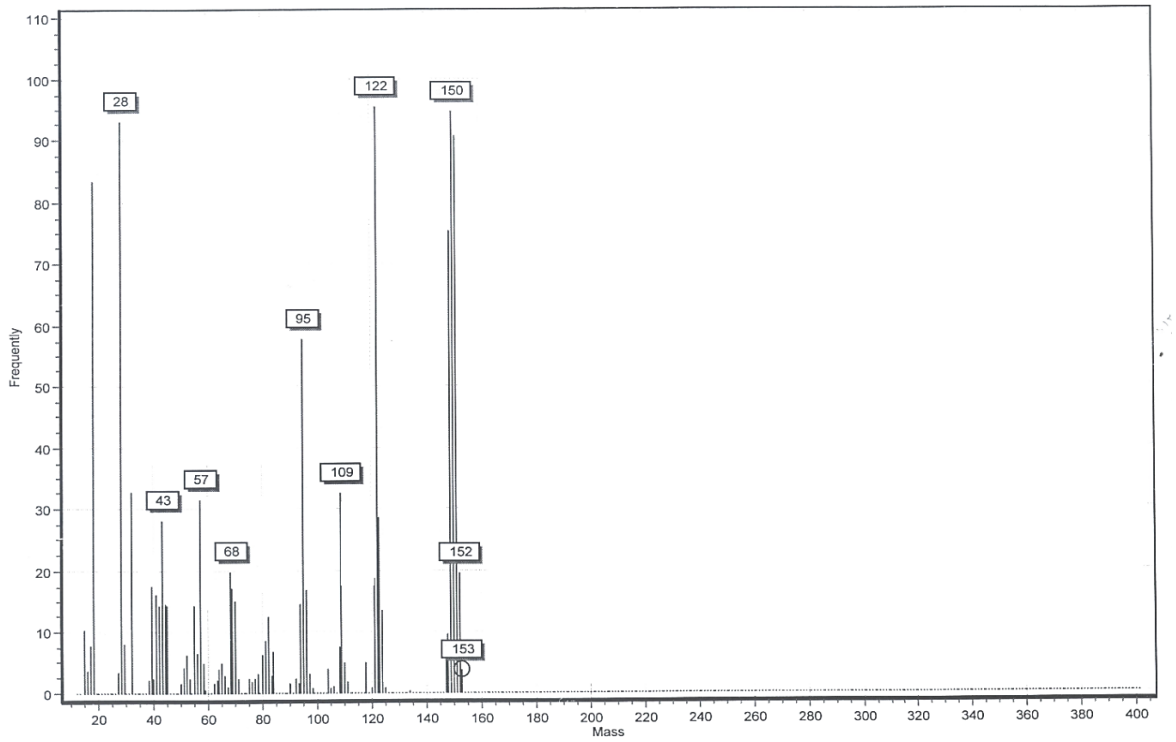

Figure 70. Mass spectrum of 2-(2-Thionyl) imidazoline (**11a**).

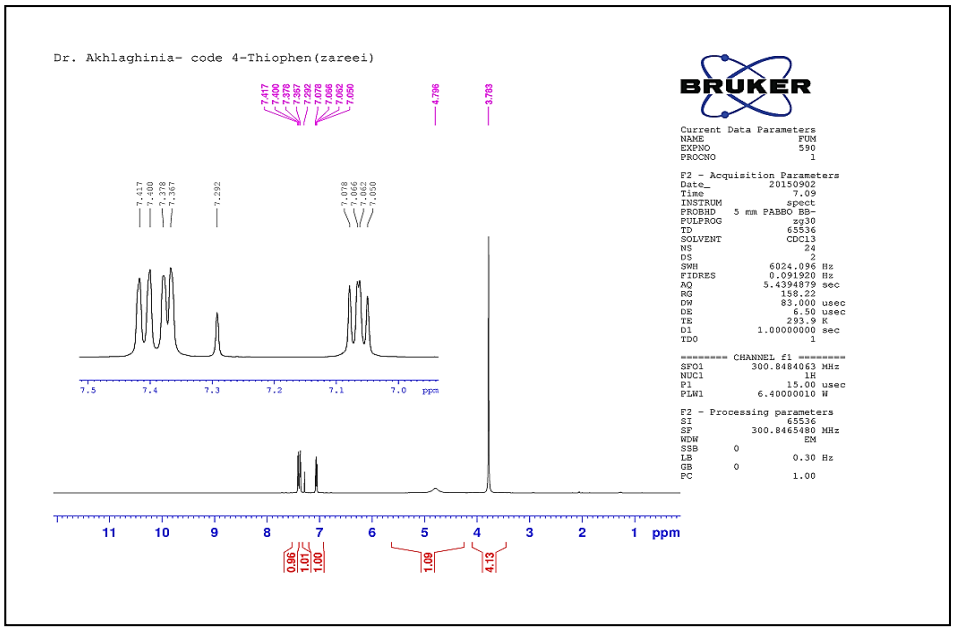

Figure 71. ^{1}H NMR (300 MHz, $CDCl_3$) spectrum of 2-(2-Thionyl) imidazoline (**11a**).

2-(2-Thionyl) oxazoline (11b). White solid, mp 57–58 °C (Lit.[1] 57–59 °C). *m/z* (ESI) 153 (3%, M^+). δ_H ($CDCl_3$, 300 MHz) 7.61 (dd, *J* 3.6 Hz, *J* 0.9 Hz, 1H, Thiophene), 7.46 (dd, *J* 3.6 Hz, *J* 0.9 Hz, 1H, Thiophene), 7.10 (t, *J* 4.2 Hz, 1H, Thiophene), 4.45 (t, *J* 9.6 Hz, 2H, CH_2), 4.06 (t, *J* 9.6 Hz, 2H, CH_2).

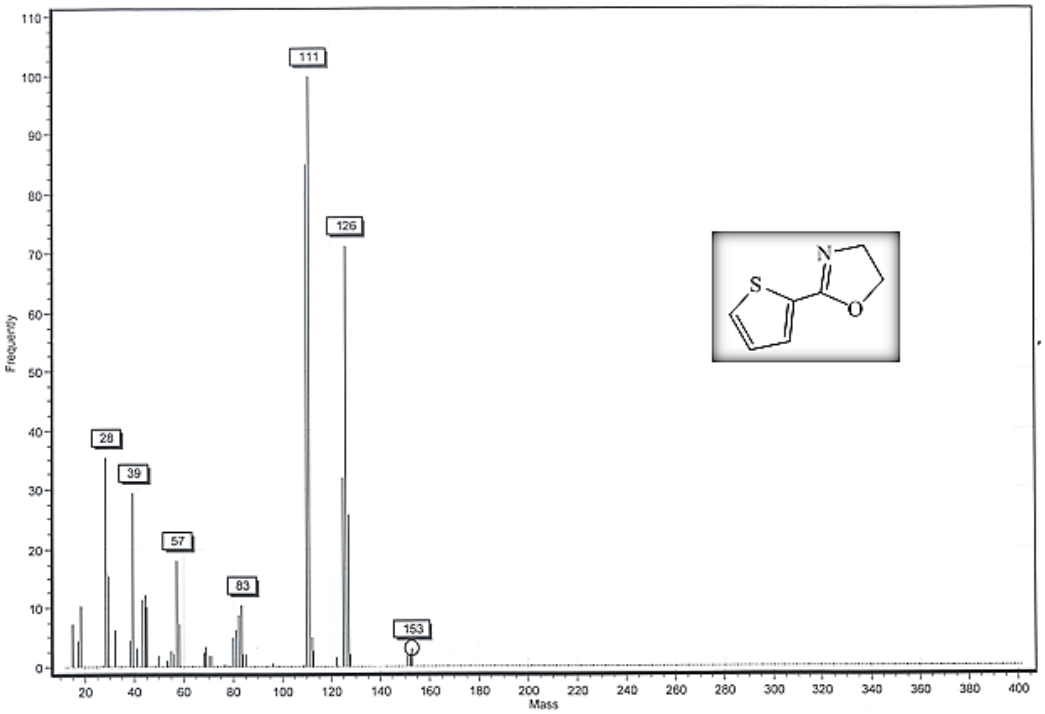

Figure 72. Mass spectrum of 2-(2-Thionyl) oxazoline (**11b**).

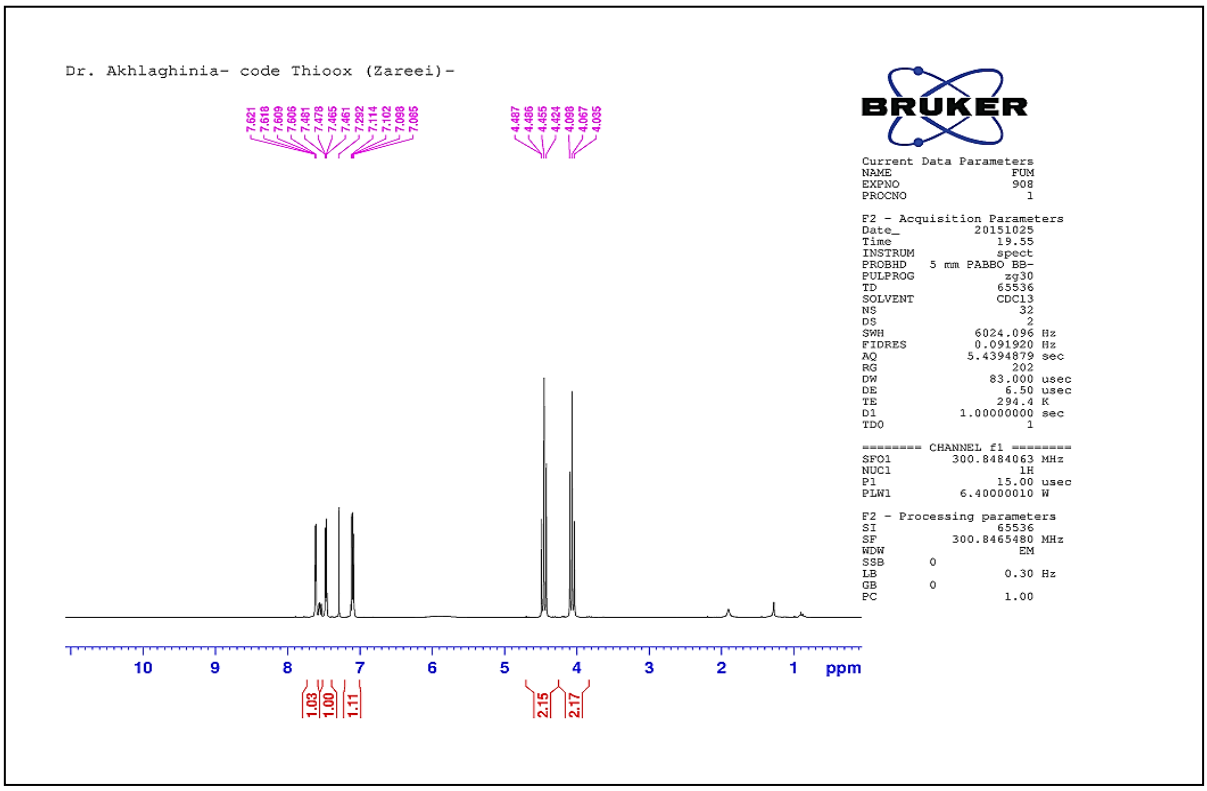

Figure 73. ^{1}H NMR (300 MHz, $CDCl_3$) spectrum of 2-(2-Thionyl) oxazoline (**11b**).

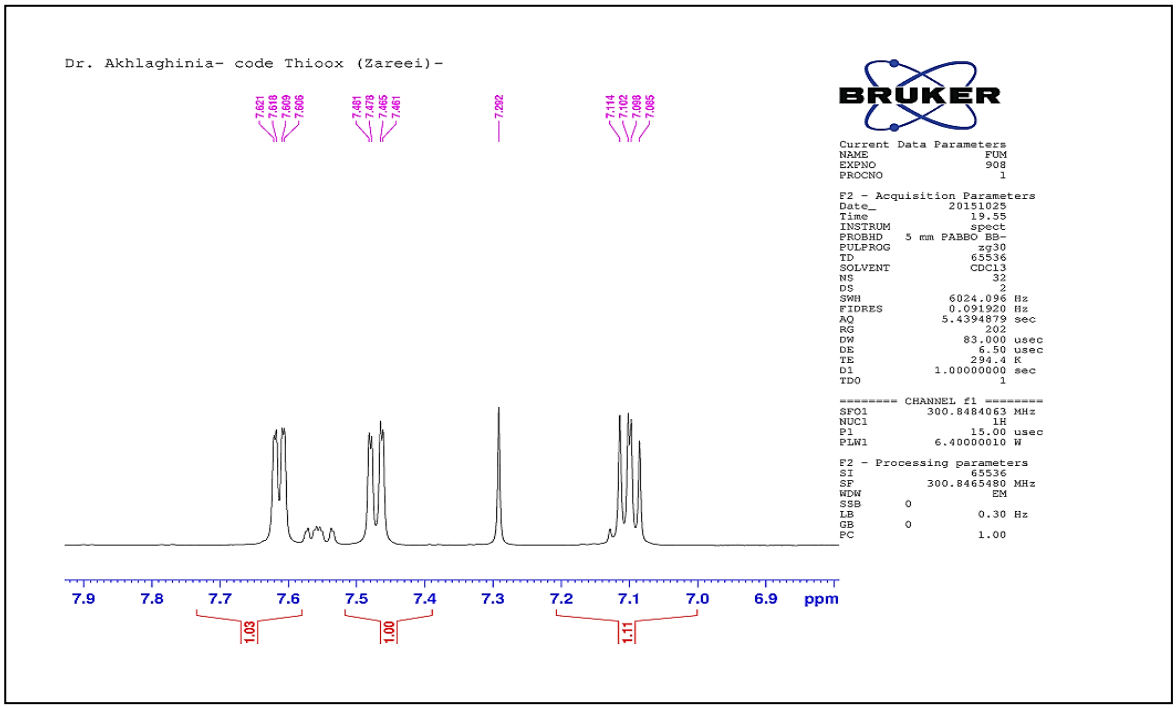

Figure 74. ^{1}H NMR (300 MHz, $CDCl_3$) spectrum of 2-(2-Thionyl) oxazoline (**11b**) expanded.

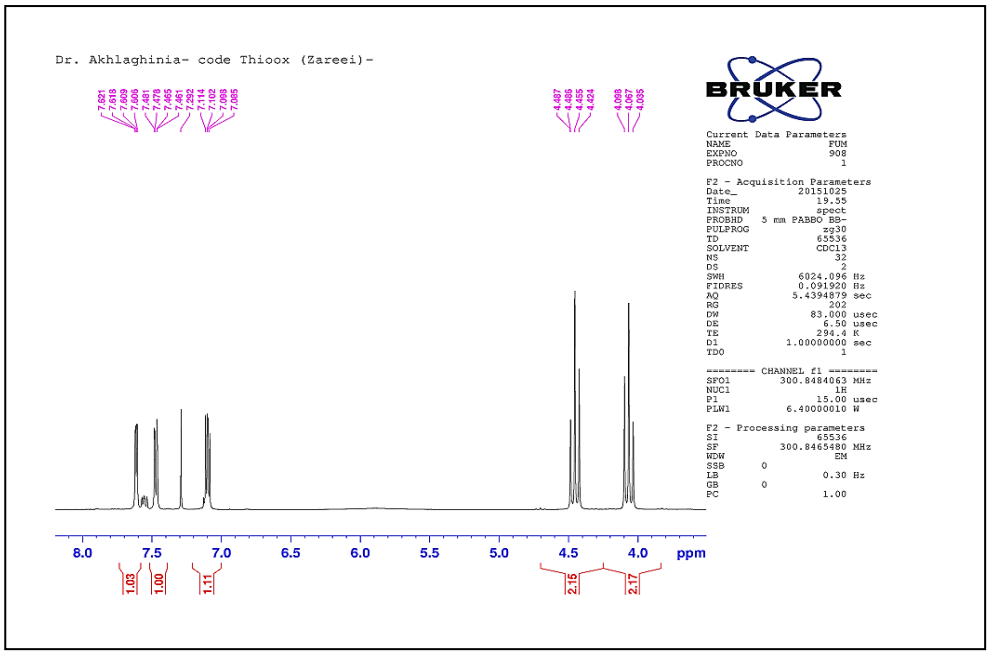

Figure 75. ^{1}H NMR (300 MHz, $CDCl_3$) spectrum of 2-(2-Thionyl) oxazoline (**11b**) expanded.

2-(2-Thionyl) thiazoline (11c). Yellow solid, mp 39–41 °C (Lit.[2] 40–42 °C). *m/z* (ESI) 170 (68%, M^+). δ_H ($CDCl_3$, 300 MHz) 7.35 (t, *J* 4.2 Hz, 2H, Thiophene), 6.98 (t, *J* 4.2 Hz, 1H, Thiophene), 4.32 (t, *J* 8.1 Hz, 2H, CH_2), 3.35 (t, *J* 8.1 Hz, 2H, CH_2). δ_C ($CDCl_3$, 75 MHz) 161.6, 137.0, 130.7, 129.6, 127.5, 64.7, 34.4.

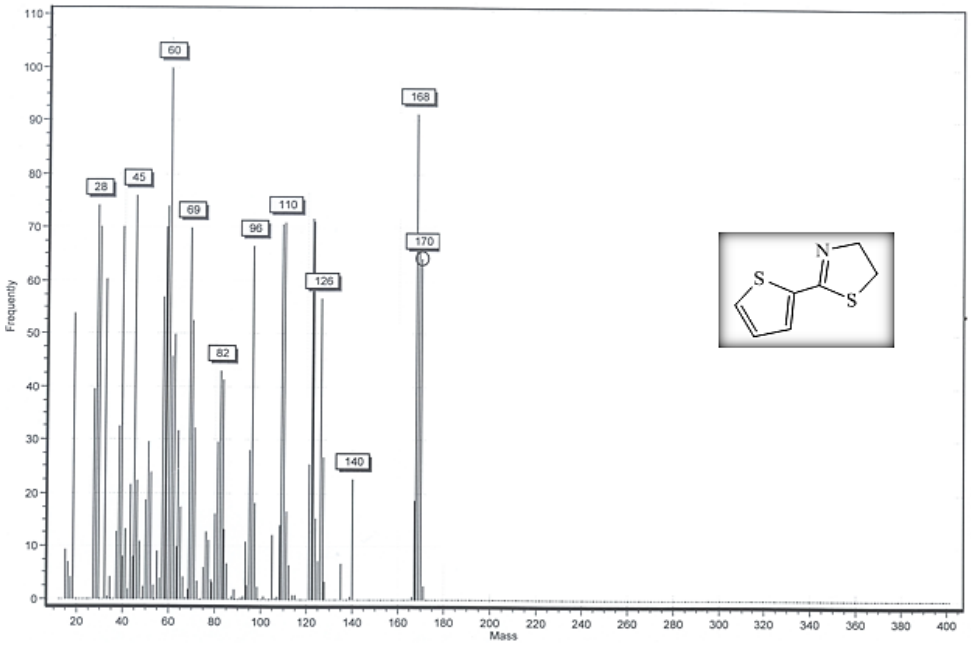

Figure 76. Mass spectrum of 2-(2-Thionyl) thiazoline (**11c**).

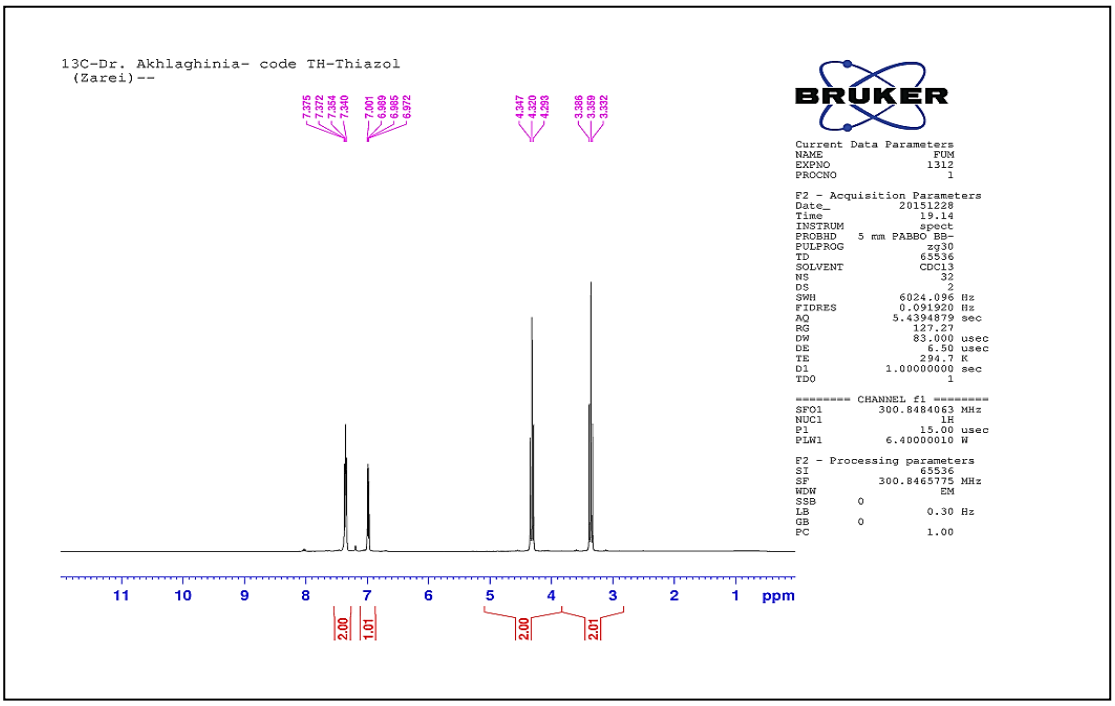

Figure 77. ^{1}H NMR (300 MHz, $CDCl_3$) spectrum of 2-(2-Thionyl) thiazoline (**11c**).

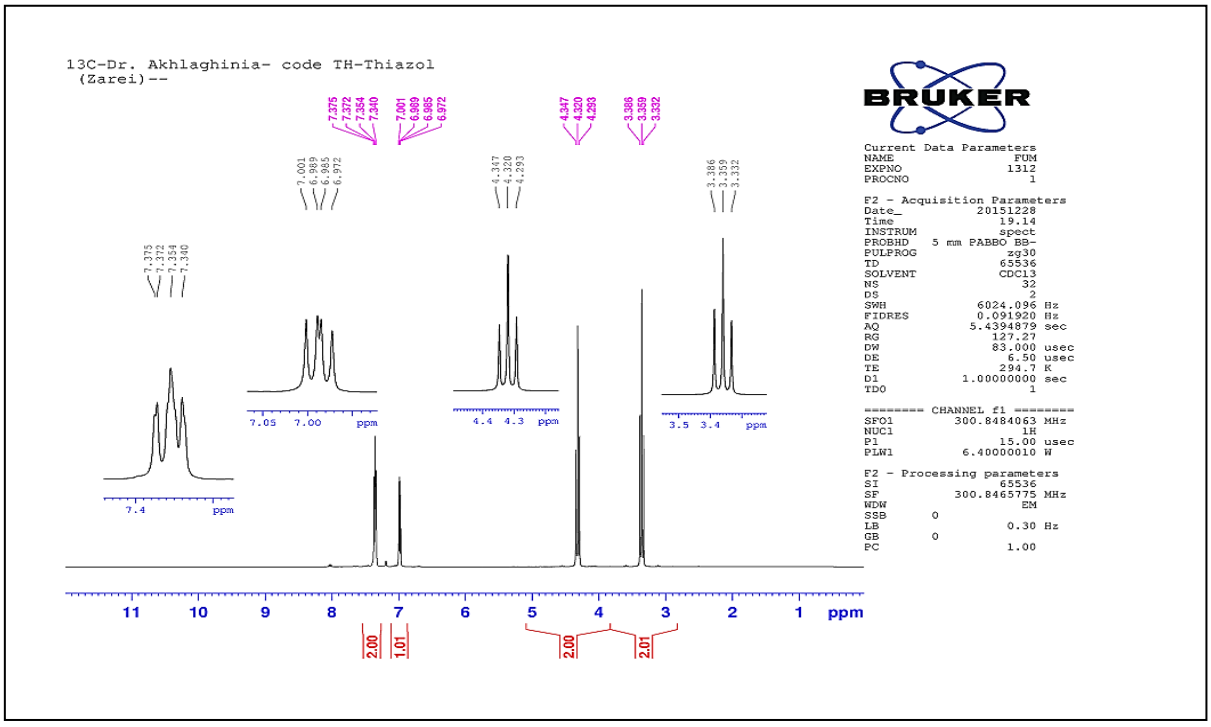

Figure 78. ^{1}H NMR (300 MHz, $CDCl_3$) spectrum of 2-(2-Thionyl) thiazoline (**11c**) expanded.

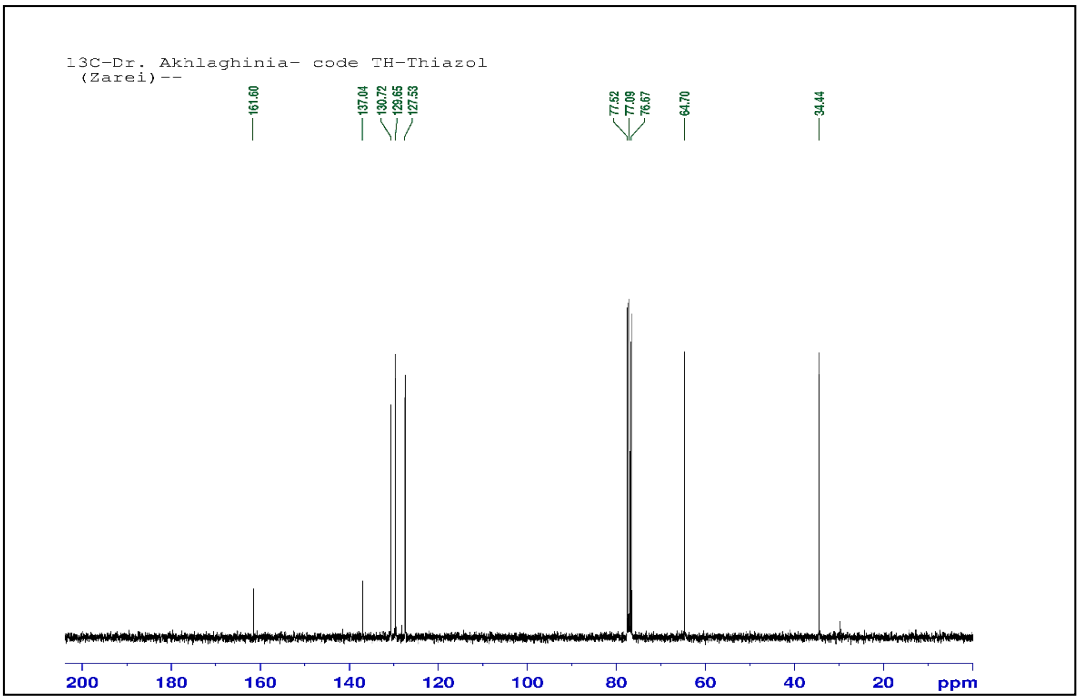

Figure 79. ^{13}C NMR (75 MHz, $CDCl_3$) spectrum of 2-(2-Thionyl) thiazoline (**11c**).

2-Butyl-2-imidazoline (12a). White solid. mp 40–41 °C (Lit.[10] 41–42 °C). *m/z* (ESI) 126 (9%, M^+).

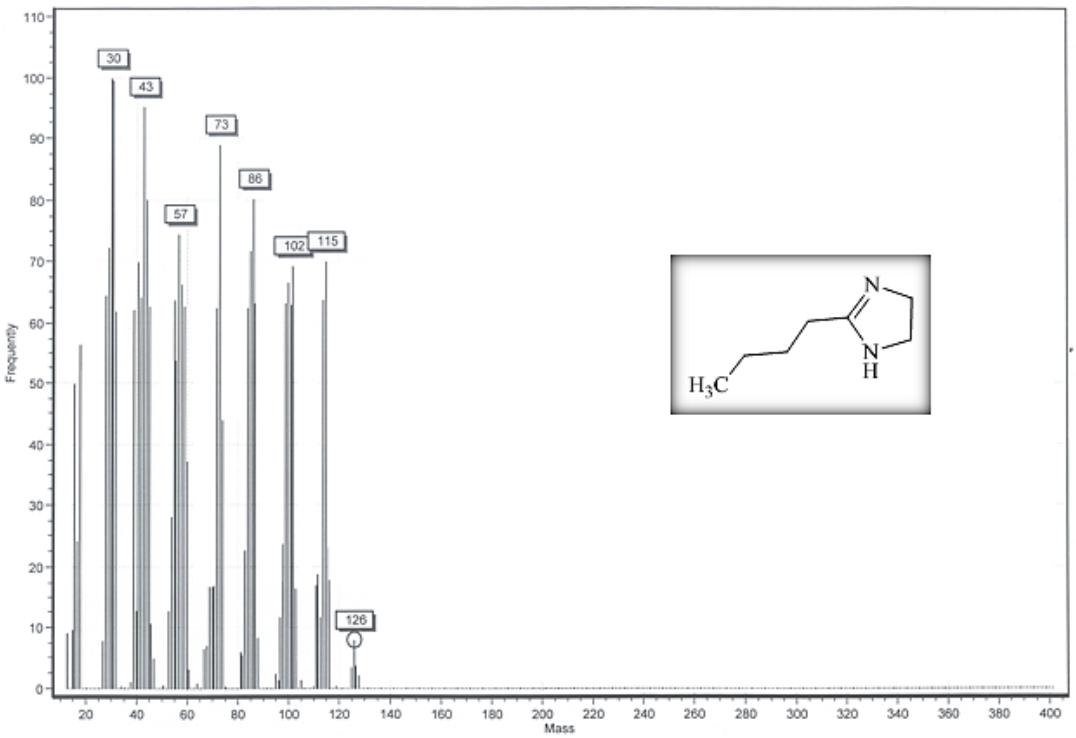

Figure 80. Mass spectrum of 2-Butyl-2-imidazoline (**12a**).

Intermediate II (X=NH). White solid; mp 120–122 °C. FT-IR (KBr): ν_{max}/cm^{-1} 3370 (NH_2), 3172 (NH), 3060 (Ph), 2917 (CH_2), 2770 (CH_2), 1658 (C=N), 1623 (C=N); MS, *m/z* (%): 121 [99%, $M^+–C_2H_4NH_2$], 105 [100%, PhC=NH], 77 [98%, Ph], 44 [64%, $CH_2CH_2NH_2$], 29 [69%, CH_2NH_2].

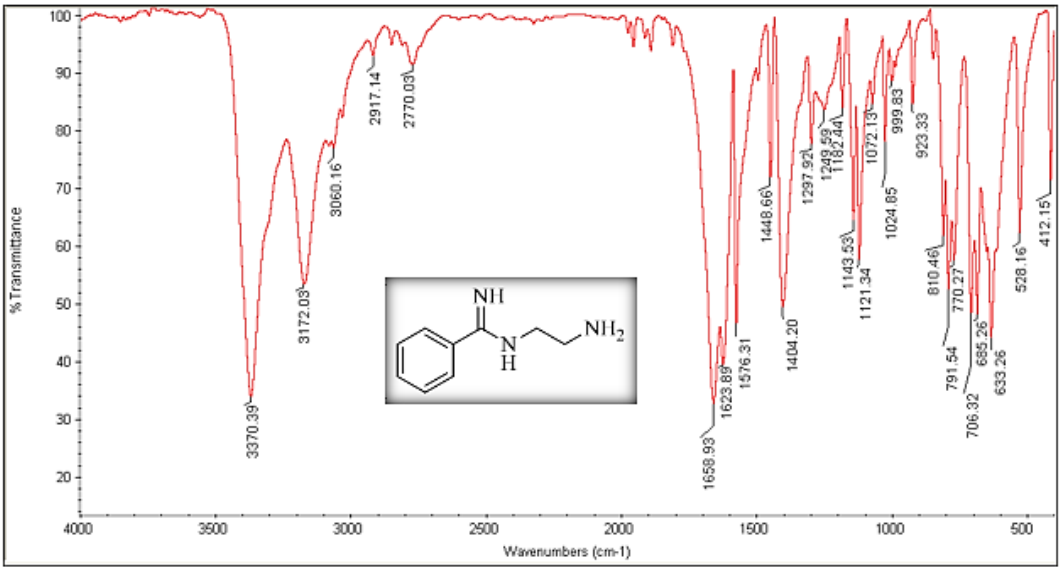

Figure 81. FT-IR (KBr) spectrum of intermediate **II** (X=NH).

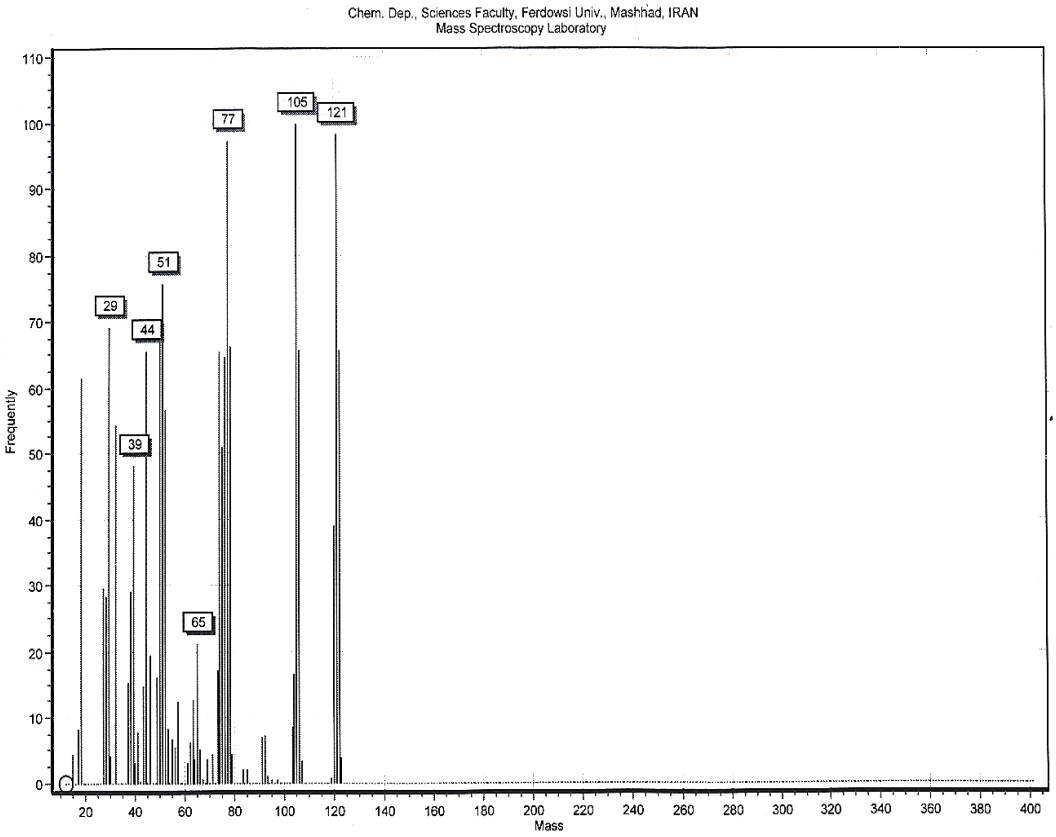

Figure 82. Mass spectrum of intermediate **II** (X=NH).

Intermediate II (X=O). Yellow oil. FT-IR (neat): ν_{max}/cm^{-1} 3481(OH), 3415 (NH), 2953 (CH_2), 2924 (CH_2), 2853 (CH_2), 1642 (C=N), 1615 (C=N); MS, *m/z* (%): 164 [43 %, M^+], 121 [87%, M^+–C_2H_4OH], 105 [100%, PhC=NH], 77 [92%, Ph], 29 [98%, CH_2OH].

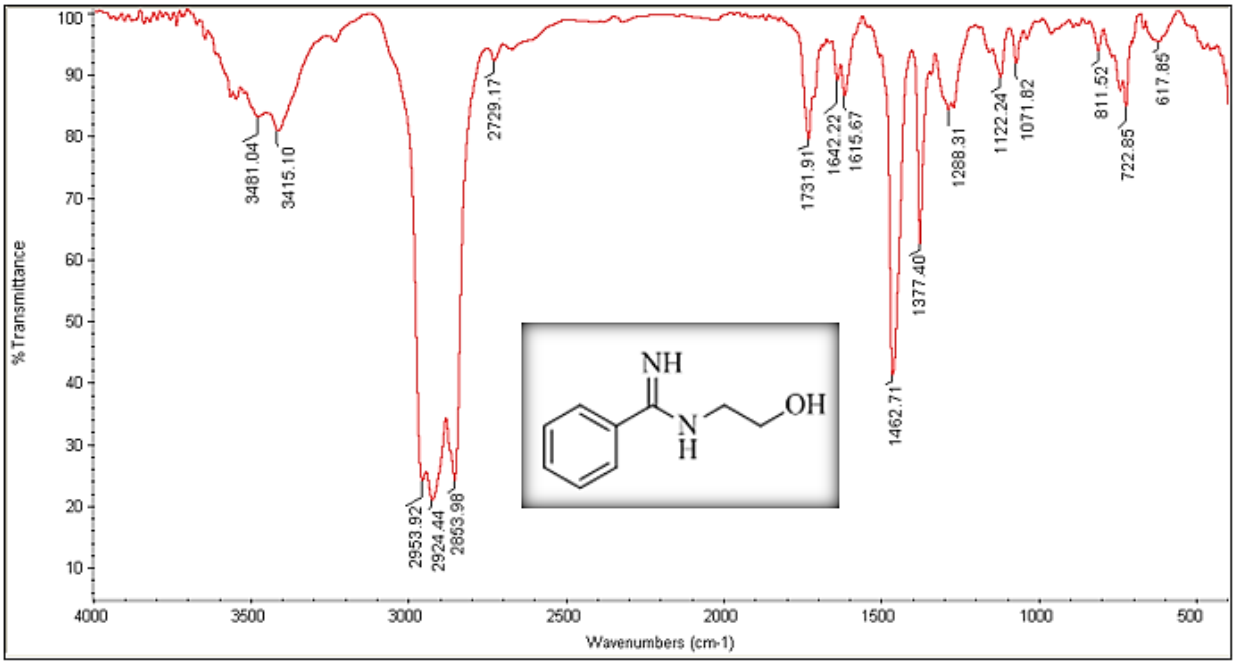

Figure 83. FT-IR (neat) spectrum of intermediate **II** (X=O).

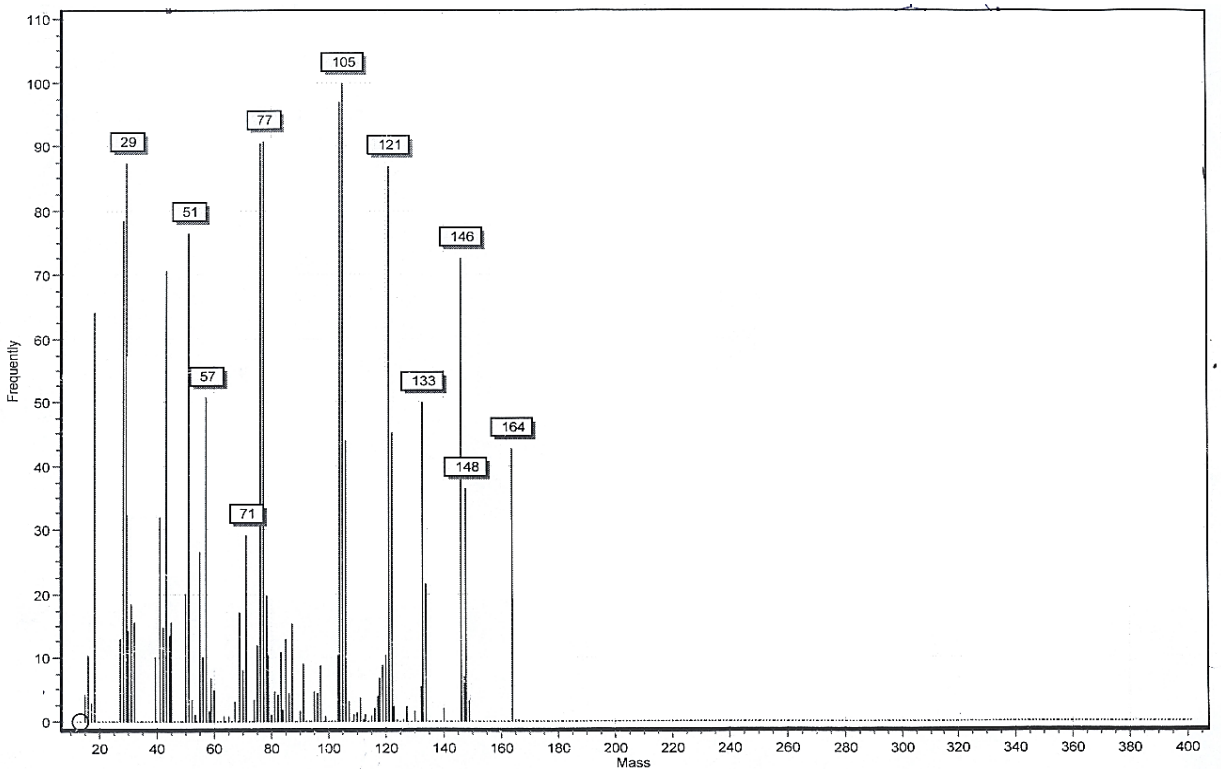

Figure 84. Mass spectrum of intermediate **II** (X=O).

Intermediate II (X=S). Yellow oil. FT-IR (neat): ν_{max}/cm^{-1} 3424 (NH), 3000 (Ph), 2914 (CH_2), 2814 (CH_2), 2263 (SH), 1675 (C=N); MS, *m/z* (%): 180 [2%, M^+], 120 [98%, M^+–C_2H_4SH], 105 [100%, PhC=NH], 77 [99%, Ph], 28 [98%, C=NH].

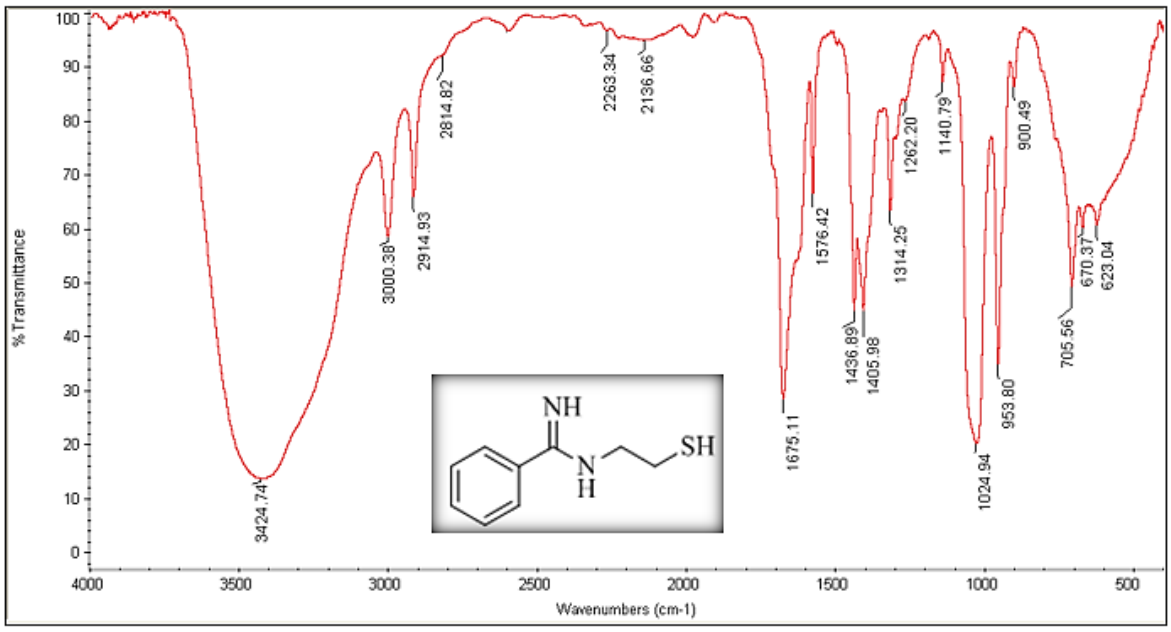

Figure 85. FT-IR (neat) spectrum of intermediate **II** (X=S).

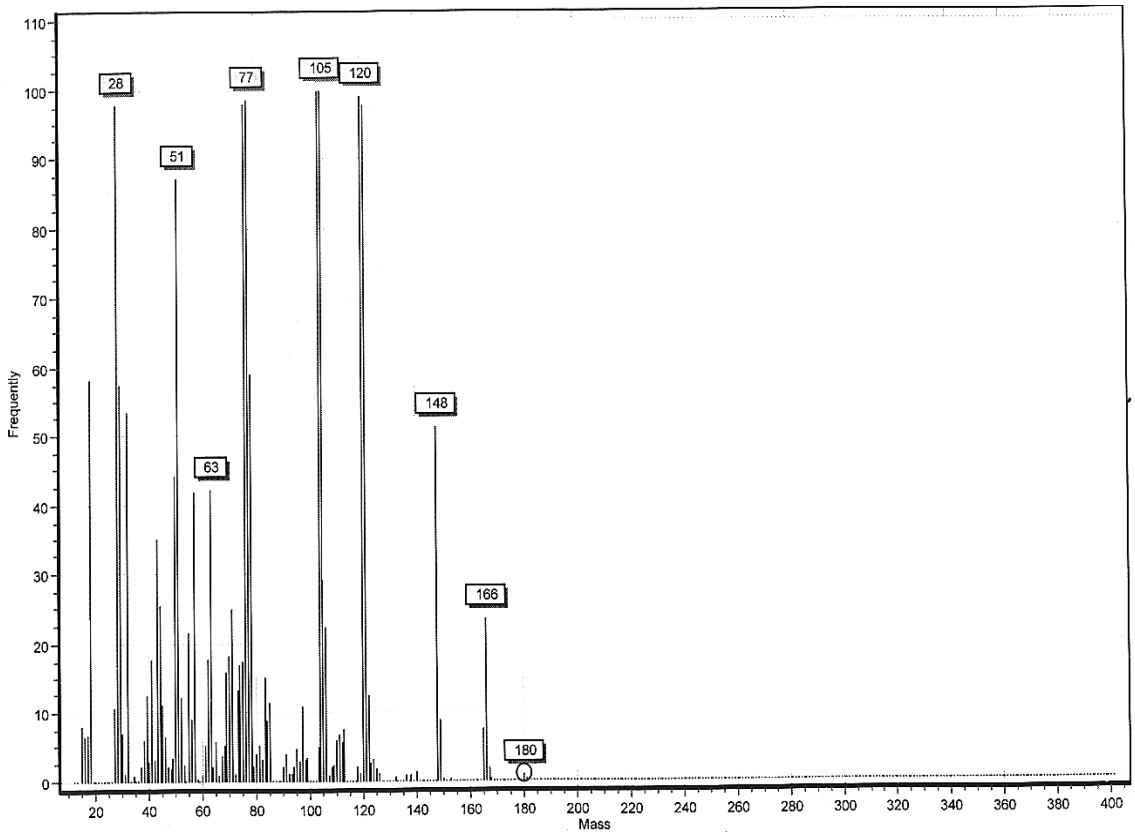

Figure 86. Mass spectrum of intermediate **II** (X=S).

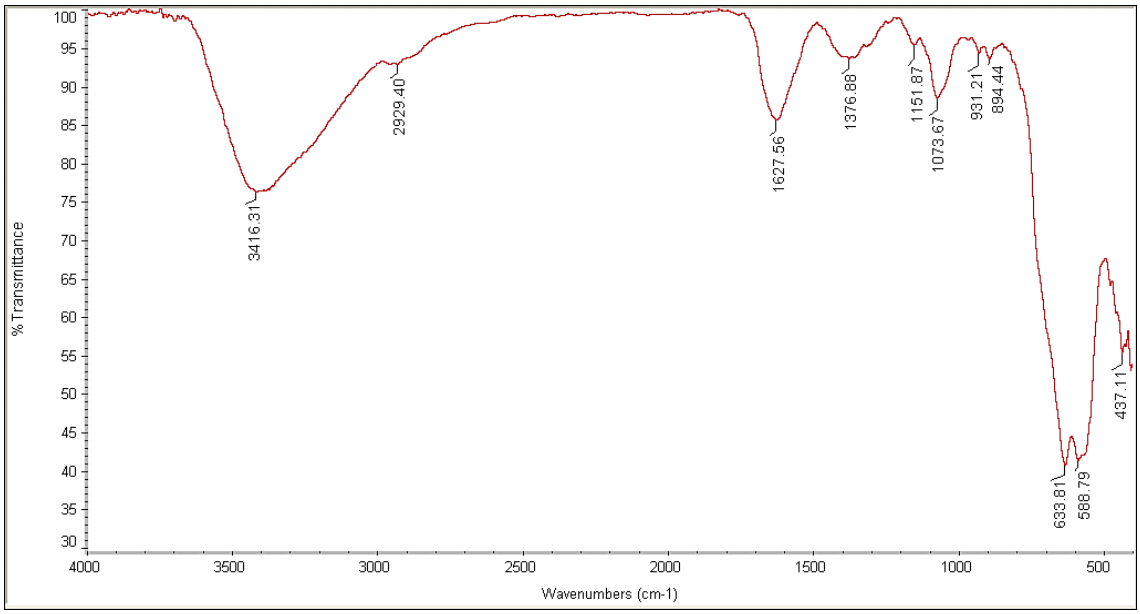

Figure 87. FT-IR spectrum of Fe_3O_4@Agarose nanocomposite (**I**).

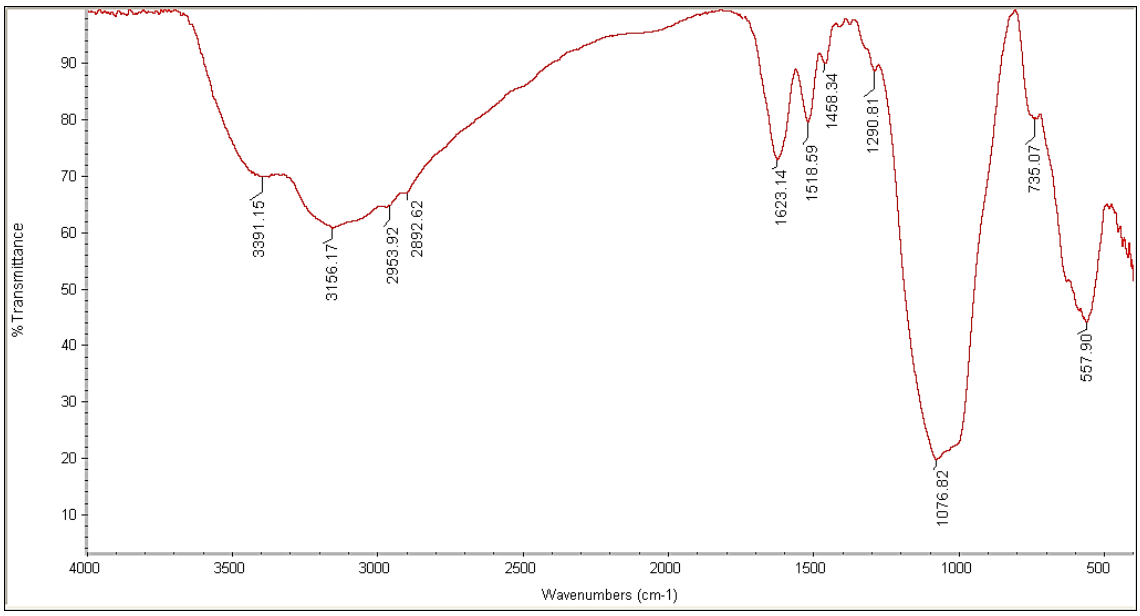

Figure 88. FT-IR spectrum of Fe_3O_4@Agarose/$AEPH_2$ **(II)**.

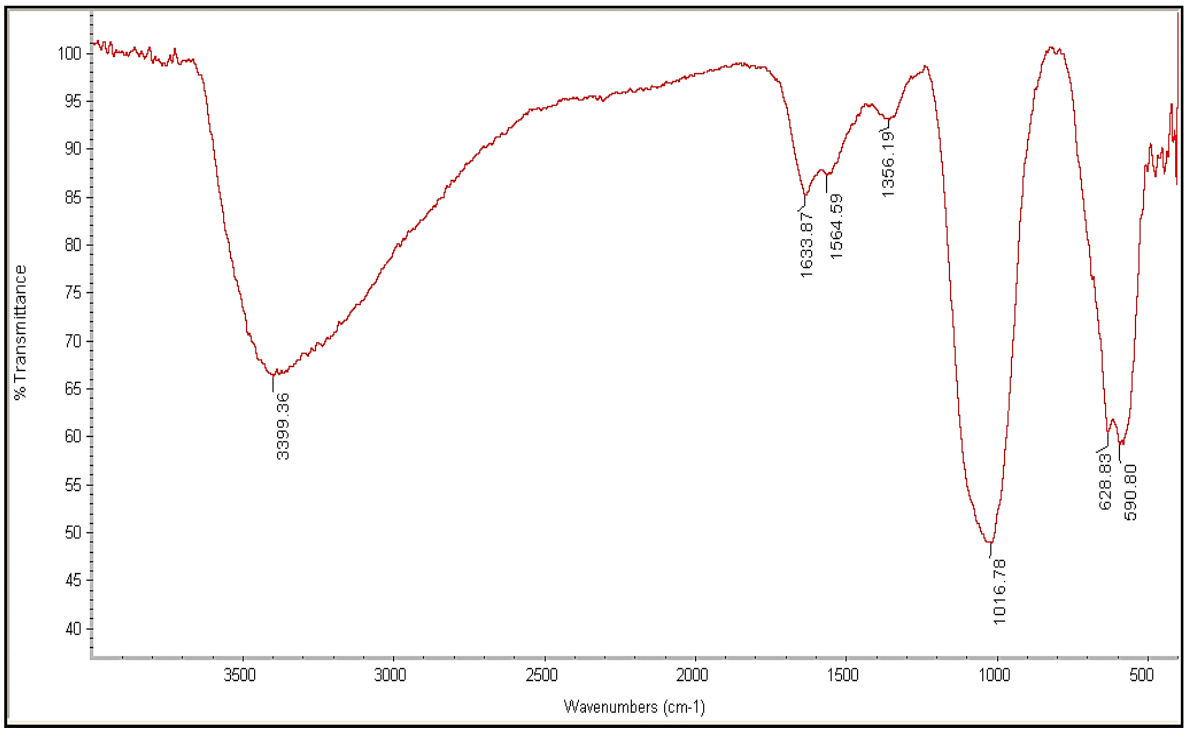

Figure 89. FT-IR spectrum of Fe_3O_4@Agarose/SAEPH$_2$ **(III)**.

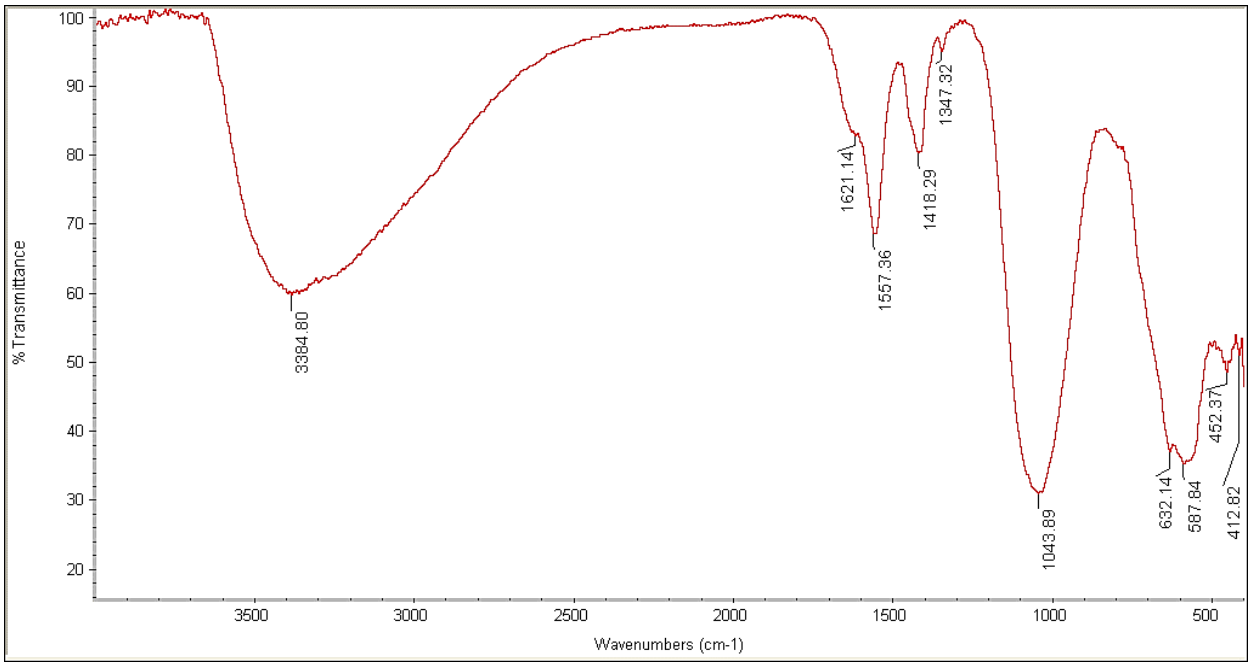

Figure 90. FT-IR spectrum of Fe_3O_4@Agarose/SAEPH$_2$/Cu(II) **(IV)**.

.

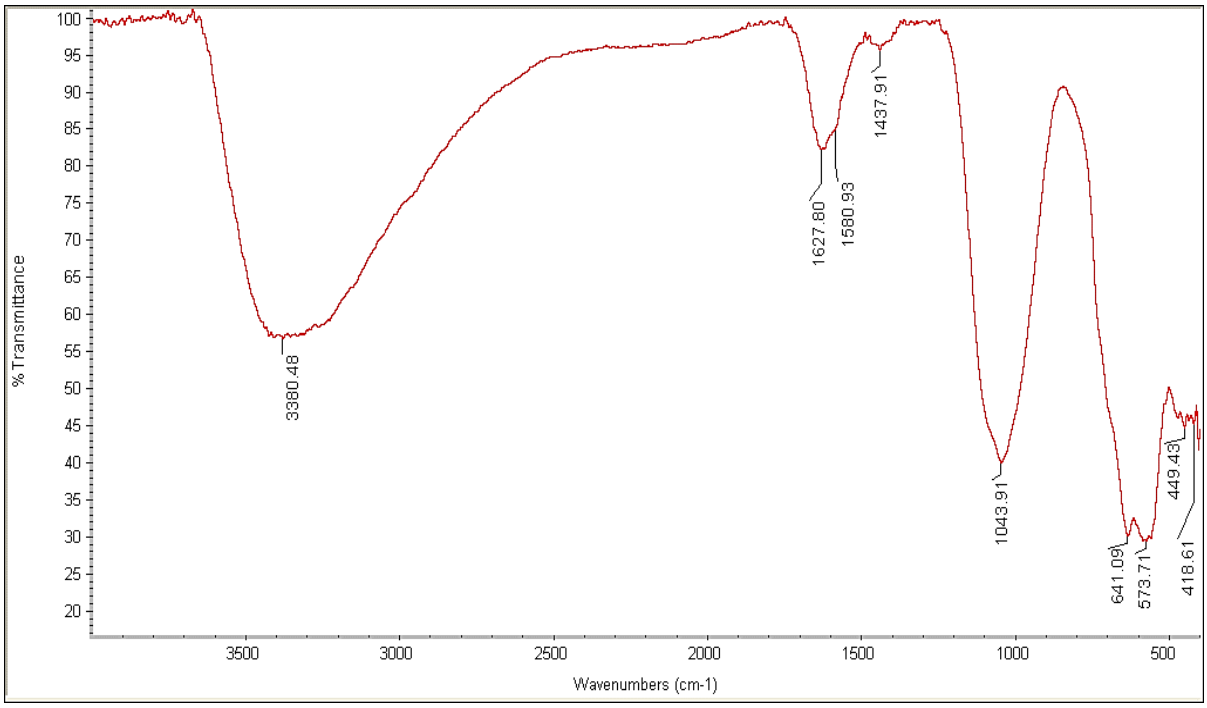

Figure 91. FT-IR spectrum of 7th reused Fe_3O_4@Agarose/SAEPH_2/Cu(II) (**IV**).

References

1. Ishihara, M.; Togo, T. *Tetrahedron* **2007**, *63*, 1474-1480.

2. Mohammadpoor-Baltork, I.; Moghadam, M.; Tangestaninejad, S.; Mirkhani, V.; Hojati, S. F. *Catal. Commun*. **2008**, *9*, 1153-1161.

3. Nasr-Esfahani, M.; Montazerozohori, M.; Mehrizi, S. *J. Heterocyclic Chem*. **2011**, *48*, 249-254.

4. Klem, R. E.; Shinner, H. F.; Walba, H.; Lsensee, R. W. *J. Heterocyclic Chem*. **1970**, *7*, 403-404.

5. Wang, L.; Guo, B.; Li, H. X.; Li, Q.; Li, H. Y.; Lang, J. P. *Dalton Trans*. **2013**, *42*, 15570-15580.

6. Trose, M.; Lazreg, F.; Lesieur, M.; Cazin, C. S. J. *Green Chem*. **2015**, *17*, 3090-3092.

7. Harfenist, M.; Soroko, F. E.; McKenzie, G. M. *J. Med. Chem*. **1978**, *21*, 405-409.

8. Boyd, B. R. N.; Rittner, R. C. *J. Am. Chem. Soc*. **1960**, *82*, 2032-2034.

9. Nalini, D.; Rajalakshmi, R.; Subashini, S. *E-J. Chem*. **2011**, *8*, 671-679.

10. Veer, S. D.; Katkar, K. V.; Akamanchi, K. G. *Tetrahedron Lett*. **2016**, *57*, 4039-4043.